Interactive comment on "Concentrations and source regions of light absorbing particles in snow/ice in northern Pakistan and their impact on snow albedo"

by Chaman Gul et al.

Anonymous Referee# 1

This manuscript reported the data of light absorbing particles (LAP, such BC, OC and dust) measured in snow/ice in northern Pakistan and estimated the induced snow albedo reduction and corresponded radiative forcing during 2015-2016. Authors found the concentration of BC, OC and dust in aged snow is higher than in fresh snow and ice and the concentration over northern Pakistan is higher than over the Himalayas and Tibetan Plateau. Estimated LAP-induced daily mean snow albedo reduction is approximately 0.07-12.0% and corresponded radiative forcing is approximately 0.16-43.5 Wm-2, depending on snow type, solar zenith angle, and locations. Also different methods are used in this study to identify the source regions of pollutants measured in this region.

Overall the results are interesting and measurement data are valuable for the community. The figures and tables in the manuscript are relevant, but not very good in quality, and need to be improved. In general the paper is well written but in many places the English could and should be improved. There are some major weaknesses in the manuscript, especially in the source region identification part (3.5) and aerosol type frequency distribution part (3.2). After the below comments are appropriately addressed, I would suggest to accept the manuscript for publication in the Atmospheric Chemistry and Physics.

Response:

We thank the reviewer for their comments that significantly contributed to improving the original manuscript. Please see below our comment-by comment-responses to each of the reviewer's comments and suggestions.

Reviewer Comments in black

Responses in blue

Modified text in the revised manuscript is in green.

Technical comments:

Introduction, I would suggest use Light-absorbing particles (LAP) instead of Light absorbing impurities, see Qian et al., 2015, which by the way is a review article for both measurement methods and modeling activities. This article is so relevant so probably should be cited in Introduction part.

Response:

Light-absorbing particles (LAP) has been used instead of Light absorbing impurities (lines 14,48,82,89,151,292,418,420, and 453). We changed the title accordingly. The recommended article has been cited in the introduction (lines 83). The text has been quoted below for your reference.

"A number of authors have described the concentration and impacts of light absorbing particles in the Tibetan glaciers (for example Qian et al., 2015; Wang et al., 2015; Que et al., 2016; Zhang et al., 2017; Li et al., 2017; Niu et al., 2017)."

Lines 62-65, Besides warming efficiency, another important characteristic of LAPs is its higher snowmelt efficiency, see Qian et al., 2011.

Response:
An additional sentence related to warming has been added in the revised manuscript (lines 67-69).

"Besides warming efficiency, another important characteristic of BC is its higher snowmelt efficiency. The snowmelt efficacy induced by BC in snow is larger for snow cover fraction and snow water equivalent than induced by carbon dioxide increase (Qian et al., 2011)."

Lines 110, precipitation 0.412 +/- 2 mm for per day or per year?

Response:
The sentences have been modified (lines 117-119), given below for your reference.

"According to the 10 years record (1999–2008) of the two nearby climatic stations, the mean total annual precipitation was 170 mm at Khunjerab (36.83°N, 75.40°E, 4730 m) station, and 680 mm at Naltar (36.29°N, 74.12°E,2858 m) station,"

Lines 123-128, again sample method is summarized in Qian et al., 2015.

Response:
We have referred to Qian et al., 2015 in the methodology section (line 138).

"Qian et al., 2015 summarized sample methods for light absorbing particles in snow and ice from different region including Arctic, Tibetan Plateau and mid-latitude regions."

Section 2.3.1, without 2.3.2, really needs 2.3.1? More details are needed regarding how the L-2 data are processed.

Response:
As per reviewer suggestions, the title/ heading of section 2.3.1 has been deleted (line 162). This part (paragraph) describes the aerosol subtypes, and CALIPSO level 2 lidar data processing. We have also added details about L-2 data processing in the modified manuscript as quoted below (lines 163, 169-174).

"The CALIPSO models define aerosol subtypes, with 532-nm (1064 nm) extinction-to-backscatter ratio. The CALIPSO Level 2 lidar vertical feature mask data product describes the vertical and horizontal distribution of clouds and aerosol layers (downloaded from https://eosweb.larc.nasa.gov/project/calipso/aerosol_profile_table). On the basis of observed backscatter strength and depolarization, the aerosol subtypes have been pre classified in the downloaded data. The details of algorithm used for the classification have been presented in Omar et al., 2009. Percentage contribution of individual aerosol subtypes were plotted using Matlab."

The number of counts for a specific aerosol type in specific month were plotted as indicated in Figure 2 and Figure S4. According to our understanding, few authors in the past (including Cong et al., 2015; Ali H. Omar et al., 2009 and Wang et al., 2016) used the sub-type aerosol data.

Lines 155-159, This paragraph should be removed or moved to Introduction section.

Response:

The paragraph has been moved to introduction section with few modifications as suggested by the reviewer (lines 47-49 of modified manuscript). The whole sentence is given below for your reference.

"However, the exact amount of albedo reduction also depends on the refractive index, snow age, grain size, solar zenith angle (SZA), snow density, dust particle size and concentration, particle morphology, surface roughness, snow depth, liquid water content, snow shape and topography (Wiscombe and Warren 1985)."

Section 2.5 is very poorly organized and kind of just present whatever tools you have or used before, without a clear goal or coherence in science structure. Must be rewritten.

Response:

The section has been reorganized and edited by a native English speaking editor (lines 210-269). The modified section has been quoted below for your reference.

2.5 Source regions of pollutants

Three methods were used to identify the potential source regions of pollutants found at the study site: wind maps, emissions inventory coupled with back trajectories, and a region-tagged chemical transport modeling analysis.

Wind vector maps were prepared using MERRA-2 reanalysis data (available from the National Aeronautics and Space Administration [NASA] https://gmao.gsfc.nasa.gov/reanalysis/MERRA-2/docs/). The U and V wind components were combined into a matrix around the study area for each individual month and then plotted against latitude/longitude values to show the spatial variance of monthly wind stress at 850 mb using arrows to indicate the direction and intensity of wind.

Air trajectories were calculated backwards from the sampling sites (S1: 36.40°N 74.50°E; S6: 35.46°N 72.54°E) to identify potential source regions for the pollutants using the web version of the Hybrid Single Particle Lagrangian Integrated Trajectory (HYSPLIT-4) model (Draxler and Hess, 1998).

The HYSPLIT-4 model has been used by others to compute air mass trajectories to identify possible source regions (Ming et al., 2009; Zhang et al., 2013). Reanalysis meteorological data from the same source as the wind data (https://www.esrl.noaa.gov/psd/data) were used as input data in the HYSPLIT model for May, June, and December 2015, and January 2016. HYSPLIT was run in a seven-day backward trajectory mode with trajectories initiating every six hours (0, 6, 12, and 18) on a daily basis from 4 May to 19 June 2015 (77 days during summer) and from 1 December 2015 to 31 January 2016 (62 during winter). The HYSPLIT model results were combined with Representative Concentration Pathways (RCPs) emission data for 2010 (available from http://sedac.ipcc-data.org/ddc/ar5_scenario_process/RCPs.html) to identify the source location. The data file used as a RCP emission inventory was "RCPs_anthro_BC_2005-2100_95371.nc". This comprises emission pathways starting from identical base year (2000) for multiple pollutants including black carbon and organic carbon. According to the description of the file, biomass burning sources were included in the RCP emission inventory that were utilized with the back-trajectory analysis. RCP had the same emissions sectors as for Hemispheric Transport Air Pollution (HTAP) emission inventory used in the molding part. The emission sectors include fuel combustion, industries, agriculture and livestock. The difference in HTAP and RCP inventories is the resolution. HTAP had relatively high resolution (0.1 x 0.1 degree) as compared to RCP (0.5 x 0.5 degree). Some discussion related to the inventory and the sectorial detail (12 sectors), which was used for the base year calibration of the RCPs is given in Lamarque et al., 2010. Monthly CALIPSO satellite based extinction data from 2006 to 2014 were used to calculate the vertical profile for aerosol extinction over the study region. The CALIPSO extinction profile was constructed for selected months – May and June for summer and December and January for winter – in 2006 to 2014 (Figure S1). The exponential equation $X = (\log(10.46) - \log(Y))/10.29$ was used to calculate the extinction profile for the trajectory heights, where Y is the vertical height in kilometers and X indicates the extinction against the height of trajectories. Height of individual trajectory points was put in the above equation and got a normalized extinction profile by assuming surface extinction =1(Figure S1).

The WRF-STEM model was used as a third approach for identifying the origin (source regions) of air masses carrying pollutants. Region tagged CO tracer is a standard air quality modeling tool used by other regional and global chemical transport models to identify pollution source regions (Chen et al., 2009; Park et al., 2009; Lamarque and Hess, 2003). The WRF-STEM model uses region tagged carbon monoxide (CO) tracers for many regions in the world to identify geographical areas contributing to observed pollutants (Adhikary et al., 2010). The model domain centered on 50.377° E longitude and 29.917° N latitude. The model horizontal grid resolution was 45x45 km with 200 grids in the east-west direction and 125 north-south. The meteorological variables needed for the chemical transport were derived from the Weather Research and Forecast (WRF) meteorological model (Grell et al., 2005) using FNL data (ds083.2) available from the UCAR website as input data. The main aim of the simulation was to identify the geographic locations contributing to the observed pollutants at the field sites. The HTAP version 2 emission inventory was used in our WRF-STEM modeling. The HTAP version 2 dataset consists of multiple pollutants including black carbon and organic carbon. This emission inventory include major sectors such as energy, industry, transport, residential except large scale open agricultural and open forest fire burning. The simulations applied in our study used the anthropogenic emissions from HTAPv2 inventory (available from http://edgar.jrc.ec.europa.eu/htap_v2/). So the results indicate the amount of pollutants reaching the study area from day-to-day planned and recurring activities in domestic, transport, industrial, and other sectors.

2.5.1 Wind maps, why not use 2005-2006 wind maps instead of 50-year average? 700mb is very high level for low-elevation region and aerosol concentration is very low at that high level. I would suggest use the terrain-oriented level like sigma level near the surface. I would also strongly suggest (a must do) use MERRA-2 reanalysis data, in which not only the data quality is better than NCEP/NCAR but also it includes aerosol data that can be used to compare with the measurement and is more appropriate for looking at the long-distance transport. Suggestion

Response:

Our sampling time period was 2015-2016 so we believe the reviewer wanted us to plot wind maps for 2015-2016.

As per your suggestions, we have used the MERRA-2 reanalysis data at 850mb and replotted the wind maps, during the selected months of 2015-2016 as shown for your reference below. The same figure has been used in the revised manuscript.

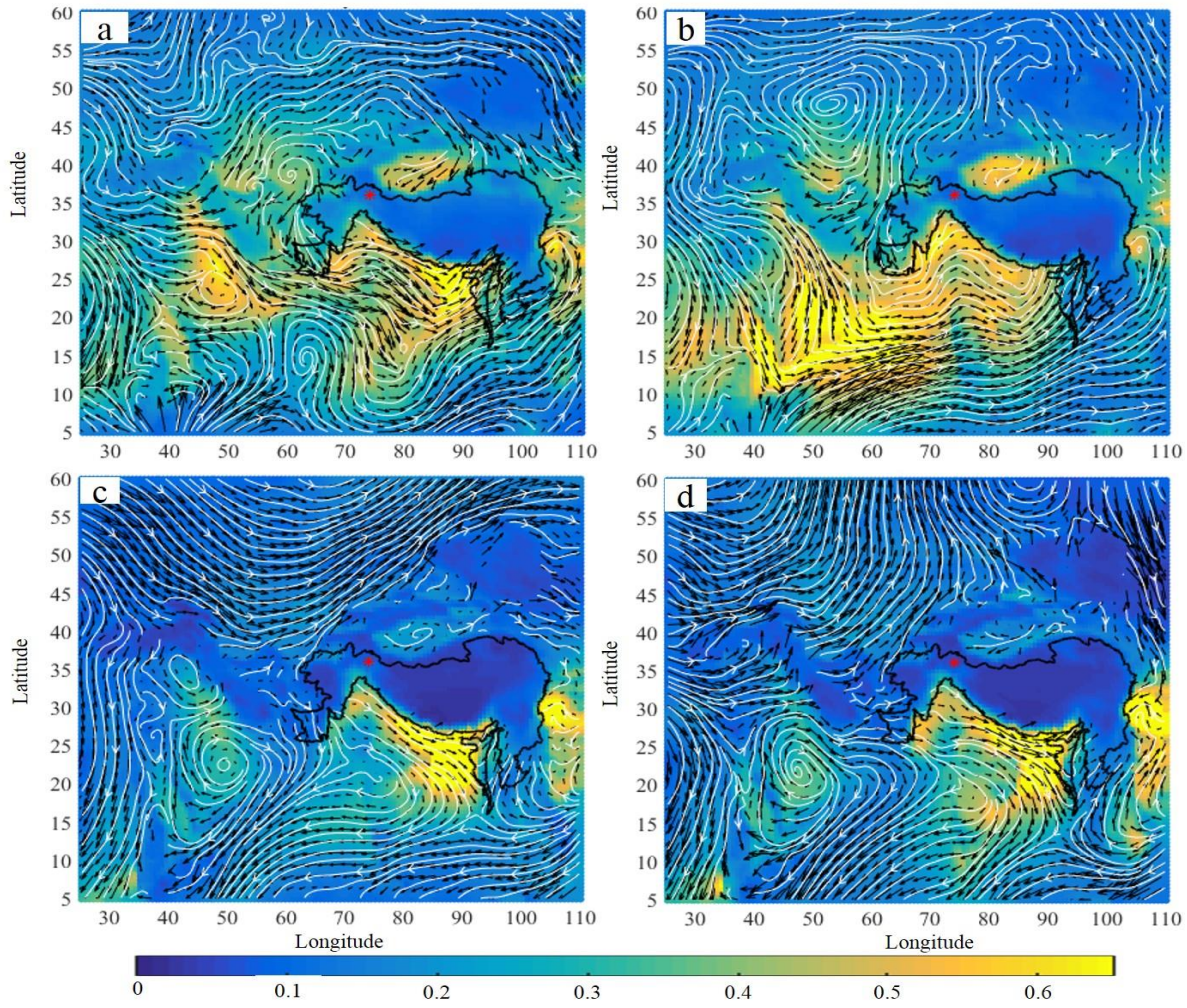

Figure 5. Monthly average horizontal wind patterns at 850 hPa during a) May, b) June, c) December, and d) January, corresponding to approximately 2500 masl, from GES DISC. The study area is indicated by a star, and white lines indicating streamlines. The background colors show monthly mean aerosol optical depth.

2.5.3,

a. **WRF-STEM can only tag CO, because of many differences between CO and LAP in such as emission sources, chemistry and removal, how to quantify their differences in long-range transport and source identifications?**
b. **How to infer the transport and source for LAPs based on CO and what's the uncertainty?**
Please see Zhang et al. 2015 and Wang et al., 2015 for source detection methods used over Tibetan Plateau region.

Response:

a. We agree with the reviewer comment, however for the time being we have CO tracer data (which has relatively good correlation with BC tracer in dry seasons) and high resolution BC tracer will be used in our next publication in near future (indicated in lines 587 and 677-680).

- BC and CO both are primary pollutants and emit from almost similar anthropogenic sources (may be different in concentration). We were more precise on the source region identification of these pollutants.
- Region tagged CO tracer is a standard air quality modeling tool used by other regional and global chemical transport models to identify pollution source regions (Chen et al., 2009; Park et al., 2009; Lamarque and Hess, 2003) lines 249-251. The WRF-STEM model uses region tagged carbon monoxide (CO) tracers for many regions in the world to identify geographical areas contributing to observed pollutants (Adhikary et al., 2010), lines 252.
- Each model has some strength and some weaknesses. The strength of our applied model is its relatively higher spatial resolution (line 253). For rough and complex topography of mountain region, it is important to use high resolution model.

b. Transport, source of LAPs based on CO and uncertainty

Source

- Depending on event, the source of LAPs (BC) and CO may be different, but in several cases the source of BC and CO might be same such as biomass burning (cooking, outdoor burning, and forest fires) and incomplete combustion process.
- During incomplete combustion of carbon-containing fuels, such as gasoline, natural gas, oil, coal, and wood, emits CO as well as BC.

Transport

- Based on chemical reactivity, the weight of the particle and its life time in the atmosphere, the transport of BC and CO may be different.
  During dry seasons, CO and BC have quite similar transport but in wet seasons (especially during monsoon seasons) BC particles are washed out with precipitation and relatively higher concentrations of CO are reaching receptor sites as compared to BC. Below quoted text has been added in the revised manuscript (lines 674-675).

  "In our case we analyze the model from 1st June to 4th July during summer season and 15th December to 17th January during winter season. In Pakistan monsoon is

generally starting during the first week of July each year, so we are expecting relatively good correlation in transport between CO and BC during pre-monsoon period. A cool, dry winter starts from December through February each year."

Uncertainty

Related uncertainty is mentioned in lines 671-680, given below for your reference.

"On modeling side the possible uncertainties are related to using CO as a tracer for light absorbing particles source region. Uncertainties are also attributed to errors in emissions inventories, simulated meteorology and removal processes built in the model. The physics and chemistry of removal for BC and CO are different from each other especially during wet seasons. We analyze the model during pre-monsoon and relatively dry periods, so we are expecting relatively good correlation in transport between CO and BC. While using global emission inventories we were unable to capture emissions at local scale. Contributions of local sources may be underestimated by coarse-resolution models. Therefore high resolution models and emission inventories at local scale are required to capture local emissions. Better-constrained measurements are required in the future for more robust results. High resolution satellite imagery, high resolution models and continuous monitoring can help us to reduce the present uncertainty."

Zhang et al. 2015 and Wang et al., 2015 are presenting impressive work for source detection methods in the Tibetan Plateau region. We have cited these papers in the proper locations.

We agreed with the reviewer comment and using high resolution BC tracer WRF-STEM model in our next publication.

Line 257, 24 hours. Considering–>considered.

Response:

Corrected (line 301, in the revised manuscript)

Line 318, Jun–>June.

Response:

Corrected (line 384, in the revised manuscript)

Section 3.2, very weak! How to connect the conclusion from this section with other parts?

Response:

We have rewritten and improved the section according to the suggestions. Repeated sentences have been removed. Some additional text has been added to improve the connection of conclusions from this section to other parts of the paper, lines 379-390.

"The CALIPSO aerosol type identifications analysis indicated that "smoke" was the most frequent-occurring type of aerosol over the study region during both summer and winter seasons. This result indicate that biomass burning sources may be the dominant contributor in this region. Frequency of

subtype aerosols for the month of June in 2006 to 2014 is shown in Figure S4. Figure 2 shows the seasonal results for month of May, June (summer) and December, January (winter) in the form of a box plot. During June smoke had the highest frequency (39%), followed by dust (21%), polluted dust (12%), and others (20%) Figure S4. Overall Smoke, dust and or polluted dust were the dominant subtype aerosols in selected months over the study region. This type of aerosol measurement in the atmosphere is important for our current study because it provides observation based data over the study region. Other approaches used (such as modeling) were based on interpolation not observation. Pollutant deposition depends on the concentration of pollutants in the atmosphere, the results are consistent with the high concentration of BC (from smoke) and dust particles in the glacier and snow surface samples."

Section 4 Summary and conclusion, one more section should be added for discussion in uncertainty and possible future direction for both modeling and measurement campaign. For example, how snow aging (snow grain size) and melting water scavenging efficiency (see Qian et al, 2014) affect the conclusions?

Response:

Agreed. We have added one more section for discussion on uncertainty and possible future directions in section 4, lines 660-671, given below for your reference.

"The overall precision in the BC, OC and TC concentrations was estimated considering the analytical precision of concentration measurements and mass contributions from field blanks. Uncertainty of the BC and OC mass concentrations was measured through the standard deviation of the field blanks, experimentally determined analytical uncertainty, and projected uncertainty associated with filter extraction. According to our understanding the major uncertainty in our study was the dust effect on BC/OC measurement. Warming role of OC was also not included in the current research which was low but significant in several regions (Yasunari et al. 2015). Beside this we think snow grain size (snow aging) and snow texture were larger sources of uncertainty in the albedo reduction / radiative forcing calculations. The measured grain size was usually different from the effective optical grain size used in the SNICAR modeling. Snow grain shape was measured with the help of snow card, but was not used in the online SNICAR albedo simulation model and assumed a spherical shape for the snow grains which may slightly affect the results, because albedo of non-spherical grain is higher than the albedo of spherical grains (Dang et al., 2016). On modeling side the possible uncertainties are related to using CO as a tracer for light absorbing particles source region. Uncertainties are also attributed to errors in emissions inventories, simulated meteorology and removal processes built in the model. The physics and chemistry of removal for BC and CO are different from each other especially during wet seasons. In order to reduce uncertainty in source region high resolution BC tracer are required. Better-constrained measurements are required in the future for more robust results. High resolution satellite imagery, high resolution models and continuous monitoring can help us to reduce the present uncertainty."

Figure 2, this is a poor figure and should be re-designed. For example, reduce the y-axis range from 300 to 150. Btw why the numbers for y-axis are 50, 100, 150, 200, 150 (should be 250?)?

Response:
Figure has been re-designed as suggested.
Revised figure 2 is given below for your reference:

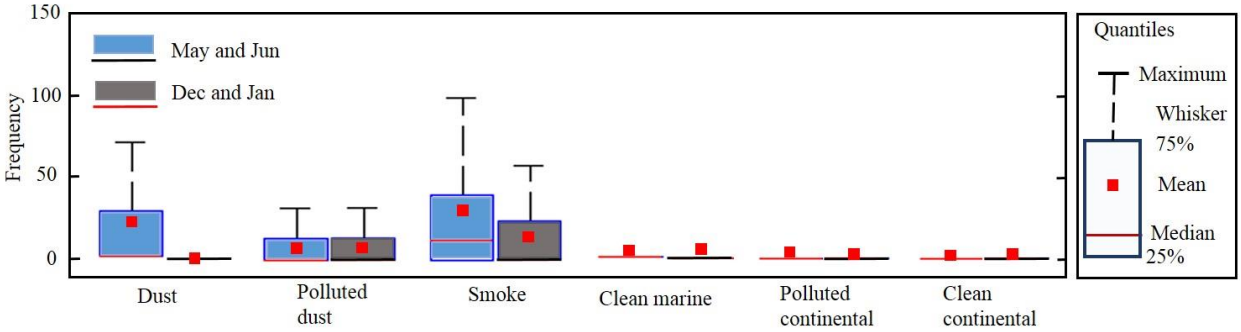

Figure 2. Frequency distribution of aerosol subtypes in the atmosphere over the study region calculated from CALIPSO data for the months in 2006 to 2014.

Figure 3, give full name for MAC in figure caption. Also consider use identical range for y-axis e.g. 0.4-1.0 and for x-axis 0.3-1.2 for Panel c and d.

Response:
Figure 3 has been re-designed as suggested. Full name for MAC has been used, identical range for y-axis e.g. 0.4-1.0 and for x-axis 0.3-1.2 for Panel c and d has been used. Quality of the figure has been improved.

Revised Figure 3 is given below for your reference:

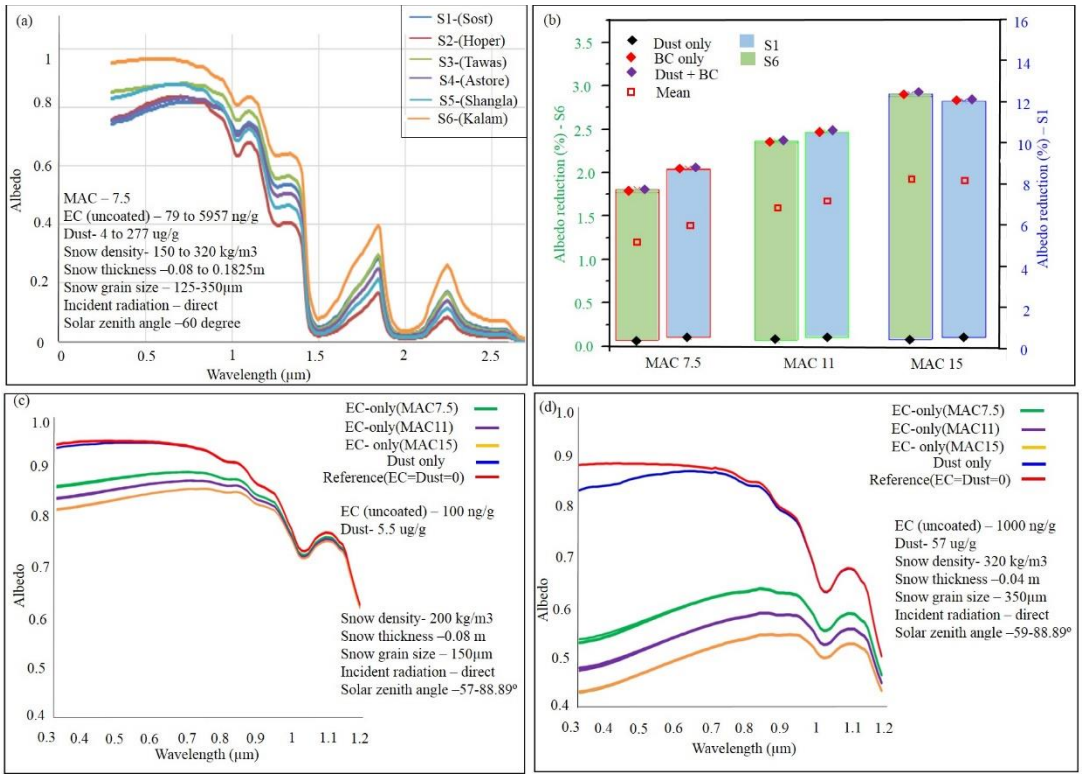

Figure 3. Spectral variation in albedo for winter sampling sites and selected Mass Absorption Cross section (MAC) values, (a) average albedo of samples at each of the sites (b) daily mean albedo reduction of fresh snow (site S6) and aged snow (site S1) snow, (note different scales of y axis) (c) albedo of fresh snow site S6, (d) albedo of aged snow site S1.

Figure 4,

a) **Suggest use identical y-axis range so can highlight the bigger effect over aged snow. The unit for radiative forcing is %?**
b) **More discussion should be provided regarding how snow aging affect the albedo reduction and radiative forcing (e.g. Qian et al., 2014)?**

Response:

a. Agreed. An identical y-axis range has been used. Radiative forcing mentioned here was calculated from albedo reductions indicated on left side of the figure. % symbol has been used in the caption of this figure. Revised Figure 4 is given below for your reference:

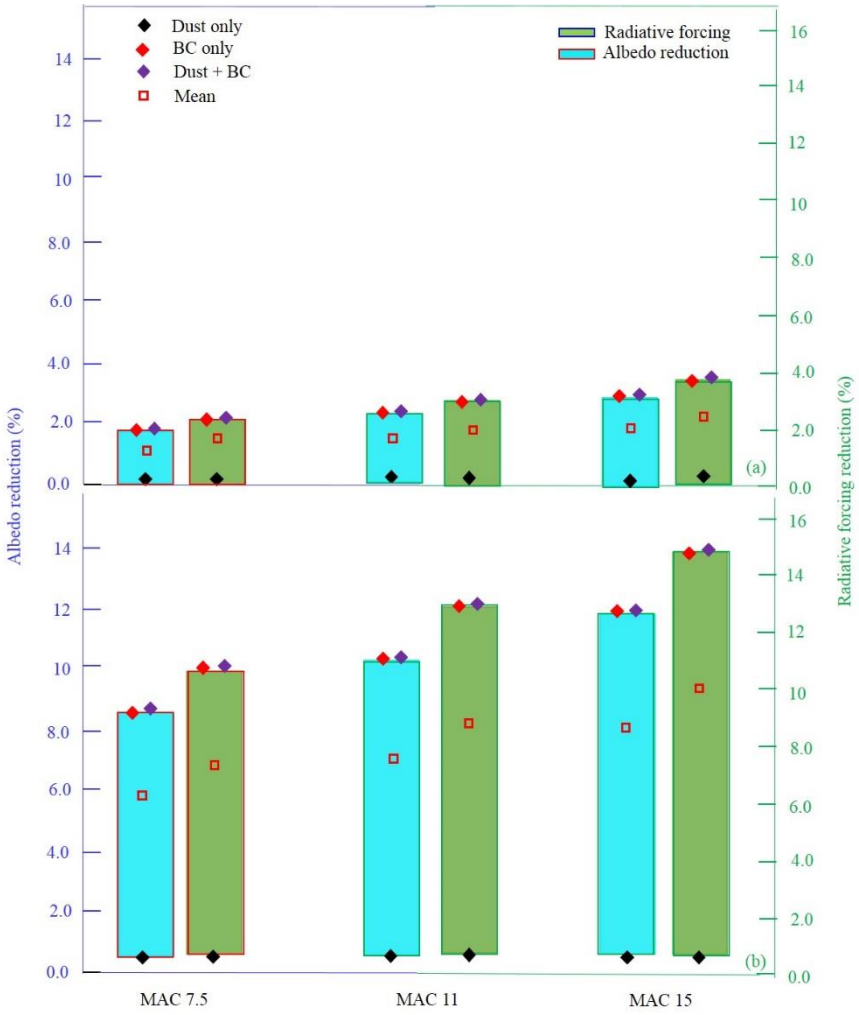

Figure 4. Daily mean radiative forcing reuction and albedo reduction caused by black carbon and dust, for different Mass Absorption Cross section (MAC) in (a) fresh (low black carbon) and (b) aged (high black carbon) snow samples (note different scales of y axis)

b. Agreed. More text has been added regarding how snow aging affects the albedo reduction and radiative forcing (line 505-510), given below for your reference

"Snow aging (snow grain size) plays an important role in albedo reduction and radiative forcing. Schmale et al., (2017) stating that the effect of snow grain size is generally larger than the uncertainty in light absorbing particles which varies with the snow type. The impact of snow aging factor on BC in snow and induced forcing are complex and had spatial and seasonal variation (Qian et al., 2014). Increase of snow aging factor reduces snow albedo and accelerate the snow melting."

Figure 5, what blue contours represent? Again 700 mb is too high and MERRA-2 is a much better dataset.

Response:

The blue lines in previous Figure 5 were indicating streamlines. We used 850 mb in the revised figure by using MERRA-2 reanalysis data, as suggested. Revised figure given below for your reference.

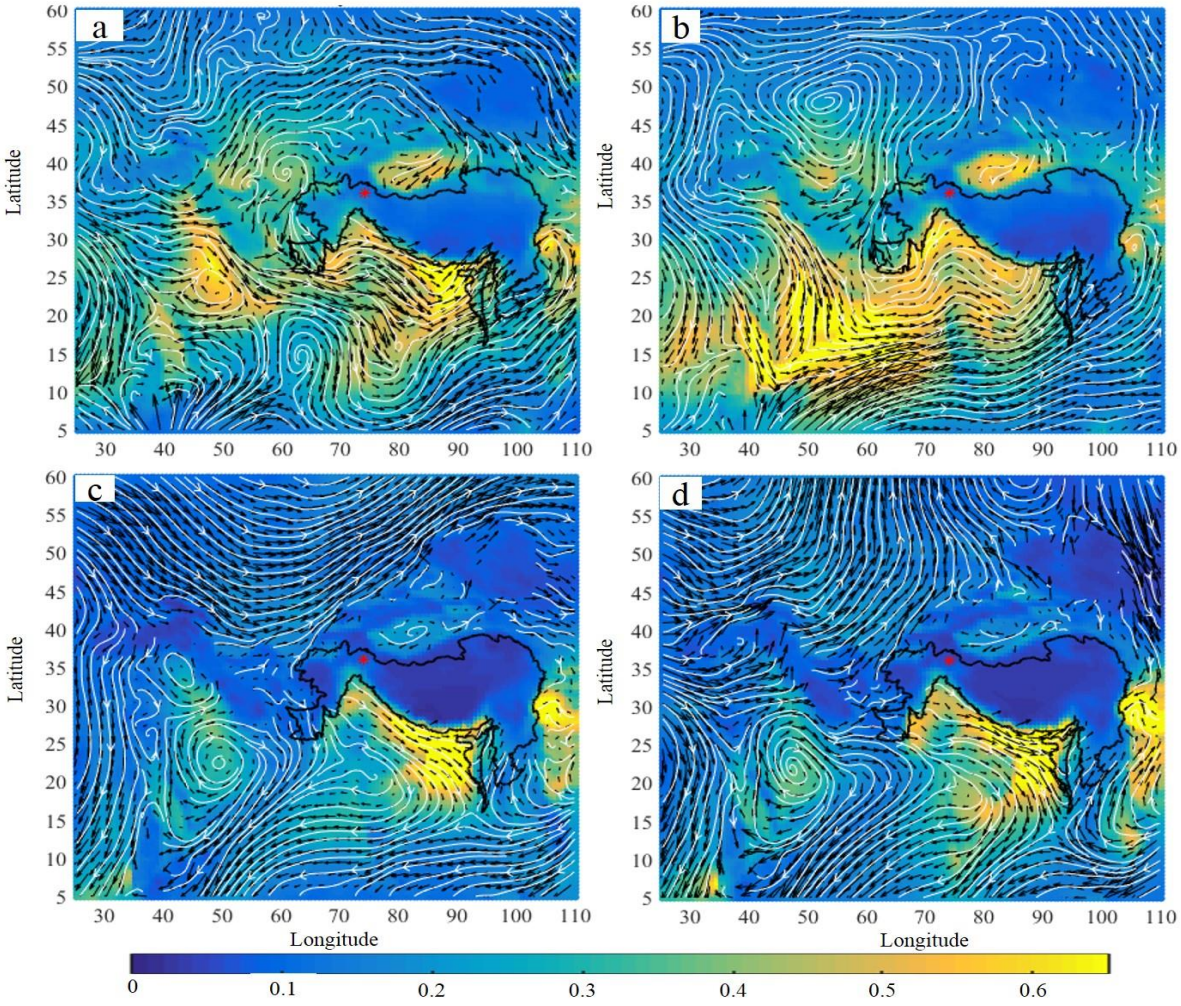

Figure 5. Monthly average horizontal wind patterns at 850 hPa during a) May, b) June, c) December, and d) January, corresponding to approximately 2500 masl, from GES DISC. The study area is indicated by a star, and white lines indicating streamlines. The background colors show monthly mean aerosol optical depth.

Figure 6, not clear what color shades represent?

Response:

Agreed. The confusing color shades have been removed. We modified the figure (line 933), as given below for your reference.

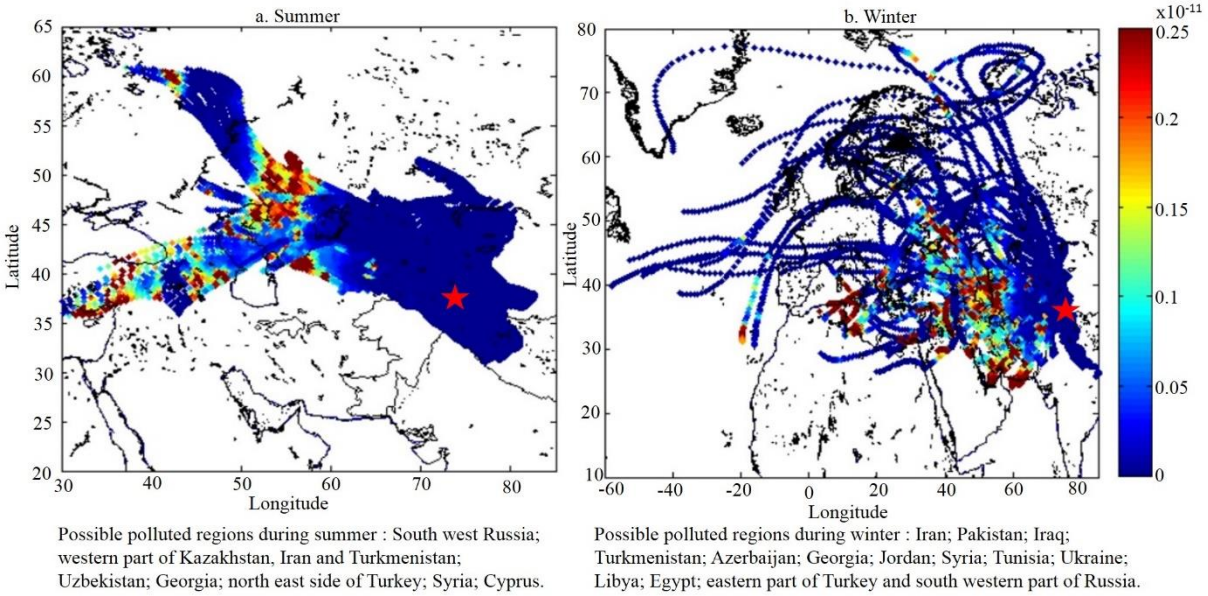

Figure 7,

(a) I am not sure how the quantitative number of contributions are meaningful because the numbers for LAP could be very different with that for CO.

(b) Anyway again, Section 2.5 is very poorly organized and kind of just present whatever tools you have or used before, without a clear goal or coherence in science structure. Need to be rewritten with a clear conclusion.

Response:

(a) Yes, we agreed that the numbers used in the Figure 7 could be different than that for LAP, especially during wet seasons. Based on following justifications, we are expecting relatively less difference between the numbers for LAP and CO.

- We analyze the model from 1 June to 4 July during the summer season. In Pakistan, monsoon generally starts during the first week of July each year, so we are expecting relatively good correlation in transport between CO and BC during the pre-monsoon period.
- During winter we analyze the model from 15 December to 17 January. A cool, dry winter starts from December through February each year. Winter season is dry but clouds during this season may bring some uncertainty in our results.

We mentioned this uncertainty in multiple places in the revised manuscript, including lines 672-680. High resolution WRF-STEM BC tagged will be used in our next publication.

(b) We have reorganized the section 2.5 and made multiple changes. We tried our best to mention a clear goal in this section with a clear conclusion, lines 205-269.

Table 2, give full name for MAC (in other tables/ figures as well).

Response:
Agreed. We used the full name for MAC at all necessary locations, such as lines 48, 58, 61 in supplementary document, and line 917 (caption of Figure 3) in the main manuscript.

Figure S7, give full names for BC1 and BC2.

Response:
Agreed. Full names for BC1 and BC2 has been used, given below for your reference

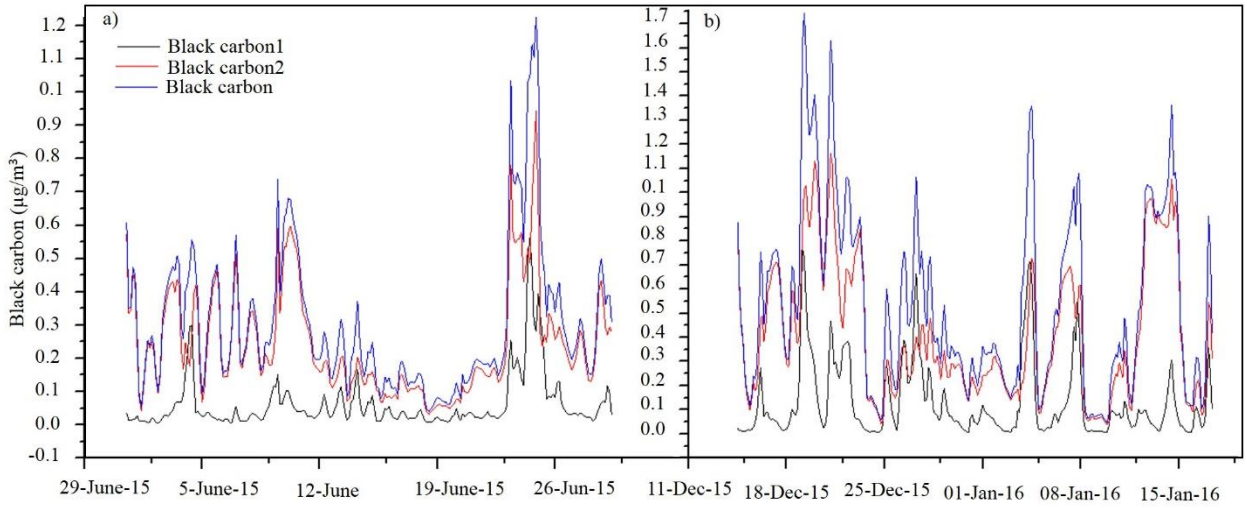

Figure S7. Concentration of black carbon1, black carbon2 and black carbon on the Sachin glacier calculated using the WRF-STEM model: a) summer, b) winter.

Suggested references

Qian et. al, 2015.
Zhang et. al, 2015.
Qian et. al, 2014.
Wang et. al, 2015.
Qian et. al, 2011.

Response:
We thank this anonymous reviewer for his careful and detailed reviews and suggestions that helped us to greatly improve this paper. Beside this the provided references/articles are very relevant and presenting a quality work in the region. So we used/cited properly these articles in the revised manuscript. We feel a big improvement in the text after revising and citing these articles.

References:

Chen, D., Wang, Y., Mcelroy, M. B., He, K., Yantosca, R. M. and Sager, P. Le: and Physics Regional CO pollution and export in China simulated by the high-resolution nested-grid GEOS-Chem model, , (2008), 3825–3839, 2009.

Cong, Z., Kawamura, K., Kang, S., Fu, P., River, G., River, Y. and River, Y.: Penetration of biomass-burning emissions from South Asia through the Himalayas : new insights from, , 1–7, doi:10.1038/srep09580, 2015.

Dang, C., et al. (2016), Effect of Snow Grain Shape on Snow Albedo. J. Atmos. Sci., 73, 3573–3583, doi:10.1175/JAS-D-15-0276.1
Ducret, J. and Cachier, H.: Particulate carbon content in rain at various temperate and tropical locations, J. Atmos. Chem., 15, 55–67, 1992.
Flanner, M. G., et al. (2012), Enhanced solar energy absorption by internally-mixed black carbon in snow grains, Atmos. Chem. Phys., 12, 4699-4721, doi:10.5194/acp- 12-4699-2012.
He, C., et al. (2014), Black carbon radiative forcing over the Tibetan Plateau, Geophys. Res. Lett., 41, 7806–7813, doi:10.1002/2014GL062191.
He, C., et al. (2017): Impact of Snow Grain Shape and Black Carbon-Snow Internal Mixing on Snow Optical Properties: Parameterizations for Climate Models. J. Climate, 0, doi:10.1175/JCLI-D-17-0300.1
LaChapelle, E. R., 1969: Field Guide to Snow Crystals. University of Washington Press, 112 pp.
Liou, K. N., et al. (2014), Stochastic parameterization for light absorption by internally mixed BC/dust in snow grains for application to climate models, J. Geophys. Res. Atmos., 119, doi:10.1002/2014JD021665.
Qian Y, TJ Yasunari, SJ Doherty, MG Flanner, WK Lau, J Ming, H Wang, M Wang, SG Warren, and R Zhang. 2015. "Light-absorbing Particles in Snow and Ice: Measurement and Modeling of Climatic and Hydrological Impact." Advances in Atmospheric Sciences 32(1):64-91. doi:10.1007/s00376-014-0010-0.
Qian Y, H Wang, R Zhang, MG Flanner, and PJ Rasch. 2014. "A Sensitivity Study on Modeling Black Carbon in Snow and its Radiative Forcing over the Arctic and Northern China." Environmental Research Letters 9(6):Article No. 064001. doi:10.1088/1748-9326/9/6/064001.
Qian Y, MG Flanner, LYR Leung, and W Wang. 2011. "Sensitivity studies on the impacts of Tibetan Plateau snowpack pollution on the Asian hydrological cycle and monsoon climate." Atmospheric Chemistry and Physics 11(5):1929-1948. doi:10.5194/acp-11-1929-2011
Qian Y, H Wang, R Zhang, MG Flanner, and PJ Rasch. 2014. "A Sensitivity Study on Modeling Black Carbon in Snow and its Radiative Forcing over the Arctic and Northern China." Environmental Research Letters 9(6):Article No. 064001. doi:10.1088/1748-9326/9/6/064001.
Shindell, D. T., Chin, M., Dentener, F.: A multi-model assessment of pollution transport to the Arctic, Atmos. Chem. Phys., 8, 5353–5372, 2008, http://www.atmos-chem-phys.net/8/5353/2008/.
Schmale, J., Flanner, M., Kang, S., Sprenger, M., Zhang, Q., Guo, J., Li, Y., Schwikowski, M. and Farinotti, D.: Modulation of snow reflectance and snowmelt from Central Asian glaciers by anthropogenic black carbon, Sci. Rep., 7(October 2016), 40501, doi:10.1038/srep40501, 2017.
Schmale, J., Flanner, M., Kang, S., Sprenger, M., Zhang, Q., Guo, J., Li, Y., Schwikowski, M. and Farinotti, D.: Modulation of snow reflectance and snowmelt from Central Asian glaciers by anthropogenic black carbon, Sci. Rep., 7(October 2016), 40501, doi:10.1038/srep40501, 2017.
Wang M, B Xu, J Cao, X Tie, H Wang, R Zhang, Y Qian, PJ Rasch, S Zhao, G Wu, H Zhao, DR Joswiak, J Li, and Y Xie. 2015. "Carbonaceous Aerosols Recorded in a Southeastern Tibetan Glacier: Analysis of Temporal Variations and Model Estimates of Sources and Radiative Forcing." Atmospheric Chemistry and Physics 15:1191-1204. doi:10.5194/acp-15-1191-2015.
Wang M, B Xu, J Cao, X Tie, H Wang, R Zhang, Y Qian, PJ Rasch, S Zhao, G Wu, H Zhao, DR Joswiak, J Li, and Y Xie. 2015. "Carbonaceous Aerosols Recorded in a Southeastern Tibetan Glacier: Analysis of Temporal Variations and Model Estimates of Sources and Radiative Forcing." Atmospheric Chemistry and Physics 15:1191-1204. doi:10.5194/acp-15-1191-2015.
Wang, Mo, et al. "Two distinct patterns of seasonal variation of airborne black carbon over Tibetan Plateau." Science of the Total Environment 573 (2016): 1041-1052.
Yasunari, T. J., Lau, K.-M., Mahanama, S. P. P., Colarco, P. R., Silva, A. M. Da, Aoki, T., Aoki, K., Murao, N., Yamagata, S. and Kodama, Y.: The GOddard SnoW Impurity Module (GOSWIM) for the NASA GEOS-5 Earth System Model: Preliminary Comparisons with Observations in Sapporo, Japan, Sola, 10(MAY), 50–56, doi:10.2151/sola.2014-011, 2014.
Zhang R, H Wang, Y Qian, PJ Rasch, RC Easter, Jr, PL Ma, B Singh, J Huang, and Q Fu. 2015. "Quantifying sources, transport, deposition, and radiative forcing of black carbon over the Himalayas and Tibetan Plateau." Atmospheric Chemistry and Physics 15(11):6205-6223. doi:10.5194/acp-15-6205-2015.

Thank you

Interactive comment on "Concentrations and source regions of light absorbing particles in snow/ice in northern Pakistan and their impact on snow albedo"

by Chaman Gul. C et al.

Anonymous Referee# 2

Major issues:

This study is valuable because it describes measurements of black carbon in snow from the Karakoram/Himalayan region of Pakistan. To my knowledge these are the first such measurements to be reported from this region. Moreover, the reported concentrations of BC in snow are extremely large, indicative of pollution being a major source of snow/ice albedo reduction in this area. The study is also comprehensive in the sense that it applies CALIPSO observations of aerosol type, back-trajectory analysis, and regional chemistry/climate modeling to ascertain dominant sources of pollution to the snow and glaciers in the study area. Despite the value of having new measurements from the Karakoram, a region with a paucity of environmental data, the study has some weaknesses that are described below. Ultimately, I believe these issues lead to conclusions which are somewhat vague. I suppose the main take-home message, however, is that there is a lot of BC in low elevation glaciers and snow of northern Pakistan, and perhaps this is a sufficient conclusion in and of itself for publication. Below, however, are the major issues I see with the current draft of the paper.

Response:

We thank the reviewer for their comments that significantly contributed to improving the original manuscript. Please see below our comment-by comment-responses to each of the reviewer's comments and suggestions.

Reviewer Comments in black

Responses in blue

Modified text in the revised manuscript is in green.

1. **(1a) The CALIPSO aerosol source identification analysis indicates that "smoke" is the most frequently-occurring type of aerosol over this region during both summer and winter. As the authors acknowledge, however, biomass burning sources were not included in the WRF-STEM modeling, and thus the dominant source regions identified through the WRF modeling may not be representative at all for the BC that was measured.**

   (1b)Moreover, were biomass burning sources included in the RCP emission inventory that was utilized with the back-trajectory analysis? (Please include more information about the RCP emissions that were used.)

(1c)A third question related to the source attribution analysis is: Potentially how important are local (e.g., within _10km) sources occurring within the same "grid cell" of the WRF and HYSPLIT models? Contributions of such local (sub-grid scale) sources may be severely underestimated by coarse-resolution models. Some of the discussion suggests that local sources may have been very important, but these sources did not really enter into the assessment (via HYSPLIT and WRF) of source attribution.

Response:

(1a). Major part from biomass burning sources (biofuel) were included in the WRF-STEM modeling, and we think the dominant source regions identified through the WRF modeling should represent majority of the BC (pollutants) regions that was measured. Apologies for not mentioning these important information in our initially submitted manuscript.

The sentence related to biomass burning has been modified in the revised manuscript (lines 260-266), given below for your reference.

"The Hemispheric Transport Air Pollution (HTAP version 2) emission inventory was used in our WRF-STEM modeling. The HTAP version 2 dataset consists of multiple pollutants including black carbon and organic carbon. All type of biomass burning (such as energy, industry, transport, residential etc...) are included in HTAP emission inventory (except large scale open agricultural and open forest fire burning). The simulations applied in our study used the anthropogenic emissions from HTAPv2 inventory (available from http://edgar.jrc.ec.europa.eu/htap_v2/). So the results indicate the amount of pollutants reaching the study area from day-to-day planned and recurring activities in domestic, transport, industrial, and other sectors."

(1b) Yes biomass burning sources were included in the RCP emission inventory that was utilized with the back-trajectory analysis. Related information about the used RCP emissions has been added in the revised manuscript (line 230-239), quoted below for your reference.

"The data file used as a RCP emission inventory was "RCPs_anthro_BC_2005-2100_95371.nc". This comprises emissions pathways starting from identical base year (2000) for multiple pollutants including black carbon and organic carbon. According to the description of the file, biomass burning sources were included in the RCP emission inventory that were utilized with the back-trajectory analysis. RCP had the same emissions sectors as for HTAP emission inventory used in the molding part. The emission sectors includes fuel combustion, industries, agriculture and livestock. The difference in HTAP and RCP emission inventories is the resolution. HTAP had relatively high resolution (0.1 x 0.1 degree) as compared to RCP (0.5 x 0.5 degree). Some discussion related to the inventory and the sectorial detail (12 sectors), which was used for the base year calibration of the RCPs is given in Lamarque et al., 2010."

(1c) Local sources and local emissions may have importance, but based on available options it was hard to capture. We are expecting minor impact of local emissions due to below reasons.

- There were limited transport on Karakorum highway and sparse residential houses in surrounding region (within_10km), near the glaciers.
- The glaciers in the surrounding region had relatively high altitude and away from main urban emission sources and urban areas.

There may be the slight effect of local transport, house cooking but we were unable to capture that local scale emissions. The chemical transport model (WRF-STEM) and RCPs were based on emission inventories and does not capture/does not collect the local emissions. In order to reduce uncertainty in source region high resolution BC tracer will be used in our next publication in near future.

Source contribution regions of pollutants identified using an emissions inventory (Representative Concentration Pathways) are shown in Figure 1 below. Lower part of the figure indicating local/regional source regions within 221Km x 276 Km region. As the resolution of RCP emission data is 0.5 x 0.5 degree so there is no change within 55 x 55 km^2 area. Using global emission inventories we are unable to capture emissions at local scale (within 10 km region). High resolution models and emission inventories at local scale are required to capture local emissions. Below text has been added in lines 675-678.

"While using global emission inventories we were unable to capture emissions at local scale. Contributions of local sources may be underestimated by coarse-resolution models. Therefore high resolution models and emission inventories at local scale are required to capture local emissions."

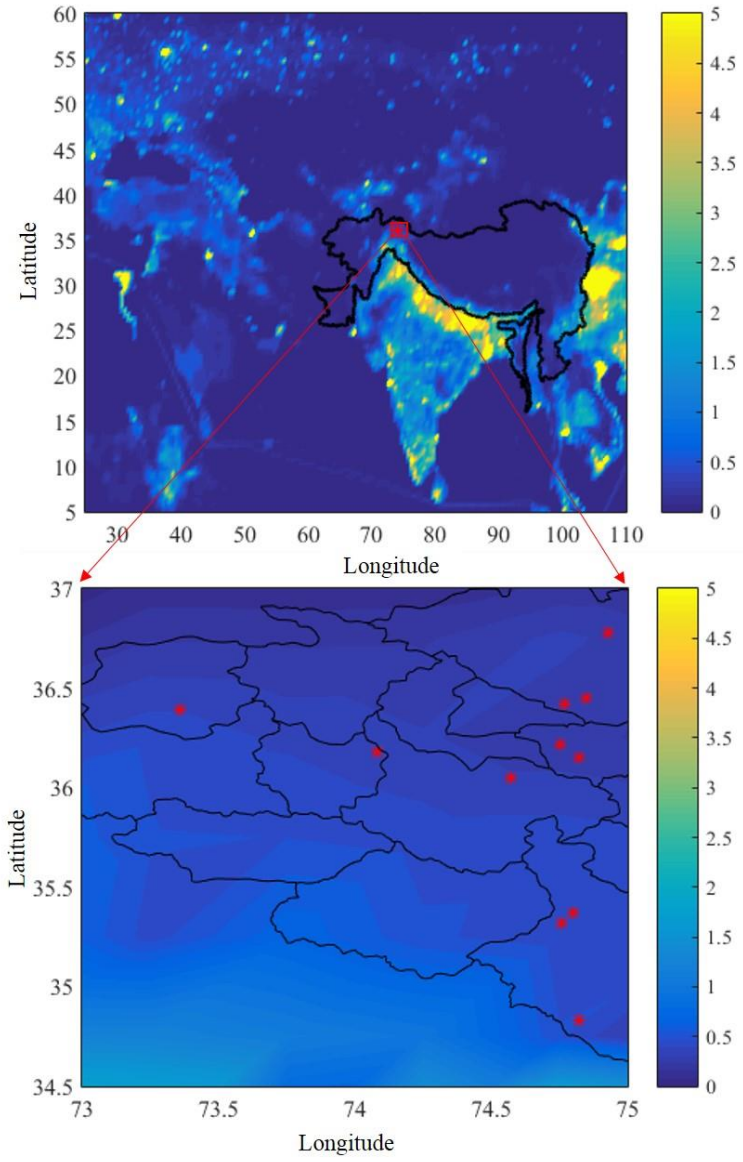

Figure1: Source contribution regions of pollutants identified using an emissions inventory (Representative Concentration Pathways). Red stars indicating sampling locations.

2. **(a) The values of BC in snow that were found are extremely large, but it is also acknowledged in the paper that the measurements were taken close to sources of pollution, namely roadways and villages.**
   (b) I am left wondering how representative the reported snow pollution values are of the broader Karakoram cryospheric region. The answer to this may not be known, but some discussion, even if speculative, about this issue would be appreciated. Do these measurements suggest that the glaciers of the Karakoram, in general, are being substantially darkened by BC, or do they simply mean that the ablation zones of a few glaciers near to obvious BC sources are quite polluted?

Response: (a) High concentration of BC in snow and ice:

The value of BC in snow and ice that was found relatively high and we justified it in our manuscript as given below for your reference.

- Sampling locations were relatively at lower elevation as compared to other studies in the past (lines 446-447). Li et al. (2017) showed a strong negative relationship between the elevation of glacier sampling locations and the concentration of light absorbing particles (lines 365-366).
- Majority of samples were from the ablation zone of the glaciers. Strong melting of surface snow and ice in the glacier ablation zone could also lead BC enrichment which causes high BC concentrations as Li et al., 2017 observed in the Southern Tibetan Plateau glacier (lines 447-448).
- In most cases snow and ice samples were collected quite a long time after snow fall, and the concentration of pollutants would also have increased in the surface snow and ice due to dry deposition (lines 352-353).
- In the past almost similar high concentration were reported by multiple authors in the region such as Xu et al. 2012 in the Tien Shan Mountains, Li et al. 2016 in the northeast of the Tibetan plateau, Wang et al. 2016 in northern China, Zhang et al., 2016 in southeastern Tibetan plateau and Zhang et al. 2017 in western Tien Shan, Central Asia (lines 341-343).

(b) Glaciers of the Karakoram, in general, are being substantially darkened by BC?

According to our understanding all the glaciers of the whole Karakoram region, may not besubstantially darkened by BC, as in case of our selected glaciers. On the basis of limited samples from selected glaciers, it is hard to conclude a general statement to represent the whole Karakorum region. Further research based on in-situ observations, satellite based observation and high resolution modeling and emission inventories are required. We are expecting that ablation zones of the debris covered glaciers which are relatively at low elevation and near to pollution sources may be quite polluted, especially during melting seasons (we have updated this information in lines 372-374, given below for your reference).

"According to our understanding all the glaciers of the whole Karakoram region, may not besubstantially darkened by BC. Ablation zones of the debris covered glaciers which are relatively at low elevation and near to pollution source may be quite polluted."

3. **The authors report that "there was no clear correlation between BC and OC concentrations" (line 269), which I found a bit worrisome given that the two species usually originate from common sources and have common transport pathways. The authors do provide some potential reasons for why we could find more BC than OC in the snow (e.g. ,greater melt scavenging of OC), which was also a bit surprising, but I would appreciate seeing some more discussion on why concentrations of BC and OC would be uncorrelated.**

Response:

Yes the concentration of BC and OC was uncorrelated. In most cases the concentration of OC was greater than the concentration of BC. In few cases the concentration of BC was greater than the concentration of OC concentration. We add an additional text in revised manuscript lines 303-315, given below for your reference.

"In most cases the concentration of OC was greater than the concentration of BC. In few cases the concentration of BC was greater than the concentration of OC, which might indicates the contribution of coal combustion and/or biomass burning to the emissions. The reported OC concentration was water-insoluble OC. Including the water soluble OC could dominate the temporal variation of the OC/BC ratio. One important factor was post-deposition process, melt water can bring dissolved organic carbon away but not for BC. Low OC/BC ratio may also be possible due to the fact that OC and BC had redistributed primarily under the control of strong melt water rather than sublimation and/or dry/wet deposition. The spatio-temporal variability of OC/BC ratio may also indicate the contribution of various sources, seasonal variation and frequent change in wind directions. The OC vs BC correlation in snow and ice samples depend on OC vs BC ratio/concentrations in the atmosphere, post deposition process and then scavenging, enrichment and melt rate of snow/snow after deposition. According to our understanding the analysis method and amount of dust loading on the sample can also alter OC/BC ratio."

Beside this, the OC to EC ratio was also affected by both emission source variability and processing during long-range transport in the atmosphere. EC is a nonvolatile and very stable species, whereas OC contains either many semi volatile species that partition between gas and particle or polar compounds that are preferentially washed out (Granat et al., 2010). So at receptor site the concentration of OC may be less especially during wet seasons.

4. **(a) Related to the point above, how precisely was OC differentiated from BC in the thermal optical technique?**
   (b) What temperature threshold or thermal evolution profile was applied to separate the two species?
   (c) Could this have had anything to do with the high BC/OC ratios that were found in the snow samples?

Response:

a. There are some uncertainties while differentiating OC from BC in thermal optical techniques. Level of uncertainty depend on amount of dust loading on the sample, temperature protocol, analysis method, and sample type. In our case we adapted IMPROVE protocol (Cao et al., 2003; Chow et al., 2004), and measured the amounts of BC and OC on the quartz filters by using a DRI® Model 2001A thermal optical carbon analyzer. BC/OC ratio may be altered due to below possible reasons.

- The different thermal optical methods used to measure OC/BC ratios often produce significantly different results (for same sample) due to variation within the temperature programming and optical techniques followed by each method (Karanasiou et al., 2015).
- The OC/BC split point is different for different method and also depend on sample type (residential cook stoves, diesel exhaust, rural aerosols, urban aerosols) (Khan et al., 2011).

- Some OC is pyrolytically converted to BC (char) when the sample is heating in inert atmosphere (Zhi et al., 2008).
- In thermal optical methods it is hard to avoid the charring of OC and considered as a big challenge to BC and OC measurements (Chow et al., 2004; Schmid et al., 2001).
- In general, BC concentrations derived from the IMPROVE method are 1.2–1.5 times higher than those derived from the NIOSH method (Chow et al.,2001; Reisinger et al., 2008), and BC concentrations from the EUSAAR_2 temperature protocol are approximately twice as high as those derived from the NIOSH protocol (Cavalli et al., 2010).

So according to our understanding it may be possible to alter OC/BC ratio by the analysis method, mentioned in lines 313, 315 in the revised manuscript, given below for your reference.

"According to our understanding the analysis method and amount of dust loading on the sample can also alter OC/BC ratio. Further details about OC and BC splitting in thermal optical method are available in Wang el al., 2012".

(b) What temperature threshold was applied to separate the two species?

The IMPROVE_A temperature protocol defines temperature plateaus for thermally derived carbon fractions of

- 120 °C for OC1,
- 250 °C for OC2,
- 450 °C for OC3,
- 550 °C for OC4

} Organic carbon.

in a helium (He) carrier gas
Total OC was calculated as OC = OC1+ OC2+ OC3+ OC4. Similarly

- 550 °C for EC1,
- 700 °C for EC2,
- 800 °C for EC3

} Elemental carbon (black carbon).

in a 98% He 2% oxygen (O2) carrier gas.
Total EC was calculated as EC = EC1+ EC2+ EC3.

These information are provided in Wang et al., 2012 and we have indicated it in lines 154-155 in the revised manuscript as given below for your reference.

"The temperature threshold that was applied to separate the two species is mentioned in Wang et al., 2012."

(c) Could this have had anything to do with the high BC/OC ratios that were found in the snow samples?

Yes, based on above explanations there may be slight effect on BC/OC ratios. This effect may be more visible in high dust loading samples. We had relatively high dust loading in few samples,

which can affect the BC/OC measurement. We have added related information in lines313-315, quoted below for your reference.

"According to our understanding the analysis method and amount of dust loading on the sample can also alter OC/BC ratios."

5. **More generally, please describe and if possible quantify, sources of uncertainty in the measurements of BC, OC, and dust in snow.**

Response:

Agreed. We have introduced a separate section to describe the possible sources of uncertainty in the measurements (lines 660-671, given below for your reference).

"The overall precision in the BC, OC and TC concentrations was estimated considering the analytical precision of concentration measurements and mass contributions from field blanks. Uncertainty of the BC and OC mass concentrations was measured through the standard deviation of the field blanks, experimentally determined analytical uncertainty, and projected uncertainty associated with filter extraction. According to our understanding the major uncertainty in our study was the dust effects on BC/OC measurement. Warming role of OC was also not included in the current research, which was low but significant in several regions (Yasunari et al. 2015). Beside this we think snow grain size (snow aging) and snow texture were larger sources of uncertainty in the albedo reduction / radiative forcing calculations than indicated. The measured grain size was usually different from the effective optical grain size used in the SNICAR modeling. Snow grain shape was measured with the help of snow card, but was not used in the online SNICAR albedo simulation model and assumed a spherical shape for the snow grains which may slightly affect the results, because albedo of non-spherical grain is higher than the albedo of spherical grains (Dang et al., 2016)."

(6a) My sense is that snow grain size and snow texture are larger sources of uncertainty in the albedo reduction / RF calculations than indicated. Although snow grain size was measured with a hand lens (with reported accuracy of 20um), this determination of grain size is usually different from the effective (surface area-weighted) / optical grain size used in the SNICAR modeling. The true uncertainty in effective/optical grain size is likely much larger than 20um, and I think the paper should include greater acknowledgment of this issue.
The discussion of albedo variability associated with snow grain size (or snow aging) should also more clearly indicate the ranges in snow grain size that were assumed for the albedo modeling.

(6b)Furthermore, references to "snow age" are sometimes used when "snow grain size" would be more appropriate, since snow grain size does not always increase monotonically with snow age, and it is really the snow grain size that matters for optical/radiative considerations. Examples of this is are on line 364: "The estimated reduction in snow albedo by dust and BC compounded by the age of snow..." and line 386: "... exact snow age ...".

Response: (6a)

We agreed with the reviewer comment. The discussion of albedo variability associated with snow grain size (or snow aging) has been added in the revised manuscript as suggested (lines 463-474), quoted below for your reference.

"According to our understanding, snow grain size (snow aging) and snow texture were larger sources of uncertainty. The effect of snow grain size is generally larger than the uncertainty in light absorbing particles which varies with the snow type (Schmale et al., 2017). For an effective snow grain radius of 80 μm, 100 μm, 120 μm, the albedo reduction caused by 100 ng g−1 of BC was 0.017, 0.019 and 0.021 respectively. As snow grain size was measured with a hand lens (with reported accuracy of 20 μm), so at least 0.002 uncertainty is present in our albedo results. Snow grain shape was measured with the help of snow card, however grain shape was not used in the online SNICAR albedo simulation model and assumed a spherical shape for the snow grains. Albedo of non-spherical grain is higher than the albedo of spherical grains (Dang et al., 2016). The shapes of snow grains and/or ice crystals is significantly changing with snow age and meteorological conditions during and after snowfall (LaChapelle 1969). Besides this, a number of recent studies (e.g., Flanner et al., 2012; Liou et al., 2014; He et al., 2014, 2017) have shown that both snow grain shape and aerosol-snow internal mixing play important roles in snow albedo calculations."

(6b) Agreed. The "snow age" were removed in the identified locations, lines 419 and 435.
Similarly we made necessary changes in few other locations including lines 457 and 435.

6. **(7a) Snow albedo and perturbations to albedo are modeled and used heavily in this study to derive radiative forcing estimates, but no observations of snow or ice albedo are reported. Are there any observations of snow and ice albedo from this region that could be utilized to help verify or support the modeling?**

   (7b)I worry in particular that debris could strongly reduce albedo of the glaciers but is neglected in the model, potentially leading to bias in the modeled albedo perturbations.

Response:

7(a) Observations based snow or ice albedo were not estimated in current study. According to our knowledge these are the first such albedo measurements to be done from this region.

7(b) Agreed. The debris could strongly reduce albedo of the glaciers, but the albedo estimated in this study were not from the surface of glaciers or debris covered area. Albedo were only estimated for the snow samples collected from the open mountain valleys as indicated in lines 126-127 and 113.

In current study we estimated the snow albedo through SNICAR model only and there is no in-situ albedo observation. In our next coming paper we are using spectrometer to measure in-situ albedo in this region and to compare it with model results and satellite based snow albedo.

Minor issues:

line 211: "... were put in the above equation and got a c extinction..." - grammar issue.
Response: Corrected, lines 245, given below for your reference.

"Height of individual trajectory points was put in the above equation and got a normalized extinction profile by assuming surface extinction =1".

line 251: "... with the generally lower deposition on the Gulkin glacier more affected by other factors" - Which factors?
Response: Other factors has been added in line 295 of revised manuscript. The whole sentence is given below for your reference.

"The marked difference on the Sachin glacier may have reflected the difference in the direction of air, which comes from Iran and Afghanistan in summer and the Bay of Bengal via India in autumn, with the generally lower deposition on the Gulkin glacier more affected by other factors (such as slope aspect of the glacier and status of local emission near the glacier)."

line 257: "is considering as" -> "considered as"

Corrected, line 301.

line 274: "... low OC/BC ratios can result from a reduction in OC, greater contributions from BC enrichment..." - It is unclear to me which processes "reduction in OC" and "BC enrichment" refer to. Could the authors please elaborate on these processes?

Response: Below are the possible reasons

- Since BC in snow was less hydrophilic than OC and thus more OC was scavenged with snow melt water as compared to BC. So OC/BC ratios decreased with time during the snow melting season.
- One most important factor is post-deposition process, melt water can bring dissolved organic carbon away but not for BC. This may be the one possible reason that we are getting more BC than OC in the snow.
- The reported OC concentrations here from snow and ice samples was representing water insoluble OC (lines 18, 148, 278, 306); because most of the water-soluble OC was not captured by the filter-based method. Including water-soluble OC could dominate the temporal variation of the OC/BC ratio.
- Higher concentration BC as compared to OC may also indicates greater melt scavenging of OC and decline of the contribution of coal combustion and/or biomass burning to the carbonaceous aerosol emissions in the major contributing source regions.

- In general, BC concentrations derived from the IMPROVE method are 1.2–1.5 times higher than those derived from the NIOSH method (Chow et al.,2001; Reisinger et al., 2008), and BC concentrations from the EUSAAR_2 temperature protocol are approximately twice as high as those derived from the NIOSH protocol (Cavalli et al., 2010).

We add an additional text in revised manuscript lines 307-315, quoted below for your reference.

"One important factor was post-deposition process, melt water can bring dissolved organic carbon away but not for BC. Low OC/BC ratio may also possible due to the fact that OC and BC had redistributed primarily under the control of strong melt water rather than sublimation and/or dry/wet deposition. The OC vs BC correlation in snow and ice samples depend on OC vs BC ratio/concentrations in the atmosphere, post deposition process and then scavenging, enrichment and melt rate of snow/snow after deposition. According to our understanding the analysis method and amount of dust loading on the sample can also alter OC/BC ratios."

line 329: "albedo of samples from the two sites simulated at a wavelength of 0.975 um ... " - Why are 0.975 um albedo values reported here? Light-absorbing impurities exert the strongest influence on blue or mid-visible albedo (e.g., _0.450 um). The 0.975 um albedo is affected less strongly by impurities, and somewhat heavily by snow grain size, so it seems an odd choice of wavelength to use for reporting albedos.

Response: Yes, the reviewer is absolutely right. Apology for using a fixed particular wavelength in previous version of manuscript. The sentence has been modified lines 397 in revised manuscript, given below for your reference.

"The values for average albedo of samples from the two sites simulated for MAC values of 7.5, 11, and 15 m^2/g and SZA of 57.0–88.9° (day time) under a clear sky ranged from 0.39 (site S1, BC only, midday, MAC 15 m^2/g) to 0.85 (site S6, dust only, early evening, MAC 7.5–15 m^2/g)."

line 336: "The results suggest that BC was the dominant forcing factor, rather than dust, as a result of the rapid snowmelt." - The identification of "rapid snowmelt" as the cause for greater BC forcing than dust forcing is confusing here. Perhaps the sentence just needs re-working. Otherwise, what role does snowmelt play in the determination of instantaneous radiative forcing?

Response: Agreed. The sentence has been modified lines 406-407, as given below for your reference.

"The results suggest that BC was the dominant forcing factor, rather than dust, which influence glacial surface albedo and accelerate glacier melt."

line 343: "... reduction in daily mean albedo of 1.8 to 2.9% ... " Are these relative or absolute reductions in albedo? If the latter, please use absolute (non-percentage) units. This also applies to other references to percent albedo reduction in the paper.

Response: The albedo reduction values presented here are relative, indicating the difference of albedo with having certain pollutants (BC, or dust, or both) and a reference albedo (with zero pollutants i.e. zero BC and zero dust concentration). Some related text has been added in lines (399 - 401), given below for your reference.

"The albedo reduction values presented here are relative, indicating the difference of albedo with having certain pollutants (BC or dust or both) and a reference albedo (with zero pollutants i.e. zero BC and zero dust concentration)."

lines 400-401: Which environments do these RF estimates apply to?

Response: Environment and small descript of each reference (used in above mentioned line 400-401) is given below

Zhang et al. 2017:

- Study region: Keqikaer Glacier (39°N–46°N and 69°E–95°E) in western Tien Shan.
- Environment: Mid-latitude winter, clearsky, cloudy, cloud amount<5 and for ≥5
- Time period: May 2015.
- Model used: SNICAR model (Flanner et al., 2007)
- Radiative forcing: Obtained by equation used in Kaspari et al., 2014; Yang et al., 2015.

Nair et al., 2013:

- Study region: Selected sites/stations in Himalayas region.
- Environment: mid-latitude winter atmospheric conditions.
- Time period: 2005-2011 mainly in pre-monsoon and winter seasons.
- Model used: SNICAR model (Flanner et al., 2007).
- Radiative forcing: Using the short-wave fluxes simulated by SBDART model.

Yang et al., 2015:

- Study region: Muji glacier (39.19° N, 73.74° E) in Tibetan Plateau.
- Environment: Clear-sky and cloudy conditions.
- Time period: During snowmelt season of 2012.
- Model used: SNICAR model (Flanner et al., 2007).
- Radiative forcing: SBDART model.

We have added further information in the revised manuscript lines 486-489, quoted below for your reference.

"To estimate these radiative forcing measurements, mid-latitude winter with clear sky and cloudy environment was used by Zhang et al. 2017; mid-latitude winter atmospheric conditions was used by Nair et al., 2013; while clear-sky and cloudy conditions environment was used by Yang et al., 2015."

lines 406-410: It should be acknowledged again that dust forcing varies strongly with dust optical properties and particle size distribution. The estimates derived here appear to have

utilized a generic representation of dust in the model that may or may no be appropriate for the dust that was actually measured.

Response: Agreed. Below sentences has been added (lines 497-502) in the revised manuscript.

"It is important to mention here that dust forcing varies strongly with dust optical properties, source material and particle size distribution. Properties for dust are unique for each of four size bins used in SNICAR online model. These size bins represent partitions of a lognormal size distribution. We used the estimated size of dust particles with generic property of dust in the model. Some dust particles can have a larger impact on snow albedo than the dust applied here (e.g., Aoki et al., 2006; Painter et al., 2007)."

lines 461: "BC from East Asia can potentially be lifted up high and transported to the northeast during the summer monsoon season. Nonetheless..." - But transport of East Asia emissions to the northeast does not seem relevant for deposition in Pakistan.
Please clarify the relevance of this statement.

Response: The sentence has been deleted and the paragraph has been slightly modified lines 561-564, given below for your reference.

"The results indicate that only a low level of pollutants (minor contribution) reached the study area from Northwest China. BC particles emitted from distant low latitude source regions such as tropical Africa barely reach the Tibetan Plateau and Himalayan regions because their emissions are removed along the transport pathways during the summer monsoon season (Zhang et al., 2015)."

line 463: "... low latitude source regions such as South Africa..." - I suggest using "tropical Africa" or something similar here instead of "South Africa" (which happens to also be the name of a country).

Response: Agreed. Tropical Africa has been used, as suggested (line 563), given below for your reference.

"BC particles emitted from distant low latitude source regions such as tropical Africa barely reach the Tibetan Plateau and Himalayan regions because their emissions are removed along the transport pathways during the summer monsoon season (Zhang et al., 2015)."

line 464: "weak emissions" - Actually, biomass burning emissions from tropical regions of Africa constitute a substantial share of global BC emissions, so "weak" may not be the best word here.

Response: Agreed. The sentence has been modified line 564, given below for your reference.

"BC particles emitted from distant low latitude source regions such as tropical Africa barely reach the Tibetan Plateau and Himalayan regions because their emissions are removed along the transport pathways during the summer monsoon season (Zhang et al., 2015)."

line 479: "considerable" -> "considerably"

Response: Corrected, lines 578.

line 482: "The concentration of hydrophobic BC, hydrophilic BC, ... " - The description earlier in Methods indicated only that CO tracers were used. Was BC also simulated with this model? If so, were BC tags applied? Please include more description of the BC simulation in Methods. This seems much more relevant for source attribution, since the physics and chemistry of removal for BC and CO are quite different from each other.

Response: BC was not simulated with the model.
The purpose of showing concentration of hydrophobic BC (BC1), hydrophilic BC (BC2) was to compare the concentration of fresh (hydrophobic) and aged (hydrophilic) BC during summer and winter seasons over the study region. In this study we applied only CO tracer and it is mentioned in lines 567-568.
We agreed that BC model simulation is relatively more relevant for source attribution. For this time we have CO tracer data (which has relatively good correlation with BC tracer in dry seasons- used by multiple authors in the past Shindell et al., 2008; Chen et al., 2009).
We will use high resolution BC tracer in our next publications in near future. Expected uncertainty in CO tag and some recommendations are stated in lines 672-680 in the revised manuscript. The indicated sentences given below for your reference.

"Future study (BC tracer) will evaluate the details of the different source region of BC reaching the glaciers as compared to region tagged CO tracers."

And

"Better-constrained measurements are required in the future for more robust results. High resolution satellite imagery, high resolution models and continuous monitoring can help us to reduce the present uncertainty."

line 520: "... and increased grain size and density." - It is not clear to me how snow grain size and snow density should affect the *concentration* of BC, as indicated in this sentence. Please clarify.

Response: Agreed. We removed this portion from the revised sentence (Line 621), the modified sentence given below for your reference.

"The samples from Sost contained the highest average concentration of BC in mountain valleys snow (winter) and those from Kalam the lowest, probably due to the impact of snow age, increased concentration of black carbon and dust (the Sost samples were aged snow and Kalam samples fresh snow)."

Figure 2: Most of the figure is white space. I suggest shrinking the y-axis range to show the plot values more clearly.
Response: Agreed. The figure has been modified as suggested, given below for your reference

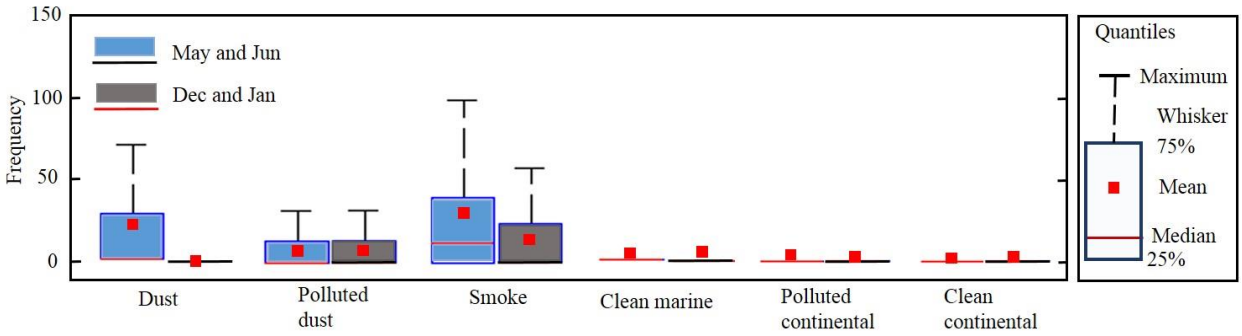

Revised Figure 2.

Figure 6: Please specify which emission inventory was used and how many days of back-trajectory were simulated.

Response: Agreed. Emission inventory has been used with number of days as given below for your reference,

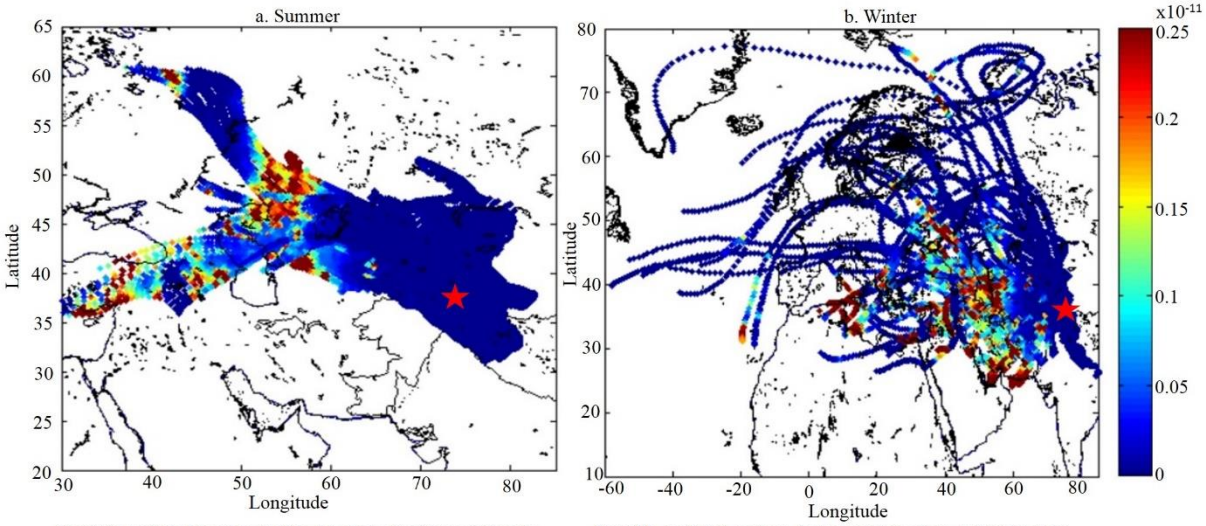

Figure 6. Source contribution regions of pollutants identified using an emissions inventory (Representative Concentration Pathways) coupled with back trajectories (a. 77 simulated days, b. 63 simulated days). Red star indicates the position of the study area.

Table 2: Are these relative or absolute snow albedo reductions?

Response: These albedos are relatives because these albedos were estimated with/from reference albedos (with no dust and no BC in the sample). Some general explanation regarding to how we estimate the albedo is given below.

Albedo were estimated using SNICAR online model by providing input parameters mentioned in Table S1. Model was run four times for one particular sample

1. No dust and no BC (reference albedo),
2. Only dust and no BC,
3. Only BC and no dust,
4. with both dust and BC concentration)

We subtract the albedos obtained in other three options with dust and/or BC from this reference albedo.

We have added these information in the revised manuscript indicated in lines 399-401, given below for your reference

"The albedo reduction values presented here are relative, indicating the difference of albedo with having certain pollutants (BC or dust or both BC and dust) and a reference albedo (with zero pollutants i.e. zero BC and zero dust concentration)."

References:

Aoki, T., Kuchiki, K., Niwano, M., Kodama, Y., Hosaka, M. and Tanaka, T.: Physically based snow albedo model for calculating broadband albedos and the solar heating profile in snowpack for general circulation models, J. Geophys. Res. Atmos., 116(11), 1–22, doi:10.1029/2010JD015507, 2011.

Cao, J. J., Lee, S. C., Ho, K. F., Zhang, X. Y., Zou, S. C., Fung, K., Chow, J. C., and Watson, J. G.: Characteristics of carbonaceous aerosol in Pearl River Delta Region, China during 2001 winter period, Atmos. Environ., 37, 1451-1460, 2003.

Cavalli, F., Viana, M., Yttri, K. E., Genberg, J., and Putaud, J. P.: Toward a standardised thermal-optical protocol for measuring atmospheric organic and elemental carbon: the EUSAAR protocol, Atmos. Meas. Tech., 3, 79–89, https://doi.org/10.5194/amt-3-79-2010, 2010.

Chen, D., Wang, Y., Mcelroy, M. B., He, K., Yantosca, R. M. and Sager, P. Le: and Physics Regional CO pollution and export in China simulated by the high-resolution nested-grid GEOS-Chem model, , (2008), 3825–3839, 2009.

Chow, J. C., Watson, J. G., Crow, D., Lowenthal, D. H., and Merrifield, T.: Comparison of IMPROVE and NIOSH carbon measurements, Aerosol Sci. Tech., 34, 23–34, https://doi.org/10.1080/027868201300081923, 2001.

Chow, J. C., Watson, J. G., Chen, L. W., Arnott, W. P., Moosmüller, H., & Fung, K. (2004). Equivalence of elemental carbon by thermal/optical reflectance and transmittance with different temperature protocols. Environmental Science & Technology, 38, 4414–4422

Cao, J.,Wu, F., Chow, J. C., Lee, S. C., Li, Y., Chen, S.W., An, Z. S., Fung, K. K.,Watson, J. G., Zhu, C. S., and Liu, S. X.: Characterization and source apportionment of atmospheric organic and elemental carbon during fall and winter of 2003 in Xi'an, China, Atmos.Chem. Phys., 5, 3127–3137, doi:10.5194/acp-5-3127-2005,2005.

Dang, C., et al. (2016), Effect of Snow Grain Shape on Snow Albedo. J. Atmos. Sci., 73, 3573–3583, doi:10.1175/JAS-D-15-0276.1

Ducret, J. and Cachier, H.: Particulate carbon content in rain at various temperate and tropical locations, J. Atmos. Chem., 15, 55–67, 1992.

Fitzgerald, W. F.: Clean hands, dirty hands: Clair Patterson and the aquatic biogeochemistry of mercury, Clean Hands, Clair Patterson's Crusade Against Environmental Lead Contamination, 119–137, 1999.

Flanner, M. G., et al. (2012), Enhanced solar energy absorption by internally-mixed black carbon in snow grains, Atmos. Chem. Phys., 12, 4699-4721, doi:10.5194/acp- 12-4699-2012.

Ganguly, D., Rasch, P. J., Wang, H. and Yoon, J.: Climate response of the South Asian monsoon system to anthropogenic aerosols, JGR-D, 117(May), 1–20, doi:10.1029/2012JD017508, 2012.

Granat, L., J. E. Engström, S. Praveen, and H. Rodhe (2010), Light absorbing material (soot) in rain water and in aerosol particles in the Maldives, J. Geophys. Res., 115, D16307, doi:10.1029/2009JD013768

He, C., et al. (2014), Black carbon radiative forcing over the Tibetan Plateau, Geophys. Res. Lett., 41, 7806–7813, doi:10.1002/2014GL062191.

He, C., et al. (2017): Impact of Snow Grain Shape and Black Carbon-Snow Internal Mixing on Snow Optical Properties: Parameterizations for Climate Models. J. Climate, 0, doi:10.1175/JCLI-D-17-0300.1

Karanasiou, A., Minguillón, M. C., Viana, M., Alastuey, A., Putaud, J. P., Maenhaut, W., Panteliadis, P., Moˇcnik, G., Favez, O., and Kuhlbusch, T. A. J.: Thermal-optical analysis for the measurement of elemental carbon (EC) and organic carbon (OC) in ambient air a literature review, Atmos. Meas. Tech. Discuss.,8, 9649–9712, https://doi.org/10.5194/amtd-8-9649-2015, 2015.

Kaspari, S., Painter, T. H., Gysel, M., Skiles, S. M. and Schwikowski, M.: Seasonal and elevational variations of black carbon and dust in snow and ice in the Solu-Khumbu, Nepal and estimated radiative forcings, Atmos. Chem. Phys., 14(15), 8089–8103, doi:10.5194/acp-14-8089-2014, 2014.

Khan, B., Hays, M. D., Geron, C., Jetter, J., Khan, B., Hays, M. D., Geron, C., Jetter, J., Khan, B., Hays, M. D., Geron, C. and Jetter, J.: Differences in the OC / EC Ratios that Characterize Ambient and Source Aerosols due to Thermal- Optical Analysis Differences in the OC / EC Ratios that Characterize Ambient and Source Aerosols due to Thermal-Optical Analysis, , 6826(October 2017), doi:10.1080/02786826.2011.609194, 2012.

Kuhlmann, J. and Quaas, J.: and Physics How can aerosols affect the Asian summer monsoon ? Assessment during three consecutive pre-monsoon seasons from CALIPSO satellite data, , 1930, 4673–4688, doi:10.5194/acp-10-4673-2010, 2010.

Kroll J Het al 2011 Carbon oxidation state as a metric for describing the chemistry of atmospheric organic aerosol Nature Chem. 3 133–9

LaChapelle, E. R., 1969: Field Guide to Snow Crystals. University of Washington Press, 112 pp.

Lamarque, J.F., Bond, T.C., Eyring, V., Granier, C., Heil, A., Klimont, Z., Lee, D., Liousse, C., Mieville, A., Owen, B., Schultz, M.G., Shindell, D., Smith, S.J., Stehfest, E., Van Aardenne, J., Cooper, O.R., Kainuma, M., Mahowald, N., McConnell, J.R., Naik, V., Riahi, K., Van Vuuren, D.P., 2010. Historical (1850-2000) gridded anthropogenic and biomass burning emissions of reactive gases and aerosols: Methodology and application. Atmospheric Chemistry and Physics 10, 7017–7039, 2010.

Li, X., Kang, S., He, X., Qu, B., Tripathee, L., Jing, Z., Paudyal, R., Li, Y., Zhang, Y., Yan, F., Li, G. and Li, C.: Light-absorbing impurities accelerate glacier melt in the Central Tibetan Plateau, Sci. Total Environ., doi:10.1016/j.scitotenv.2017.02.169, 2017.

Li, Y., Chen, J., Kang, S., Li, C., Qu, B., Tripathee, L., Yan, F., Zhang, Y., Guo, J., Gul, C. and Qin, X.: Impacts of black carbon and mineral dust on radiative forcing and glacier melting during summer in the Qilian Mountains, northeastern Tibetan Plateau, Cryosph. Discuss., (April), 1–14, doi:10.5194/tc-2016-32, 2016.

Liou, K. N., et al. (2014), Stochastic parameterization for light absorption by internally mixed BC/dust in snow grains for application to climate models, J. Geophys. Res. Atmos., 119, doi:10.1002/2014JD021665.

Ming, J., Xiao, C., Cachier, H., Qin, D., Qin, X., Li, Z. and Pu, J.: Black Carbon (BC) in the snow of glaciers in west China and its potential effects on albedos, Atmos. Res., 92(1), 114–123, doi:10.1016/j.atmosres.2008.09.007, 2009.

Nair, V. S., Babu, S. S., Moorthy, K. K., Sharma, A. K., Marinoni, A. and Ajai: Black carbon aerosols over the Himalayas: Direct and surface albedo forcing, Tellus, Ser. B Chem. Phys. Meteorol., 65(1), doi:10.3402/tellusb.v65i0.19738, 2013.

Niu, H., Kang, S., Shi, X., Paudyal, R., He, Y., Li, G. and Wang, S.: Science of the Total Environment In-situ measurements of light-absorbing impurities in snow of glacier on Mt . Yulong and implications for radiative forcing estimates, Sci. Total Environ., 581–582, 848–856, doi:10.1016/j.scitotenv.2017.01.032, 2017.

Novakov, T., Menon, S., Kirchstetter, T. W., Koch, D. and Hansen, J. E.: Aerosol organic carbon to black carbon ratios : Analysis of published data and implications for climate forcing of soot emissions maybe a useful approach to slow global warming ., , 110, 1–13, doi:10.1029/2005JD005977, 2005.

Ohara, T. et al., 2007, An Asian emission inventory of anthropogenic emission sources for the period 1980-2020. Atmospheric Chemistry and Physics 7, 4419-4444

Painter, T. H., Barrett, A. P., Landry, C. C., Neff, J. C., Cassidy, M. P., Lawrence, C. R., McBride, K. E. and Farmer, G. L.: Impact of disturbed desert soils on duration of mountain snow cover, Geophys. Res. Lett., 34(12), 1–6, doi:10.1029/2007GL030284, 2007.

Qian, Y., Flanner, M. G., Leung, L. R. and Wang, W. 2011. Sensitivity studies on the impacts of Tibetan Plateau snowpack pollution on the Asian hydrological cycle and monsoon climate. Atmos. Chem. Phys. 11, 1929-1948.

Qu, B., Ming, J., Kang, S. C., Zhang, G. S., Li, Y. W., Li, C. D., Zhao, S. Y., Ji, Z. M. and Cao, J. J.: The decreasing albedo of the Zhadang glacier on western Nyainqentanglha and the role of light-absorbing impurities, Atmos. Chem. Phys., 14(20), 11117–11128, doi:10.5194/acp-14-11117-2014, 2014.

Ram Kand SarinMM2010 Spatio-temporal variability in atmospheric abundances of EC,OC and WSOC over Northern India J. Aerosol Sci. 41 88–98

Reisinger, P., Wonaschütz, A., Hitzenberger, R., Petzold, A., Bauer, H., Jankowski, N., Puxbaum, H., Chi, X., and Maenhaut, W.: Intercomparison of measurement techniques for black or elemental carbon under urban background conditions in wintertime: influence of biomass combustion, Environ. Sci. Technol., 42, 884–889, https://doi.org/10.1021/es0715041, 2008.

Saarikoski S et al 2008 Sources of organic carbon in fine particulate matter in Northern European urban air Atmos. Chem. Phys. 8 6281–95

Schmid, H., Laskus, L., Abraham, H. J., Baltensperger, U., Lavanchy, V., Bizjak, M., et al. (2001). Results of the "carbon conference" international aerosol carbon round robin test stage I. Atmospheric Environment, 35, 2111–2121.

Schmale, J., Flanner, M., Kang, S., Sprenger, M., Zhang, Q., Guo, J., Li, Y., Schwikowski, M. and Farinotti, D.: Modulation of snow reflectance and snowmelt from Central Asian glaciers by anthropogenic black carbon, Sci. Rep., 7(October 2016), 40501, doi:10.1038/srep40501, 2017.

Shindell, D. T., Chin, M., Dentener, F.: A multi-model assessment of pollution transport to the Arctic, Atmos. Chem. Phys., 8, 5353–5372, 2008, http://www.atmos-chem-phys.net/8/5353/2008/.

Wang M, B Xu, J Cao, X Tie, H Wang, R Zhang, Y Qian, PJ Rasch, S Zhao, G Wu, H Zhao, DR Joswiak, J Li, and Y Xie. 2015. "Carbonaceous Aerosols Recorded in a Southeastern Tibetan Glacier: Analysis of Temporal Variations and Model Estimates of Sources and Radiative Forcing." Atmospheric Chemistry and Physics 15:1191-1204. doi:10.5194/acp-15-1191-2015.

Wang, X., Pu, W., Ren, Y., Zhang, X., Zhang, X., Shi, J., Jin, H., Dai, M. and Chen, Q.: Snow albedo reduction in seasonal snow due to anthropogenic dust and carbonaceous aerosols across northern China, Atmos. Chem. Phys. Discuss., (September), 1–52, doi:10.5194/acp-2016-667, 2016.

Wang, X., Pu, W., Ren, Y., Zhang, X., Zhang, X., Shi, J., Jin, H., Dai, M. and Chen, Q.: Snow albedo reduction in seasonal snow due to anthropogenic dust and carbonaceous aerosols across northern China, Atmos. Chem. Phys. Discuss., (September), 1–52, doi:10.5194/acp-2016-667, 2016.

Wang M, B Xu, J Cao, X Tie, H Wang, R Zhang, Y Qian, PJ Rasch, S Zhao, G Wu, H Zhao, DR Joswiak, J Li, and Y Xie. 2015. "Carbonaceous Aerosols Recorded in a Southeastern Tibetan Glacier: Analysis of Temporal Variations and Model Estimates of Sources and Radiative Forcing." Atmospheric Chemistry and Physics 15:1191-1204. doi:10.5194/acp-15-1191-2015.

Xu, B., Yao, T., Liu, X. and Wang, N.: Elemental and organic carbon measurements with a two-step heating-gas chromatography system in snow samples from the Tibetan Plateau, Ann. Glaciol., 43(June 2015), 257–262, doi:10.3189/172756406781812122, 2006.

Xu, B., Cao, J., Joswiak, D. R., Liu, X., Zhao, H. and He, J.: Post-depositional enrichment of black soot in snow-pack and accelerated melting of Tibetan glaciers, Environ. Res. Lett., 7(1), 14022, doi:10.1088/1748-9326/7/1/014022, 2012.

Yamaji, K. et al., 2003, A country-specific, high-resolution emission inventory for methane from livestock in Asia in 2000. Atmospheric Environment 37(31), 4393-4406, doi:10.1016/S1352-2310(03)00586-7

Yan X. et al., 2003, Development of region-specific emission factors and estimation of methane emission from rice field in East, Southeast and south Asian countries, Global Change Biology, 9, 237-254.

Yang, S., Xu, B., Cao, J., Zender, C. S. and Wang, M.: Climate effect of black carbon aerosol in a Tibetan Plateau glacier, Atmos. Environ., 111, 71–78, doi:10.1016/j.atmosenv.2015.03.016, 2015.

Zhang R, H Wang, Y Qian, PJ Rasch, RC Easter, Jr, PL Ma, B Singh, J Huang, and Q Fu. 2015. "Quantifying sources, transport, deposition, and radiative forcing of black carbon over the Himalayas and Tibetan Plateau." Atmospheric Chemistry and Physics 15(11):6205-6223. doi:10.5194/acp-15-6205-2015.

Zhang, Y., Kang, S., Xu, M., Sprenger, M., Gao, T., Cong, Z., Li, C., Guo, J., Xu, Z., Li, Y., Li, G., Li, X., Liu, Y. and Han, H.: Sciences in Cold and Arid Regions Light-absorbing impurities on Keqikaer Glacier in western Tien Shan : concentrations and potential impact on albedo reduction, , 9(2), doi:10.3724/SP.J.1226.2017.00097.Light-absorbing, 2017.

Zhang, Y., Hirabayashi, Y., Liu, Q. and Liu, S.: Glacier runoff and its impact in a highly glacierized catchment in the southeastern Tibetan Plateau: Past and future trends, J. Glaciol., 61(228), 713–730, doi:10.3189/2015JoG14J188, 2015.

Zhi, G.: Effects of temperature parameters on thermal- optical analysis of organic and elemental carbon in aerosol, , (November 2014), doi:10.1007/s10661-008-0393-4, 2008.

Zhang, Y., Hirabayashi, Y., Liu, Q. and Liu, S.: Glacier runoff and its impact in a highly glacierized catchment in the southeastern Tibetan Plateau: Past and future trends, J. Glaciol., 61(228), 713–730, doi:10.3189/2015JoG14J188,

2015.

Thank you

Concentrations and source regions of light absorbing ~~impurities~~ particles in snow/ice in northern Pakistan and their impact on snow albedo

Chaman Gul[1,2,5], Siva Praveen Puppala[2], Shichang Kang[1,3,5], Bhupesh Adhikary[2], Yulan Zhang[1], Shaukat Ali[4], Yang Li[3], Xiaofei Li[1]

[1]State Key Laboratory of Cryosphere Science, Northwest Institute of Eco-Environment and Resources, Chinese Academy of Sciences, Lanzhou 73000, China
[2]International Centre for Integrated Mountain Development (ICIMOD), G.P.O. Box 3226, Kathmandu, Nepal
[3]CAS Center for Excellence in Tibetan Plateau Earth Sciences, Beijing, 100101, China
[4]Global Change Impact Studies Centre (GCISC), Ministry of Climate Change, Islamabad, Pakistan
[5]University of Chinese Academy of Sciences, Beijing, China

Correspondence to: Chaman Gul (chaman.gul@icimod.org; chaman@lzb.ac.cn), SivaPraveen.Puppala@icimod.org.

Abstract. Black carbon (BC), water-insoluble organic carbon (OC), and mineral dust are important ~~particulate impurities~~particles in snow and ice, which significantly reduce albedo and accelerate melting. Surface snow and ice samples were collected from the Karakoram-Himalayan region of northern Pakistan during 2015 and 2016 in summer (six glaciers), autumn (two glaciers), and winter (six mountain valleys). The average BC concentration overall was 2130 ± 1560 ngg^{-1} in summer samples, 2883±3439 ngg^{-1} in autumn samples, and 992 ± 883 ngg^{-1} in winter samples. The average water insoluble OC concentration overall was 1839 ± 1108 ngg^{-1} in summer samples, 1423 ± 208 ngg^{-1} in autumn samples, and 1342 ± 672 ngg^{-1} in winter samples. The overall concentration of BC, OC, and dust in aged snow samples collected during the summer campaign was higher than the concentration in ice samples. The values are relatively high compared to reports by others for the Himalayas and Tibetan Plateau. This is probably the result of taking more representative samples at lower elevation where deposition is higher and the effects of ageing and enrichment more marked. A reduction in snow albedo of 0.1–8.3% for fresh snow and 0.9–32.5% for aged snow was calculated for selected solar zenith angles during day time using the Snow, Ice, and Aerosol Radiation (SNICAR) model. Daily mean albedo was reduced by 0.07–12.0%. The calculated radiative forcing ranged from 0.16 to 43.45 Wm^{-2} depending on snow type, solar zenith angle, and location. The potential source regions of the deposited pollutants were identified using spatial variance in wind vector maps, emission inventories coupled with backward air trajectories, and simple region tagged chemical transport modelling. Central, South, and West Asia were the major sources of pollutants during the sampling months, with only a small contribution from East Asia. Analysis based on the Weather Research and Forecasting (WRF-STEM) chemical transport model identified a significant contribution (more than 70%) from South Asia at selected sites. Research into the presence and effect of pollutants in the glaciated areas of Pakistan is economically significant because the surface water resources in the country mainly depend on the rivers (the Indus and its tributaries) that flow from this glaciated area.

1 Introduction

Carbon is an essential component of atmospheric aerosols, where it appears in the form of black carbon (BC, or elemental carbon EC), and organic carbon (OC). BC is emitted into the atmosphere from incomplete combustion of carbon-based fuels (mainly fossil fuels and biomass) (Jacobson, 2004) while OC can be directly emitted into or formed in the atmosphere. After deposition on snow and ice surfaces, BC particles significantly reduce the snow albedo (hemispheric reflectance) in the visible part of the electromagnetic spectrum, cause snow albedo feedback (Doherty et al., 2013), enhance solar radiation absorption (Warren and Wiscombe, 1980), and accelerate snow melting (Hansen and Nazarenko, 2004). BC, both in air and deposited on snow, is important in net positive forcing of the climate. Clean snow is one of the most reflective natural surfaces on Earth at the ultraviolet and visible wavelengths, while BC is the most efficient light-absorbing species in the visible spectral range (Horvarth, 1993). One ngg^{-1} of BC has almost the same effect on albedo reduction as 100 ngg^{-1} mineral dust at 500 nm wavelength (Warren et al., 1982). However, the exact amount of albedo reduction also depends on the refractive index, ~~snow age,~~ grain size, solar zenith angle (SZA), snow density, dust particle size and concentration, particle morphology, surface roughness, snow depth, liquid water content, snow shape and topography ~~and dust particle size~~(Wiscombe and Warren 1985). Albedo reduction usually results in amplification of the energy absorbed by dirty snow (Painter et al., 2010). An albedo feedback is triggered and amplified by deposition of impurities on the snow surface which reduces snow albedo thus accelerating melting and further reducing albedo (Doherty et al., 2013; Flanner et al., 2009). Albedo feedback is amplified by the presence of light-absorbing ~~impurities~~ particles (Doherty et al., 2013). Studies conducted in Greenland showed that at visible wavelengths 10 ngg^{-1} coarse-grained BC particles in aged snow and 40 ngg^{-1} BC particles in new snow could reduce snow albedo by around 1 to 3% (Warren and Wiscombe, 1985).

Increased BC mass concentration and deposition on the Tibetan glaciers over the last 20 years (Xu et al., 2009a) has played a significant role in rapid glacier melting in the region (Xu et al., 2012; Yao et al., 2012). A high concentration of aerosol has deposited on the snow surface and increased the BC content in snow over the southern edge of the Tibetan Plateau to the north of the Himalayas (Gertler et al., 2016). The southern slope of the Himalayas is relatively even more exposed to BC due to emissions from India and transport through southwesterly and westerly winds (Xu et al., 2009; Yasunari et al., 2010). BC deposited on snow in the Himalayan region induces an increase in net shortwave radiation at the snow surface with an annual mean of about 1 to 3 Wm^{-2}, producing an estimated 0.05–0.3°C warming (Ménégoz et al., 2014). Deposition of anthropogenic BC has been observed to contribute significantly to the decrease in snow cover extent over recent decades (Dery et al., 2007), and shortening the duration of the snow cover season by several days (Ménégoz et al., 2013a). The climate warming efficiency of BC in snow is greater than the warming efficiency of other anthropogenic pollutants, including carbon dioxide (Hansen et al., 2005). Besides warming efficiency, another important characteristic of BC is its higher snowmelt efficiency. The snowmelt efficacy induced by BC in snow is larger for snow cover fraction and snow water equivalent than induced by carbon dioxide increase (Qian et al., 2011). The annual snow albedo reduction effect due to BC outweighs the

aerosol dimming effect (reduction in solar radiation reaching the surface) by a factor of about six over the global snow cover (Flanner et al., 2009).

At present, South and East Asia are considered to be the two largest BC emission regions in the world and likely to remain so (Menon et al., 2010). BC transported from East Asia can be lifted high and moved towards the northeast during the summer monsoon season (Zhang et al., 2015; Cong et al., 2015; Lüthi et al., 2015), affecting the life of glaciers and snow-covered areas.

Research into the glaciers of the extended Himalayan region and Tibetan Plateau has prime importance because these glaciers act as a water storage tower for South and East Asia, and shrinking could affect water resources for up to a billion people (Immerzeel et al., 2010). The glaciated area in northern Pakistan may be more exposed to BC effects than that in other regions because potentially it can receive emissions generated from both South and Central Asia as well as from the Middle East. Meltwater coming from these glaciers flows into the river Indus, which has major economic importance for the people of Pakistan.

A number of authors have described the concentration and impacts of light absorbing ~~impurities~~ particles in the Tibetan glaciers (for example Qian et al., 2015; Wang et al., 2015; Que et al., 2016; Zhang et al., 2017; Li et al., 2017; Niu et al., 2017~~;~~). However, until now, no studies have been published related to the concentration of light absorbing aerosols in the surface snow and ice of northern Pakistan, and although several authors have investigated transport pathways over the Himalayan region (e.g. Babu et al., 2011 for the western trans-Himalayas; Lu et al., 2012~~, and Kopacz et al., 2011~~ for the Tibetan Plateau and Himalayas) little is known about the potential sources and transport pathways of pollutants affecting the Pakistan area.

In this study, we looked at the concentration of light absorbing ~~impurities~~ particles (BC, OC, dust) in snow and ice in northern Pakistan, their impact on snow albedo and radiative forcing, and the likely source regions. Albedo was estimated from the BC and dust concentrations identified in collected samples of snow and ice using the online snow albedo simulation SNICAR model (Flanner et al., 2009). Radiative forcing was calculated from the albedo reduction obtained from the SNICAR model together with the incident short-wave solar radiation obtained from the SBDART (Santa Barbara DISORT Atmospheric Radiative Transfer) model. The frequency distribution of aerosol subtypes (smoke, continental polluted, dust, and others) in the atmosphere over the study area was calculated for the snow and ice sampling periods using Cloud-Aerosol Lidar and Infrared Pathfinder Satellite Observations (CALIPSO) satellite data from 2006 to 2014 as a further indication of the types of aerosol contributing to the observed deposition. The potential source regions of pollutants were identified using spatial variance in wind vector maps prepared using ~~50 years of~~MERRA-2 reanalysis data, calculation of back air trajectories using the HYSPLIT-4 (Hybrid Single Particle Lagrangian Integrated Trajectory) model, and a simple region tagged chemical transport model (WRF-STEM). The back air trajectories approach has been used in many studies to identify possible source regions for atmospheric and deposited BC (Zhang et al., 2013). Pollutant source regions identified using the different approaches were compared and the most likely source regions of the pollutants identified.

2 Methodology

2.1 Study area

The study area was located around 35.40°N 74.38°E in the mountains and adjacent mountain valleys of the Karakoram and Himalayan region in northern Pakistan (Figure 1). Snow and ice samples were collected in summer from six glaciers – Passu, Gulkin, Barpu, Mear, Sachin, and Henarche – and in autumn from Gulkin and Sachin (Figure 1). The Passu and Gulkin glaciers are located very near to the Karakoram highway connecting Pakistan with China, and there are a number of small villages (Passu, Hussaini, Gulmit, and others) close by. The Barpu and Mear glaciers are located very close to each other and around ~~2~~ 3 km away from the residential area of the Hopar and Nagar valleys. There is a small city (Astore) near the Sachin glacier and some restaurants near its terminus. Winter snow samples were collected from mountain valleys near to Passu, Barpu and Sachin glaciers, and three other areas to the west with a number of small villages (Figure 1). The average elevation of the selected glaciers was quite low comparted to the elevation of the glaciers studied for BC, OC and dust on the Tibetan plateau by previous researchers. The mountains around the selected glaciers are mostly dry and rocky. ~~The mean annual precipitation (rain) at Gilgit was approximately 0.412 ± 2 mm during the period 1980–2013 (Gul et al., 2017)~~ According to the 10 years record (1999–2008) of the two nearby climatic stations, the mean total annual precipitation was 170 mm at Khunjerab (36.83°N, 75.40°E, 4730 m) station, and 680 mm at Naltar (36.29°N, 74.12°E,2858 m) station, while the daily average temperature during winter and pre-monsoon showed an increasing trend between 1980 and 2014 (Gul et al., 2017).The study area is mostly exposed to the westerlies and emission from South Asia. Most of the people in the region use wood for cooking and heating.

2.2 Sample collection

A total of 50 surface ice and 49 snow samples were collected from the glaciers in summer 2015 and 2016 (Passu 15, Gulkin 31, Barpu 6, Mear 8, Sachin 35, Henarche 4), and 13 in autumn 2016 (Gulkin 7, Sachin 6) at elevations ranging from 2,569 to 3,895 masl (Figure 1). Eighteen snow samples were collected in winter 2015 and 2016 from nearby mountain valleys at elevations of 1,958 to 2,698 masl; the winter sampling region was divided into six sites (S1 to S6) based on geographical location and elevation (Figure 1). Samples were collected using the "clean hands – dirty hands" principle (Fitzgerald, 1999). Ice samples were collected from the surface (5 cm depth) at different points on the glaciers. The elevation difference between collection points on the same glacier ranged from 30 to 100 meters.

The samples were preserved in ultra clean plastic bags, allowed to melt in a temporary laboratory near the sampling location, and filtered through quartz-filters immediately after melting. An electric vacuum pump was used to accelerate filtration. The melted snow/ice volume of the samples was measured using a graduated cylinder. Sampled filters were carefully packed inside petri-slides marked with a unique code representing the sample.

The snow density of winter snow samples was measured using a balance; snow/ice grain sizes were observed with a hand lens (25×) with an accuracy of 0.02 mm (Aoki et al., 2011) and snow shape were estimated through

snow card. We assumed external mixing of snow and aerosol particles and considered spherical snow grains. Qian et al., 2015 summarized sample methods for light absorbing particles in snow and ice from different region including Arctic, Tibetan Plateau and mid-latitude regions. Snow grain size and snow texture were larger sources of uncertainty in the albedo reduction mentioned in section 3.3.

2.3 Dust, OC, and BC analysis

Before analysis, sampled filters were allowed to dry in an oven for 24 hours and then weighed using a microbalance. The dust mass on the filters was calculated from the mass difference in weight before and after sampling (Kaspari et al., 2014; Li et al., 2017).

There are many methods available for analyzing BC and OC. The three methods considered most effective for measuring BC and water insoluble OC concentrations in snow are thermal optical analysis, filter-based analysis, and single particle soot photometer analysis (Ming et al., 2008). The thermal optical analysis method has been used by many researchers (e.g., Li et al., 2017) and was chosen for the study. This is an indirect method for measuring BC and OC on sampled filters; it follows Beer's law and uses stepwise combustion of the ~~impurities~~ particles deposited on quartz filters (Boparai et al., 2008), followed by measurement of light transmission and/or reflectance of the filters. The BC and OC content present in the collected samples was measured using a thermal optical DRI carbon analyzer, similar to the IMPROVE protocol (Cao et al., 2003). The temperature threshold that was applied to separate the two species is mentioned in Wang et al., 2012. A few (less than ten) filters had higher dust loads; for these the method was slightly modified using a 100% helium atmosphere and temperature plateau (550°C). A very few (less than 5) samples with very dense dust concentrations were not properly analyzed by the instrument and were excluded from the results. The extremely high dust value of one sample from Passu (15 times the level in the next highest sample) which had low values of other pollutants was excluded as a probable error. In some cases, a single sample was analyzed two or three times to ensure accurate results were obtained. Beside this filter based BC, OC and dust analysis

~~2.3.1 Frequency of different aerosol subtypes in the atmosphere~~

the CALIPSO models define multiple aerosol sub-types, with 532-nm (1064 nm) extinction-to-backscatter ratio. The frequency of different aerosol subtypes – clean marine, dust, polluted continental, clean continental, polluted dust, smoke, and other – present in the atmosphere over the study region was investigated using CALIPSO data for the same months in which ice and snow samples were collected i.e. January, May, June, and December – over the period June 2006 to December 2014. ~~The Level 2 aerosol profile data products were downloaded from https://eosweb.larc.nasa.gov/project/calipso/aerosol_profile_table. A set of feature classification flags (including aerosol subtype) detected in different layers of the CALIPSO backscatter data were derived.~~ The CALIPSO Level 2 lidar vertical feature mask data product describes the vertical and horizontal distribution of clouds and aerosol layers (downloaded from https://eosweb.larc.nasa.gov/project/calipso/aerosol_profile_table). On the basis of observed

Formatted: Normal

Formatted: Left, Adjust space between Latin and Asian text, Adjust space between Asian text and numbers

backscatter strength and depolarization, aerosol subtypes have been pre classified in the downloaded data. The details of algorithm used for the classification have been presented in Omar et al., 2009. Percentage contribution of individual aerosol subtypes were plotted using matlab.

The frequencies of different subtypes were calculated along the specific paths followed by CALIPSO over the study region.

2.4 Albedo simulations and estimation of radiative forcing

~~Light absorbing impurities (BC and dust particles) present on surface snow can reduce the snow surface albedo in the visible portion of the electromagnetic spectrum, increase solar radiation absorption, and accelerate melting (Yasunari et al., 2014). SZA, snow grain size, BC and dust concentration in snow, the presence of other light absorbing impurities, particle morphology, surface roughness, snow depth, liquid water content, snow shape, and topography are all important factors in reducing snow albedo (Wiscombe and Warren 1985).~~

Snow albedo was estimated for each of the 18 winter samples and the average calculated for samples at each of the sites (1 to 6). Albedo from two sites – S1 (Sost), which had the highest average concentration of BC and dust, and S6 (Kalam), which had the lowest average concentration of BC and dust – were further explored using the SNICAR model (Flanner et al., 2007). The aim was to quantify the effect of BC, dust, and Mass Absorption Cross section (MAC) on albedo reduction. Sensitivity model experiments were carried out using various combinations of BC, dust, and MAC values, while other parameters were kept constant (parameters for sites 1 and 6 shown in supplementary materials, Table S1). Snow albedo was simulated for different daylight times, with the SZA set in the range 57.0–88.9° based on the position of the sun in the sky for the sampling date and locations. The daily mean was calculated from the mean of the albedo values simulated for 24 different SZA values (one per hour), and the daytime mean from the mean of the albedo values simulated for 10 SZA values (one per hour during daylight). The mid-latitude winter clear-sky option was selected for surface spectral distribution. The parameters used for sensitivity analysis are shown in Table S1. MAC values of 7.5, 11, and 15 m^2/g were selected based on a literature review (Que et al., 2014; Pandolfi et al., 2014). In order to reduce the uncertainty, the dust concentration in the samples was divided into four diameter classes (as per the model requirements): size 1 (0.1–1.0 µm) was taken to be 2%, size 2 (1–2.5 µm) to be 13%, size 3 (2.5–5 µm) to be 31%, and size 4 (5–10 µm) to be 54% of total dust mass present in the sample, based on results published by others (Gillette et al., 1974; Mahowald et al., 2014). Radiative forcing (RF) was estimated for the same samples following Eq. (1):

$$RF_x = R_{in-short} * \Delta \boldsymbol{\alpha}_x \quad (1)$$

where $R_{in\text{-}short}$ denotes incident short-wave solar radiation (daily mean), as measured by the SBDART (Santa Barbara DISORT Atmospheric Radiative Transfer) model, and $\Delta\alpha_x$ denotes the daily mean reduction in albedo, as simulated by the SNICAR model.

Formatted: Justified

2.5 Source regions of pollutants

~~Black carbon particles have a residence time of days to weeks in the atmosphere (Cape et al., 2012) and may be transported a long way away from the source location (Kopacz et al., 2011; Aruna et al., 2013).~~ Three methods were used to identify the potential source regions of pollutants found at the study site: wind maps, emissions inventory coupled with back trajectories, and a region-tagged chemical transport modeling analysis.

~~2.5.1 Wind maps~~

~~Wind speed and direction were represented using the two perpendicular vectors U (the zonal velocity towards the east) and V (the meridional velocity towards the north).~~ Wind vector maps were prepared using ~~50 years of~~MERRA-2 reanalysis data ~~from the joint National Centers for Environmental Prediction and the National Center for Atmospheric Research (NCEP/NCAR) Reanalysis Project~~ (available from the National Aeronautics and Space Administration~~National Oceanic and Atmospheric Administration~~ [N~~O~~AASA] https://gmao.gsfc.nasa.gov/reanalysis/MERRA-2/docs/~~https://www.esrl.noaa.gov/psd/data/gridded/data.ncep.reanalysis.html~~). The U and V wind components were combined into a matrix around the study area for each individual month and then plotted against latitude/longitude values to show the spatial variance of monthly wind stress at ~~700~~ 850 mb using arrows to indicate the direction and intensity of wind.

~~2.5.2 Back air trajectories~~

Air trajectories were calculated backwards from the sampling sites (S1: 36.40°N 74.50°E; S6: 35.46°N 72.54°E) to identify potential source regions for the pollutants using the web version of the Hybrid Single Particle Lagrangian Integrated Trajectory (HYSPLIT-4) model (Draxler and Hess, 1998). The HYSPLIT-4 model has been used by others to compute air mass trajectories to identify possible source regions (Ming et al., 2009; Zhang et al., 2013). Reanalysis meteorological data from the same source as the wind data (https://www.esrl.noaa.gov/psd/data) were used as input data in the HYSPLIT model for May, June, and December 2015, and January 2016. HYSPLIT was run in a seven-day backward trajectory mode with trajectories initiating every six hours (0, 6, 12, and 18) on a daily basis from 4 May to 19 June 2015 (77 days during summer) and from 1 December 2015 to 31 January 2016 (62 during winter). The HYSPLIT model results were combined with Representative Concentration Pathways (RCPs) emission data for 2010 (available from http://sedac.ipcc-data.org/ddc/ar5_scenario_process/RCPs.html) to identify the source location. The data file used as a RCP emission inventory was "RCPs_anthro_BC_2005-2100_95371.nc". This comprises emission~~s~~ pathways starting from identical base year (2000) for multiple pollutants including black carbon and organic carbon. According to the description of the file, biomass burning sources were included in the RCP emission inventory that were utilized with the back-trajectory analysis. RCP had the same emissions sectors as for Hemispheric Transport Air Pollution (HTAP) emission inventory used in the molding part. The emission sectors include~~s~~ fuel combustion, industries, agriculture and livestock. The difference in HTAP and RCP inventories is the

Formatted: Justified

resolution. HTAP had relatively high resolution (0.1 x 0.1 degree) as compared to RCP (0.5 x 0.5 degree). Some discussion related to the inventory and the sectorial detail (12 sectors), which was used for the base year calibration of the RCPs is given in Lamarque et al., 2010.

Monthly CALIPSO satellite based extinction data from 2006 to 2014 were used to calculate the vertical profile for aerosol extinction over the study region. The CALIPSO extinction profile was constructed for selected months – May and June for summer and December and January for winter – in 2006 to 2014 (Figure S1). The exponential equation $X = (\log(10.46) - \log(Y))/10.29$ was used to calculate the extinction profile for the trajectory heights, where Y is the vertical height in kilometers and X indicates the extinction against the height of trajectories. Height of individual trajectory points ~~were~~ was put in the above equation and got a normalized extinction profile by assuming surface extinction =1(Figure S1).

~~2.5.3 WRF-STEM model~~

The WRF-STEM model was used as a third approach for identifying the origin (source regions) of air masses carrying pollutants. Region tagged CO tracer is a standard air quality modeling tool used by other regional and global chemical transport models to identify pollution source regions (Chen et al., 2009; Park et al., 2009; Lamarque and Hess, 2003). The WRF-STEM model uses region tagged carbon monoxide (CO) tracers for many regions in the world to identify geographical areas contributing to observed pollutants (Adhikary et al., 2010). The model domain centered on 50.377° E longitude and 29.917° N latitude. The model horizontal grid resolution was 45x45 km with 200 grids in the east-west direction and 125 north-south. The meteorological variables needed for the chemical transport were derived from the Weather Research and Forecast (WRF) meteorological model (Grell et al., 2005) using FNL data (ds083.2) available from the UCAR website as input data. The main aim of the simulation was to identify the geographic locations contributing to the observed pollutants at the field sites. ~~, thus emissions from open biomass burning were not included in the simulation. The simulations used the anthropogenic emissions from HTAPv2 (available from http://edgar.jrc.ec.europa.eu/htap_v2/), thus the results indicate the amount of pollutants reaching the study area from day-to-day planned and recurring activities in domestic, transport, industrial, and other sectors.~~ The HTAP version 2 emission inventory was used in our WRF-STEM modeling. The HTAP version 2 dataset consists of multiple pollutants including black carbon and organic carbon. This emission inventory include major sectors such as energy, industry, transport, and residential are included except large scale open agricultural and open forest fire burning). The simulations applied in our study used the anthropogenic emissions from HTAP inventory (available from http://edgar.jrc.ec.europa.eu/htap_v2/). So the results indicate the amount of pollutants reaching the study area from day-to-day planned and recurring activities in domestic, transport, industrial, and other sectors.

The model was run for a month prior to the field campaign dates to allow for model spin up (normal practice for a regional chemical transport model), and then for the months of December, January, and June, to match the field campaign dates.

3. Results and discussion

3.1 BC, OC and dust concentrations

Reported concentrations of OC and BC have been field blank subtracted. Total carbon (TC), OC and BC concentration values were blank corrected by subtracting an average of the field blanks. Blank concentrations were used to calculate detection limits as mean ± standard deviation. The minimum, maximum, and average concentrations of BC, OC, and dust in the ice and snow samples are given in Table 1. We represent water insoluble organic carbon as OC in this manuscript. The average BC concentration overall was 2130 ± 1560 ngg^{-1} in summer samples, 2883 ± 3439 ngg^{-1} in autumn samples (both from glaciers), and 992 ± 883 ngg^{-1} in winter samples. The average water insoluble OC concentration overall was 1839 ± 1108 ngg^{-1} in summer samples, 1423 ± 208 ngg^{-1} in autumn samples, and 1342 ± 672 ngg^{-1} in winter samples. There was considerable variation in individual samples, with summer values of BC ranging from 82 ngg^{-1} (Gulkin glacier) to 10,502 ngg^{-1} (Henarche glacier), autumn values from 125 ngg^{-1} (Gulkin glacier) to 6481 ngg^{-1} (Sachin glacier), and winter samples from 79 ngg^{-1} (Kalam) to 5957 ngg^{-1} (Sost).

The lowest BC (82 ngg^{-1}) and OC (128 ngg^{-1}) concentrations were observed in summer samples collected from the Gulkin and Sachin glaciers, respectively. The average values of BC and OC were low in all samples from the Passu glacier, even though it lies close to the Karakoram highway which links Pakistan with China. The low concentrations of BC may have been due to the east facing aspect of the glacier shielding it from pollutants transported from west to east. Slope aspect of a glacier is important for snow cover dynamics (Gul et al., 2017). Dust concentrations are known to vary with slope aspect due to the effects of wind direction on deposition.

The highest average concentration of BC was found in autumn samples from the Sachin glacier, and highest average concentration of OC in summer samples from the same glacier. The average concentration of BC was much greater in autumn than in summer on the Sachin glacier, but somewhat greater in summer than in autumn on the Gulkin glacier, indicating highly spatiotemporal patterns in the deposition of ~~impurities~~particles. The marked difference on the Sachin glacier may have reflected the difference in the direction of air, which comes from Iran and Afghanistan in summer and the Bay of Bengal via India in autumn, with the generally lower deposition on the Gulkin glacier more affected by other factors (such as slope aspect of the glacier and status of local emission near the glacier).

Most summer samples were collected from surface ice (Figure S2a), but a few samples for Gulkin and Sachin were collected from aged snow on the glacier surface (Figure S2 b,c). Dust was visible on the relatively aged snow, and the BC and OC concentrations in these snow samples were much higher than those in ice. The highest average BC values in winter were also observed in aged snow (from Sost) and the lowest in fresh snow (from Kalam) (Table 1). Generally, snow samples collected within 24hours after snowfall event ~~is considering~~considered as a fresh snow.

There was no clear correlation between average BC concentration of glacier samples and glacier elevation, while the winter snow samples showed a weak increasing trend in average BC with site elevation (Table 1, Figure S3). In most cases the concentration of OC was greater than the concentration of BC. In few cases the concentration of BC

Formatted: Normal

was greater than the concentration of OC, which might indicates the contribution of coal combustion and/or biomass burning to the emissions. The reported OC concentration was water insoluble OC. Including the water soluble OC could dominate the temporal variation of the OC/BC ratio. One important factor was post-deposition process, melt water can bring dissolved organic carbon away but not for BC. Low OC/BC ratio may also possible due to the fact that OC and BC had redistributed primarily under the control of strong melt water rather than sublimation and/or dry/wet deposition. The spatio-temporal variability of OC/BC ratio may also indicate the contribution of various sources, seasonal variation and frequent change in wind directions. The OC vs BC correlation in snow and ice samples depend on OC vs BC ratio/concentrations in the atmosphere, post deposition process and then scavenging, enrichment and melt rate of snow/snow after deposition. According to our understanding the analysis method and amount of dust loading on the sample can also alter OC/BC ratio. Further details about OC and BC splitting in thermal optical method are available in Wang et al., 2012.

We analyzed the ratios of OC to BC in the different samples as in atmospheric fractions this can be used as an indicator of the emission source, although apportionment is not simple and only indicative. The BC fraction is emitted during combustion of fossil fuels, especially biomass burning in rural areas in winter, and urban emissions from road transport. The OC fraction can be directly emitted to the atmosphere as particulate matter (primary OC) from fossil fuel emissions, biomass burning, or in the form of biological particles or plant debris; it can also be generated in the atmosphere as gases are converted to particles (secondary OC). In general, lower OC/BC ratios are associated with fossil fuel emissions and higher OC/BC ratios with biomass burning. The lowest OC/BC ratio of 0.041 was observed in a summer sample from Henarche glacier, and the highest ratio of 5 in a winter sample from Kalam. The higher value at Kalam may indicate greater contributions from biomass burning than from fossil fuel combustion in the region. There was no clear correlation between BC and OC concentrations. In summer samples, the average concentration of OC was greater than the average concentration of BC in samples from four of the six glaciers, but it was much lower in Barpu and Henarche. In winter, individual snow samples indicated that concentration of OC was greater than BC at low elevation sites and vice versa; the average OC was greater than average BC at all except the highest elevation site (Table 1).

In deposited samples, low OC/BC ratios can result from a reduction in OC (Niu et al., 2017), greater contributions from BC enrichment and OC scavenging, and/or the contribution of different emission sectors (including quantity, combustion conditions, and fuel type). Often, the OC/BC ratio reflects the impact of dilution of dissolved organic carbon and enrichment of primary organic carbon during snow/ice melting, and differences in OC/BC ratios may reflect differences in the enrichment process. The low OC/BC ratio in the samples from Henarche, the glacier at the lowest elevation, could, for example, be due to preferential washing out of OC particles with meltwater. Overall, there was a higher positive correlation between BC and dust compared to OC suggesting that for BC and dust particle precipitation and enrichment processes were similar.

A wide range of values has been reported by different authors for BC concentrations in snow and ice samples

Formatted: Justified

from different regions (Table S2). The concentrations of BC in our samples were higher than those reported by many authors (Table S2), but were comparable with the results reported by Xu et al. (2012) in the Tien Shan Mountains, Li et al. (2016) in the northeast of the Tibetan plateau, and Wang et al. (2016) in northern China and Zhang et al. (2017) in western Tien Shan, Central Asia. High concentrations indicate high deposition rates on the snow and ice surface, but there are several possible reasons for a wide variation in values apart from differences in deposition rates, including differences in sampling protocols, geographical/sampling location (Qu et al., 2014) and elevation of sampling site, and year/season of sampling. Majority of samples were from the ablation zone of the glaciers. Strong melting of surface snow and ice in the glacier ablation zone could also lead BC enrichment which causes high BC concentrations as Li et al., 2017 observed in the Southern Tibetan Plateau glacier. ~~T~~ The sampling season (May to September in our case) is an important factor because during the melting season rapid enrichment occurs immediately as snow melts. The peak melting period is May to August/September, thus the concentration of BC, OC, and dust in our samples would have been increased as melting progressed due to the enrichment in melting snow and scavenging by the melting water. In most cases snow and ice samples were collected quite a long time after snow fall, and the concentration of pollutants would also have increased in the surface snow and ice due to dry deposition. It seems likely that the pollutants in surface samples would be affected by sublimation and deposition until the next melt season (Yang et al., 2015). In some of the cases in our study, the average concentration of BC, OC, and/or dust for a particular glacier/site was increased as a result of a single highly concentrated sample, reflecting the wide variation that results from the interplay of many factors.

Enrichment is more marked at lower elevations as the temperatures are higher which enhances melting and ageing of surface snow, while deposition also tends to be higher because the pollutant concentrations in the air are higher (~~Wang et al., 2012~~ Wang et al., 2012; Nair et al., 2013). Previous studies have tended to focus on the accumulation area of glaciers (e.g. ice cores and snow pits) where enrichment influences are less marked, and on high elevation areas, where deposition is expected to be lower, in both cases leading to lower values. In our study, the majority of samples collected in summer and autumn were collected from the ablation area of debris-covered glaciers where enrichment influences are marked due to the relatively high temperature, and this is reflected in the relatively high values of BC, OC, and dust. Li et al. (2017) showed a strong negative relationship between the elevation of glacier sampling locations and the concentration of light absorbing ~~impurities~~particles. Stronger melt at lower elevations leads to higher pollutant concentrations in the exposed snow. Equally, BC may be enriched in the lower elevation areas of glaciers as a result of the proximity to source areas, as well as by the higher temperatures causing greater melting. Thus the main reason for the high concentrations of BC, OC, and dust in our samples may have been that the samples were taken from relatively low elevation sites. Human activities near the sampling sites in association with the summer pilgrimage season probably also contributed to an increase in pollutant concentrations. According to our understanding all the glaciers of the whole Karakoram region, may not substantially darkened by BC. Ablation zones of the debris covered glaciers which are relatively at low elevation and near to pollution source may be quite polluted.

3.2 Frequency distribution of aerosol sub types in the atmosphere

~~The frequency of different aerosol subtypes present in the atmosphere over the study region was investigated using CALIPSO subtype aerosol data (clean marine, dust, polluted continental, clean continental, polluted dust, smoke, and other) for January, May, June, and December (the months in which samples were collected) from June 2006 to December 2014. The frequency was calculated along the tracks followed by the CALIPSO satellite.~~ The CALIPSO aerosol type identifications analysis indicated that "smoke" was the most frequent-occurring type of aerosol over the study region during both summer and winter seasons.~~-~~ This result indicate that biomass burning sources may be the dominant contributor in this region. Frequency of sub type aerosol for the month of June in 2006 to 2014 is shown in Figure S4. Figure 2 shows the seasonal results for month of May, June (summer) and December, January (winter) in the form of a box plot. During June smoke had the highest frequency (39%), followed by dust (21%), polluted dust (12%), and others (20%) Figure S4. Overall Smoke, dust and or polluted dust were the dominant subtype aerosols in selected months over the study region. This type of aerosol measurement in the atmosphere is important for our current study because it provides observation based data over the study region. Other approaches used (such as modeling) were based on interpolation not observation. Pollutant deposition depends on the concentration of pollutants in the atmosphere, the results are consistent with the high concentration of BC (from smoke) and dust particles in the glacier and snow surface samples.

3.3 Snow albedo reduction

The albedo of individual winter snow samples was calculated using the SNICAR model and then averaged for each site (S1 to S6). Figure 3a shows the average for each site across the visible and infrared spectrum. Two sites were chosen for further analysis: S1 (Sost) which had the highest average concentration of BC, and S6 (Kalam) which had the lowest average concentration of BC. The albedo was simulated for different MAC values and SZA for samples at the two sites as described in the methods. The values for average albedo of samples from the two sites simulated ~~at a wavelength of 0.975 µm~~ for MAC values of 7.5, 11, and 15 m^2/g and SZA of 57.0–88.9° (day time) under a clear sky ranged from 0.39 (site S1, BC only, midday, MAC 15 m^2/g) to 0.85 (site S6, dust only, early evening, MAC 7.5–15 m^2/g). The albedo reduction values presented here are relative, indicating the difference of albedo with having certain pollutants (BC or dust or both) and a reference albedo (with zero pollutants i.e. zero BC and zero dust concentration). The detailed values are shown in Table S3.

Table 2 show the calculated percentage reduction (compared to a reference value with zero BC, OC, and dust) in daily minimum, maximum, and mean broadband snow albedo at different MAC values (7.5, 11, 15 m^2/g) resulting from the average BC, dust, and combined BC and dust concentrations found in samples at each of the sites. The reduction was strongly dependent on BC concentration and almost independent of dust concentration, and increased with increasing MAC value. The results suggest that BC was the dominant forcing factor, rather than dust, ~~as a result of the rapid snowmelt~~which influence glacial surface albedo and accelerate glacier melt.~~-~~ BC was found to play an important role in forcing in the northern Tibetan plateau (Li et al., 2016), whereas in the central Tibetan plateau and

Himalayas, dust played a more important role (Qu et al., 2014; Kaspari et al., 2014). The MAC value affected the albedo more in the visible range than at 1.2 µm (near infrared) wavelength (Fig 3c, d). The combined concentration of BC and dust, or BC alone, strongly reduced the snow albedo for a given combination of other input parameters. The effect at the low pollutant site (S6) was small: the values for day time snow albedo at 0.975 µm due to BC, or BC plus dust with different MAC and SZA, ranged from 0.70 to 0.83, with a reduction in daily mean albedo of 1.8 to 2.9%, and those for dust alone from 0.79 to 0.85, with a reduction in daily mean albedo of less than 0.1%. The effect at the high pollutant site (S1) was much more marked: BC or BC and dust reduced day time snow albedo to values ranging from 0.39 to 0.64, a reduction in daily mean albedo of 8.8 to 12.0%, but the effect of dust alone was still low with values of 0.70 to 0.78, again a reduction in daily mean albedo of less than 0.1%.

Both the snow albedo and the impact of ~~impurities~~ light absorbing particles depend on a range of factors including the SZA, snow depth, snow grain size, and ~~snow age~~snow density. For example, the snow albedo reduction due to BC is known to be less in the presence of other light absorbing ~~impurities~~ particles as these will absorb some of the available solar radiation (Kaspari et al., 2011). The snow albedo calculated for our samples was strongly dependent on the SZA with albedo increasing with decreasing SZA, especially at near infrared wavelengths (Table S3).

The impact of snow ageing was also investigated. The winter samples from S1 (Sost) were aged snow, whereas those from S6 (Kalam) were fresh snow (Table 1, Figure S5 b,c). Not only was dust clearly visible on the surface of the aged snow, the grain size was large and the snow was dense. The aged snow had a much higher concentration of BC and dust, which reduced the albedo, but the extent of reduction is also affected by other factors. Albedo reduction by BC and dust particles is known to be greater for aged snow than for fresh snow (Warren and Wiscombe, 1985). In our samples, the calculated reduction in snow albedo for high MAC values (15) compared to low MAC values (7.5) was greater in aged snow than in fresh snow (Figure 3b). The effective grain size of snow increases with time as water surrounds the grains. Snow with larger grain size absorbs more radiation because the light can penetrate deeper into the snowpack, thus decreasing surface albedo (Flanner et al., 2006). In the melting season, the snowpack becomes optically thin and more ~~impurities~~ particles are concentrated near the surface layer, which further increases the effect on albedo.

The estimated reduction in snow albedo by dust and BC ~~compounded by the age of snow~~ (up to 29% of daytime maximum value, Table 2) was higher than that reported by others for High Asia based on farmers' recordings (e.g 1.5 to 4.6% reported by Nair et al., 2013) and in the Himalayas (Ming et al., 2008; Kaspari et al., 2014; Gertler et al., 2016). However, although the values were relatively high, they were at the same level or lower than the estimates for albedo reduction of 28% by BC and 56% by dust in clean ice samples, and of 36% by BC and 29% by dust in aged snow samples, reported by Qu et al. (2014) for surface samples from the Zhadang glacier, China. Simulation results by Ming et al. (2013a) showed BC, dust, and grain growth to reduce broadband albedo by 11%, 28%, and 61%, respectively, in a snowpack in central Tibet. Dust was the most significant contributor to albedo reduction when mixed inside the snow and ice, or when the glacier was covered in bare ice. In our case BC was a more influential

445 factor than dust during a similar study period to that reported by Li et al. (2017), indicating that BC plays a major
446 role in albedo reduction.
447 The possible reasons for the relatively high values for albedo reduction in our samples include the lower
448 elevation of the sampling locations, relatively high concentrations of BC and dust, high MAC values, low snow
449 thickness, underlying ground quality, presence of small and large towns near the sampling sites, and predominance
450 of aged snow samples. Most of the samples collected in winter were from places with snow depth less than 50 cm
451 (Figure S5a), thus mud, stones, and clay below the snow layer would be expected to increase the absorption of solar
452 radiation and reduce the albedo.
453 The high albedo reduction in the visible range of the electromagnetic spectrum could be due to the relatively
454 high concentration of surface (~1cm) snow impurities. The total amount of deposited ~~impurities~~ particles in the
455 surface layer of aged snow was relatively high, indicating a high deposition rate of atmospheric pollutants.
456 Flanner et al. (2007) reported that BC emission and snow ageing are the two largest sources of uncertainty in
457 albedo estimates. The uncertainties in our estimated albedo reduction include the BC type (uncoated or sulfate
458 coated), ~~exact snow age,~~ the size distribution of dust concentration, the accuracy of snow grain size, snow texture,
459 snow density, and albedo of the underlying ground. Sulfate-coated particles have an absorbing sulfate shell
460 surrounding the carbon; recent studies confirm that coated BC has a larger absorbing power than non-coated BC
461 (Naoe et al., 2009). We used uncoated black carbon concentration in the SNICAR model, but the pollutants at the
462 remote site are presumed to be mainly from long range transport, thus the BC may have gained some coating. The
463 albedo reduction for sulfate-coated black carbon was calculated to be 3–8.5% higher, depending on the MAC and
464 SZA values, than for uncoated black carbon at low concentrated site S6 (Figure S6). According to our
465 understanding, snow grain size (snow aging) and snow texture are larger sources of uncertainty. The effect of snow
466 grain size is generally larger than the uncertainty in light absorbing particles which varies with the snow type
467 (Schmale et al., 2017). For an effective snow grain radius of 80 μm, 100 μm, 120 μm, the albedo reduction caused
468 by 100 ng g−1 of BC was 0.017, 0.019 and 0.021 respectively. As snow grain size was measured with a hand lens
469 (with reported accuracy of 20 μm), so at least 0.002 uncertainty is present in our albedo results. Snow grain shape
470 was measured with the help of snow card, however grain shape was not used in the online SNICAR albedo
471 simulation model and assumed a spherical shape for the snow grains. Albedo of non-spherical grain is higher than
472 the albedo of spherical grains (Dang et al., 2016). The shapes of snow grains and/or ice crystals is significantly
473 changing with snow age and meteorological conditions during and after snowfall (LaChapelle 1969). Besides this, a
474 number of recent studies (e.g., Flanner et al., 2012; Liou et al., 2014; He et al., 2014, 2017) have shown that both
475 snow grain shape and aerosol-snow internal mixing play important roles in snow albedo calculations.
476

477 **3.4 Radiative forcing (RF)**

478 Radiative forcing (RF) is a measure of the capacity of a forcing agent to affect the energy balance in the

Formatted: Justified

Formatted: Font: 10 pt

atmosphere – the difference between sunlight absorbed by the Earth and energy radiated back to space – thereby contributing to climate change. Changes in albedo contribute directly to radiative forcing: a decrease in albedo means that more radiation will be absorbed and the temperature will rise. In snow and ice, the additional energy absorbed by any pollutants present also increases and accelerates the melting rate.

Various authors have described the impact of albedo change in snow and ice on radiative forcing. Zhang et al. (2017) reported that a reduction in albedo by 9% to 64% can increase the instantaneous radiative forcing by as much as 24.05–323.18 Wm^{-2}. Nair et al. (2013) estimated that in aged snow a BC concentration of 10–200 ngg^{-1} can increase radiative forcing by 2.6 to 28.1 Wm^{-2}; while Yang et al. (2015) reported radiative forcing of 18–21 Wm^{-2} for aged snow in samples from the westernmost Tibetan Plateau. To estimate these radiative forcing measurements, mid-latitude winter with clear sky and cloudy environment was used by Zhang et al. 2017; mid-latitude winter atmospheric conditions was used by Nair et al., 2013; while clear-sky and cloudy conditions environment was used by Yang et al., 2015.

We calculated the radiative forcing in the samples assessed for day time albedo and daily (24h) mean albedo. The radiative forcing at different daylight times caused by BC deposition varied from 3.93 to 43.44 Wm^{-2} (3.93–11.54 Wm^{-2} at the low BC site and 20.88–43.45 Wm^{-2} at the high BC site), and that by dust from 0.16 to 2.08 Wm^{-2} (0.16–0.30 Wm^{-2} at the low BC site and 1.38–2.08 Wm^{-2} at the high BC site) (detailed values given in Table S4), indicating that BC was the dominant factor. The RF due to combined BC and dust was very similar to that for BC alone. Based on optical properties and size distribution of dust particles some studies in past showed higher forcing due to dust as compared to BC (Qu et al., 2014). The increase in daily mean radiative forcing ranged from 0.1% for dust only at the low pollutant site to 14.9% for BC at the high pollutant site. It is important to mention here that dust forcing varies strongly with dust optical properties, source material and particle size distribution. Properties for dust are unique for each of four size bins used in SNICAR online model. These size bins represent partitions of a lognormal size distribution. We used the estimated size of dust particles with generic property of dust in the model. Some dust particles can have a larger impact on snow albedo than the dust applied here (e.g., Aoki et al., 2006; Painter et al., 2007).

Both radiative forcing and albedo reduction increased with decreasing daytime SZA, indicating higher melting at midday compared to morning and evening. Figure 4 shows the daily mean albedo reduction and corresponding radiative forcing caused by BC for fresh (low BC) and aged (high BC) snow with different MAC values. Snow aging (snow grain size) plays an important role in albedo reduction and radiative forcing. Schmale et al., (2017) stating that the effect of snow grain size is generally larger than the uncertainty in light absorbing particles which varies with the snow type. The impact of snow aging factor on BC in snow and induced forcing are complex and had spatial and seasonal variation (Qian et al., 2014). Increase of snow aging factor reduces snow albedo and accelerate the snow melting.

An increase in MAC value from 7.5 to 15 led to an increase in radiative forcing by 1.48 Wm^{-2} in fresh snow and 4.04 Wm^{-2} in aged snow. This suggests that when the surface of snow, ice, and glaciers experience strong melting,

Formatted: Justified, Don't adjust space between Latin and Asian text, Don't adjust space between Asian text and numbers

enrichment with BC and dust could cause more forcing. Previous studies of ice cores and snow pits probably underestimated the albedo reduction and radiative forcing in glacier regions as samples were taken from high elevation areas where there is less ageing and melting and thus lower surface enrichment of BC and dust than at lower elevation. Our results are higher than those reported in other studies on the northern slope of the Himalayas (Ming et al., 2012), western Tibetan Plateau (Yang et al., 2015b), and Tien Shan mountains (Ming et al., 2016). However, they are comparable to values for radiative forcing reported more recently by others, for example for the Muji glacier (Yang et al., 2015), Zhadang glacier (Qu et al., 2014), in high Asia (Flanner et al., 2007; Nair et al., 2013), and in the Arctic (Wang et al., 2011; Flanner, 2013). The results suggest that enrichment of black carbon (in our case) and mineral dust (other authors) can lead to increased absorption of solar radiation, exerting a stronger effect on climate and accelerating glacier melt.

3.5 Potential source regions

3.5.1 Wind vector maps

Figure 5 shows the spatial variance of wind vector maps (U and V) at ~~700~~ 850 mb in May, June, January, and December prepared using ~~50 years of~~MERRA-2 reanalysis data for the year 2015 and 2016. The wind blows primarily from west to east but there were variations over the year. Central ~~and South~~ Asia contributed ~~a large~~ some part of the air in ~~December, January, and~~ May and June. In winter (December and January), the wind blew from Azerbaijan and northwest Iran, reaching the study site via Syria, Iraq, Turkmenistan, and Afghanistan. In May, the prevailing air masses were from Syria, Turkey, Turkmenistan, Iraq, Azerbaijan, northwest Iran, Afghanistan, Nepal, South west China and southern Pakistan. In June, the trend ~~shifted gradually towards~~was almost same as in May ~~air arriving from the east (Myanmar and Thailand) through the Bay of Bengal, India, the Arabian Sea, and southeast Pakistan, especially to lower elevation areas,~~with relatively less contribution from Nepal ~~and~~ and South west China~~becoming dominated by these easterlies in autumn~~. In ~~November~~ January and December, the western trade winds ~~again became~~were stronger than the easterlies.

3.5.2 Coupled emissions inventory with back air trajectory

Trajectory analysis using the HYSPLIT model showed that in May and June 2015 air parcels reached the study site along three different pathways: one from north Asia (Russia) via Central Asia (Kazakhstan), one from western Asia (Cyprus and Syria) via Central and Southern Asia (Georgia), and one via India, which was more local (Figure 6). The trajectories in summer had distinct pathways, while those in winter were dispersed in all directions, partially covering West, East, and South Asia, and completely covering Central Asia. Figure 6 shows the product of extinction and emission calculated along the pathways of trajectories calculated using the vertical profile for aerosol extinction over the study region obtained from the monthly CALIPSO satellite-based extinction data. Scattering and absorption decreased exponentially with increasing elevation (Figure S1) but was still visible at elevations above 5 km in summer.

The RCP emission data combined with back trajectories and extinction data showed that the hotspot regions of pollution that affected the study sites during winter were mainly to the southwest rather than very distant (Figure 6b). Iran, Turkmenistan, Azerbaijan, Georgia, the eastern part of Turkey, and the southwestern part of Russia all showed comparatively high pollutant emissions in winter which moved towards northern Pakistan. The western part of Kazakhstan, Uzbekistan, and northeastern Turkey emitted particularly high concentrations of pollutants.

Combination of the back-trajectory results and surface-wind direction analysis indicated that during the sampling months, aerosols were significantly influenced by the long-range transport of pollutants coming from Central and South Asia, with a small contribution from West and East Asia. This differs somewhat from previous reports which suggested that the Tibetan Plateau and Himalayan region are mainly effected by pollutants from East and South Asia (Zhang et al., 2015). An increasing trend has been reported for black carbon emissions in Central and South Asia over the past 150 years (Bond et al., 2007), and a significant increase has been found in black carbon concentrations in glacier snow in west China in the last 20 years, especially during the summer and monsoon seasons (Ming et al., 2008). In South Asia, the largest source of atmospheric black carbon is emission from biomass and biofuels used for cooking and heating (dung, crop residues, wood) (Venkataraman et al., 2005).

~~BC from East Asia can potentially be lifted up high and transported to the northeast during the summer monsoon season (Zhang et al., 2015). Nevertheless, t~~The results indicate that only a low level of pollutants (minor contribution) reached the study area from ~~this source~~Northwest China. BC particles emitted from distant low latitude source regions such as ~~South~~ tropical Africa barely reach the Tibetan Plateau and Himalayan regions because their ~~weak~~ emissions are removed along the transport pathways during the summer monsoon season (Zhang et al., 2015).

3.5.3 Chemical transport modelling

The contribution of pollutants from potential source regions was also investigated using the WRF-STEM model with tagged carbon monoxide tracers and source regions of East Asia, South Asia, Central Asia, the Middle East, Europe, the Russian Federation, and West Asia. (The individual countries in the regions are listed in Table S5).

Figure 7 shows the results of the model simulations for summer (1 June to 4 July 2015) and winter (15 December 2015 to 17 January 2016) at two glacier sites (Sachin and Shangla) where the model terrain elevation was close to the observation terrain elevation. The model simulations showed Pakistan to be the major contributor of pollutants in summer (77% at Shangla and 43% at Sachin) followed by the South Asian countries; and the south Asian countries in winter (47% at Shangla and 71% at Sachin) followed by Pakistan, which is in line with the findings by Lu et al. (2012) that South Asia contributed 67% black carbon in the Himalayas. There were minor contributions of 2–7% of pollutants from Afghanistan, Iran, Central Asia, and the Middle East, and extremely small amounts from East Asia, Europe, Africa, West Asia, and China. The contribution from Iran, the Middle East, and Europe was greater in winter than in summer, while the contribution from Central Asia and China was greater in summer than in winter. The proportion of daily contributions fluctuated ~~considerable~~considerably: with higher contributions from Iran, the Middle East, and Europe on individual days in winter, ranging for example from 2–30%

for the Middle East.

The concentration of hydrophobic BC (BC1), hydrophilic BC (BC2), and total black carbon (BC = BC1 + BC2) given by the model for Sachin glacier grid point in the summer and winter seasons is shown in supplemental material (Figure S7). Freshly emitted BC particles are hydrophobic and gradually acquire a hygroscopic coating over time in the model. Time series analysis of BC1 and BC2 concentration show influence of both freshly emitted BC as well as aged BC reaching the observation location. The highest concentration of BC1 was observed on 20th December 2015 followed by 25th June 2015, indicating influence of freshly emitted air mass both in the summer as well as winter months. Future study (BC tracer) will evaluate the details of the different source region of BC reaching the glaciers as compared to region tagged CO tracers.

3.5.4 Comparison of the different approaches used to identify potential source regions

The high BC concentration in the atmosphere over the study region was attributed to long-range transport from urban source regions. Potential source regions of the pollutants deposited on glaciers and snow were identified using wind vector mapping with ~~50 years~~ MERRA-2 ~~of~~ reanalyzed data, calculation of back air trajectories using the HYSPLIT-4 model, and chemical transport pathways using the WRF-STEM tagged chemical transport model. The back trajectory results indicated that the majority of pollutants in summer were from Central and South Asia, and in winter from Iran, Pakistan, Iraq, Turkmenistan, Azerbaijan, Georgia, Jordan, Syria, Tunisia, Ukraine, Libya and Egypt. The WRF-STEM model indicated that most anthropogenic pollutants were from Pakistan and South Asia during both summer and winter. However, both approaches showed a reasonable contribution from Central Asian countries and limited contribution from East Asian countries in summer. The wind vector maps also indicated that the study site was mostly effected by westerly winds. All three approaches showed a reasonable contribution from neighboring countries such as Afghanistan, Pakistan, Iran, and India in specific months. Overall, the results indicate that South, Central, and West Asia were the major sources of the pollutants detected at the sampling sites.

There was some mismatching in source regions among the three approaches. The WRF-STEM model and wind vector maps both identified a small contribution from East Asia, but this was not identified in the back trajectories approach. Similarly, the wind vector maps and back air trajectories showed a dominant contribution from the west, while the WRF-STEM model showed a major contribution from Pakistan and South Asia. The differences in the results obtained by the different methods may be due in part to the complex topography of the region and the different altitudes used by the methods; the coarse resolution of the WRF-STEM model; and differences in the emission source inventories and meteorological parameters used by the WRF-STEM and HYSPLIT-4 models. Limitation of using back trajectories to identify source region is explained further in a paper by (Jaffe et al., 1999).

Furthermore, the atmospheric BC concentration over the Himalayas has significant temporal variations associated with synoptic and meso scale changes in the advection pattern (Babu et al., 2011) which can affect pollutant transport and deposition. The large uncertainty among different emission inventories can also affect the results, especially in the Himalayan region.

4 Summary and conclusion

Black carbon (BC) and organic carbon (OC) concentrations were measured using thermal optical analysis of snow and ice surface samples collected from glacier and mountain valleys in northern Pakistan in summer, autumn, and winter. The samples contained high concentrations of BC, OC, and dust in low elevation glaciers and surface snow in mountain valleys. The samples from Sost contained the highest average concentration of BC in mountain valleys snow (winter) and those from Kalam the lowest, probably due to the impact of snow age, increased concentration of black carbon and dust (the Sost samples were aged snow and Kalam samples fresh snow), ~~and increased grain size and density~~. The average concentration of BC in surface samples from Sachin glacier was higher in autumn than in summer; the BC values in summer snow samples collected from Sachin and Gulkin glaciers (aged snow from the glacier surface) were much higher than those in ice. The average BC concentration in summer samples collected from glaciers was 2130 ± 1560 ngg^{-1} and that in autumn samples 2883± 3439ngg^{-1}. The average concentration of OC was 1839 ± 1108 ngg^{-1} in summer samples, 1423 ± 208 ngg^{-1} in autumn samples, and 1342 ± 672 ngg^{-1} in winter samples, with the highest variability in summer samples. The individual lowest BC (82 ngg^{-1}) and OC (129 ngg^{-1}) concentrations were observed in summer samples collected from the Gulkin and Sachin glaciers, respectively. Dust and other pollutants were clearly visible on aged snow and ice surfaces; the results indicate considerable enrichment during ageing. The pollutant concentrations in our samples were relatively higher than those reported by others in earlier studies, which tended to focus on the accumulation area of glaciers (e.g. ice cores and snow pits), where enrichment influences are less marked and measured values are likely to be lower, and high elevation areas, where deposition of pollutants is expected to be lower. It is likely that pollutant concentrations were underestimated in these earlier studies, particularly when there was strong surface melting.

Snow albedo was calculated for winter samples using the SNICAR model with various combinations of BC and dust concentrations, three values for MAC, and a range of values for SZA (57 – 88.89º during daytime), with other parameters kept constant. BC was the major component responsible for albedo reduction, dust had little effect. The reduction by BC ranged from 2.8 to 32.5% during daytime, which is quite high, with albedo reduced to below 0.6. The reduction was greater for higher concentrations of BC and greater MAC. The reduction in 24 h average albedo ranged from <0.07–2.9% for fresh snow samples and <0.05–12.0% for aged snow. Changes in albedo contribute directly to radiative forcing: a decrease in albedo means that more radiation will be absorbed and the temperature will rise. The radiative forcing by BC was also higher than that caused by dust, indicating that BC was the dominant factor. The day time albedo values in winter snow samples ranged from 0.39 to 0.82 with BC alone or BC plus dust, and from 0.70 to 0.85 with dust alone; the corresponding radiative forcing was 3.93–43.44 Wm^{-2} for BC alone, 4.01–43.45 Wm^{-2} for BC and dust, and 0.16–2.08 Wm^{-2} with dust alone. The radiative forcing calculated from the daily mean albedo reduction ranged from 0.1% for dust only at the low pollutant site to 14.9% for BC at the high pollutant site.

The potential source regions of the pollutants deposited on glaciers and snow were identified using spatial variance in wind vector maps, emission inventories coupled with back air trajectories, and region tagged chemical

transport modelling. The wind vector maps identified Central Asian and South Asian countries (such as Azerbaijan, Turkmenistan, Pakistan, Afghanistan, Syria, Iraq, Turkey) as more important. The trajectory analysis coupled with emission inventories showed that air parcels reached northern Pakistan along three pathways, one from north Asia (Russia) via Central Asia (Kazakhstan), one from western Asia (Cyprus and Syria) via Central and Southern Asia (Georgia), and one via India. Combination of the back-trajectory results and surface-wind direction analysis indicated that aerosols were significantly influenced by the long-range transport of pollutants from Central and South Asia. The region tagged chemical transport model indicated that Pakistan and South Asia were the main contributors of pollutants. Analysis based on the WRF-STEM model identified a significant contribution from Pakistan (up to 77%) and South Asia (up to 71%) at selected sites. Overall, the results indicate that Central, South, and West Asia were the major sources of the pollutants detected at the sampling sites, with only a small contribution from East Asia.

The overall precision in the BC, OC and TC concentrations was estimated considering the analytical precision of concentration measurements and mass contributions from field blanks. Uncertainty of the BC and OC mass concentrations was measured through the standard deviation of the field blanks, experimentally determined analytical uncertainty, and projected uncertainty associated with filter extraction. According to our understanding the major uncertainty in our study was the dust effect on BC/OC measurement. Warming role of OC was also not included in the current research which was low, but significant in several regions (Yasunari et al. 2015). Beside this we think snow grain size (snow aging) and snow texture were larger sources of uncertainty in the albedo reduction / radiative forcing calculations ~~than indicated~~. The measured grain size was usually different from the effective optical grain size used in the SNICAR modeling. Snow grain shape was measured with the help of snow card, but was not used in the online SNICAR albedo simulation model and assumed a spherical shape for the snow grains which may slightly affect the results, because albedo of non-spherical grain is higher than the albedo of spherical grains (Dang et al., 2016). On modeling side the possible uncertainties are related to using CO as a tracer for light absorbing particles source region. Uncertainties are also attributed to errors in emissions inventories, simulated meteorology and removal processes built in the model. The physics and chemistry of removal for BC and CO are different from each other especially during wet seasons. We analyze the model during pre-monsoon and relatively dry periods, so we are expecting relatively good correlation in transport between CO and BC. While using global emission inventories we were unable to capture emissions at local scale. Contributions of local sources may be underestimated by coarse-resolution models. Therefore high resolution models and emission inventories at local scale are required to capture local emissions. Better-constrained measurements are required in the future for more robust results. High resolution satellite imagery, high resolution models and continuous monitoring can help us to reduce the present uncertainty.

Acknowledgments

This study was supported by the National Natural Science Foundation of China (41630754, 41671067, and 41501063), the Chinese Academy of Sciences (KJZD-EW-G03-04), the State Key Laboratory of Cryosphere Science (SKLCS-ZZ-2015), program funding to ICIMOD from the Governments of Sweden and Norway, and ICIMOD core funds contributed by the Governments of Afghanistan, Australia, Austria, Bangladesh, Bhutan, China, India, Myanmar, Nepal, Norway, Pakistan, Switzerland, and the United Kingdom. The authors wish to thank the unknown reviewers for their invaluable comments and advice on an earlier draft.

References

Adhikary, B., Carmichael, G. R., Kulkarni, S., Wei, C., Tang, Y., D'Allura, a., Mena-Carrasco, M., Streets, D. G., Zhang, Q., Pierce, R. B., Al-Saadi, J. a., Emmons, L. K., Pfister, G. G., Avery, M. a., Barrick, J. D., Blake, D. R., Brune, W. H., Cohen, R. C., Dibb, J. E., Fried, a., Heikes, B. G., Huey, L. G., O'Sullivan, D. W., Sachse, G. W., Shetter, R. E., Singh, H. B., Campos, T. L., Cantrell, C. a., Flocke, F. M., Dunlea, E. J., Jimenez, J. L., Weinheimer, a. J., Crounse, J. D., Wennberg, P. O., Schauer, J. J., Stone, E. a., Jaffe, D. a. and Reidmiller, D. R.: A regional scale modeling analysis of aerosol and trace gas distributions over the eastern Pacific during the INTEX-B field campaign, Atmos. Chem. Phys., 10(5), 2091–2115, doi:10.5194/acp-10-2091-2010, 2010.

Aoki, T., Kuchiki, K., Niwano, M., Kodama, Y., Hosaka, M. and Tanaka, T.: Physically based snow albedo model for calculating broadband albedos and the solar heating profile in snowpack for general circulation models, J. Geophys. Res. Atmos., 116(11), 1–22, doi:10.1029/2010JD015507, 2011.

~~Aruna, K., Kumar, T. V. L., Rao, D. N., Murthy, B. V. K., Babu, S. S. and Moorthy, K. K.: Black carbon aerosols in a tropical semi-urban coastal environment: Effects of boundary layer dynamics and long range transport, J. Atmos. Solar-Terrestrial Phys., 104(March), 116–125, doi:10.1016/j.jastp.2013.08.020, 2013.~~

Babu, S. S., Chaubey, J. P., Krishna Moorthy, K., Gogoi, M. M., Kompalli, S. K., Sreekanth, V., Bagare, S. P., Bhatt, B. C., Gaur, V. K., Prabhu, T. P. and Singh, N. S.: High altitude (~4520 m amsl) measurements of black carbon aerosols over western trans-Himalayas: Seasonal heterogeneity and source apportionment, J. Geophys. Res. Atmos., 116(24), 1–15, doi:10.1029/2011JD016722, 2011.

Bond, T. C., Bhardwaj, E., Dong, R., Jogani, R., Jung, S., Roden, C., Streets, D. G. and Trautmann, N. M.: Historical emissions of black and organic carbon aerosol from energy-related combustion, 1850-2000, Global Biogeochem. Cycles, 21(2), 1–16, doi:10.1029/2006GB002840, 2007.

Boparai, P., Lee, J. and Bond, T. C.: Revisiting Thermal-Optical Analyses of Carbonaceous Aerosol Using a Physical Model, Aerosol Sci. Technol., 42(11), 930–948, doi:10.1080/02786820802360690, 2008.

Cao, J. J., Lee, S. C., Ho, K. F., Zhang, X. Y., Zou, S. C., Fung, K., Chow, J. C. and Watson, J. G.: Characteristics of carbonaceous aerosol in Pearl River Delta Region, China during 2001 winter period, Atmos. Environ., 37(11), 1451–1460, doi:10.1016/S1352-2310(02)01002-6, 2003.

~~Cape J. N., Coyle. M., Dumitrean, P.: The atmospheric lifetime of black carbon, J. Atmospheric Environment, Volume 59, doi.org/10.1016/j.atmosenv.2012.05.030, 2012.~~

Chen, D., Wang, Y., Mcelroy, M. B., He, K., Yantosca, R. M. and Sager, P. Le: and Physics Regional CO pollution and export in China simulated by the high-resolution nested-grid GEOS-Chem model, , (2008), 3825–3839, 2009.

Cong, Z., Kawamura, K., Kang, S., Fu, P., River, G., River, Y. and River, Y.: Penetration of biomass-burning emissions from South Asia through the Himalayas : new insights from, , 1–7, doi:10.1038/srep09580, 2015.

Dang, C., et al. (2016), Effect of Snow Grain Shape on Snow Albedo. J. Atmos. Sci., 73, 3573–3583, doi:10.1175/JAS-D-15-0276.1

Déry, S. J. and Brown, R. D.: Recent Northern Hemisphere snow cover extent trends and implications for the snow-albedo feedback, Geophys. Res. Lett., 34(22), 2–7, doi:10.1029/2007GL031474, 2007.

Doherty, S. J., Grenfell, T. C., Forsström, S., Hegg, D. L., Brandt, R. E. and Warren, S. G.: Observed vertical redistribution of black carbon and other insoluble light-absorbing particles in melting snow, J. Geophys. Res. Atmos., 118(11), 5553–5569, doi:10.1002/jgrd.50235, 2013.

Draxler, R. R. and Hess, G. D.: An Overview of the HYSPLIT_4 Modelling System for Trajectories, Dispersion, and Deposition, Aust. Meteorol. Mag., 47(February), 295–308, 1998.

Fitzgerald, W. F.: Clean hands, dirty hands: Clair Patterson and the aquatic biogeochemistry of mercury, Clean Hands, Clair Patterson's Crusade Against Environmental Lead Contamination, 119–137, 1999.

Flanner, M. G.: Arctic climate sensitivity to local black carbon, J. Geophys. Res. Atmos., 118(4), 1840–1851, doi:10.1002/jgrd.50176, 2013.

Flanner, M. G. and Zender, C. S.: Linking snowpack microphysics and albedo evolution, J. Geophys. Res. Atmos., 111(12), 1–12, doi:10.1029/2005JD006834, 2006.

Flanner, M. G., Zender, C. S., Randerson, J. T. and Rasch, P. J.: Present-day climate forcing and response from black carbon in snow, J. Geophys. Res. Atmos., 112(11), 1–17, doi:10.1029/2006JD008003, 2007.

Flanner, M. G., Zender, C. S., Hess, P. G., Mahowald, N. M., Painter, T. H., Ramanathan, V. and Rasch, P. J.: Springtime warming and reduced snow cover from carbonaceous particles, Atmos. Chem. Phys. Discuss., 8(6), 19819–19859, doi:10.5194/acpd-8-19819-2008, 2009.

Gertler, C. G., Puppala, S. P., Panday, A., Stumm, D. and Shea, J.: Black carbon and the Himalayan cryosphere: A review, Atmos. Environ., 125(SEPTEMBER), 404–417, doi:10.1016/j.atmosenv.2015.08.078, 2016.

Gillette, D.A., Blifford, I.H., Fryrear, D.W.: Influence of wind velocity on size distributions of aerosols generated by wind erosion of soils. J. Geophys. Res. 79, 4068–4075, doi: 10.1029/JC079i027p04068, 1974.

Grell, G. A., Peckham, S. E., Schmitz, R., McKeen, S. A., Frost, G., Skamarock, W. C. and Eder, B.: Fully coupled chemistry within the WRF model, Atmos. Environ., 39(37), 6957–6975, doi:DOI: 10.1016/j.atmosenv.2005.04.027, 2005.

Gul, C., Kang, S. et al.: Using Landsat images to monitor changes in the snow-covered area of selected glaciers in

Formatted: Font color: Auto

752 northern Pakistan, Journal of Mountain Science, DOI：10.1007/s11629-016-4097-x.2017.
753 Hansen, J. and Nazarenko, L.: Soot climate forcing via snow and ice albedos, Proc. Natl. Acad. Sci. U. S. A., 101(2),
754 423–428, doi:10.1073/pnas.2237157100, 2004.
755 Hansen, J., Sato, M., Ruedy, R., Nazarenko, L., Lacis, A., Schmidt, G. A., Bell, N.:Climate and Dynamics-D18104-
756 Efficacy of climate forcings, J. Geophys. Res., Part D-Atmospheres, 110(18), doi: 10.
757 1029/2005JD005776, 2005.
758 Immerzeel, W. W., van Beek, L. P. H. and Bierkens, M. F. P.: Climate change will affect the Asian water towers.,
759 Science, 328(5984), 1382–5, doi:10.1126/science.1183188, 2010.
760 Jacobson, M. Z.: Climate response of fossil fuel and biofuel soot, accounting for soot's feedback to snow and sea ice
761 albedo and emissivity, J. Geophys. Res., 109, D21201, doi:10.1029/2004JD004945, 2004
762 Jaffe, D., Anderson, T., Covert, D., Kotchenruther, R., Trost, B., Danielson, J., Simpson, W., Blake, D., Harris, J. and
763 Carmichael, G.: Transport of Asian Air Pollution to North America, , 26(6), 711–714, 1999.
764 Kaspari, S., Painter, T. H., Gysel, M., Skiles, S. M. and Schwikowski, M.: Seasonal and elevational variations of
765 black carbon and dust in snow and ice in the Solu-Khumbu, Nepal and estimated radiative forcings, Atmos.
766 Chem. Phys., 14(15), 8089–8103, doi:10.5194/acp-14-8089-2014, 2014.
767 Kaspari, S. D., Schwikowski, M., Gysel, M., Flanner, M. G., Kang, S., Hou, S. and Mayewski, P. A.: Recent
768 increase in black carbon concentrations from a Mt. Everest ice core spanning 1860-2000 AD, Geophys. Res.
769 Lett., 38(4), 11–16, doi:10.1029/2010GL046096, 2011.
770 Lamarque, J. and Hess, P. G.: Model analysis of the temporal and geographical origin of the CO distribution during
771 the TOPSE campaign, , 108, 1–12, doi:10.1029/2002JD002077, 2003.
772 Lamarque, J.-F., Bond, T.C., Eyring, V., Granier, C., et al.: Historical (1850–2000) gridded anthropogenic and
773 biomass burning emissions of reactive gases and aerosols: methodology and application, Atmos. Chem. Phys.,
774 10, 7017–7039, doi:10.5194/acp-10-7017-2010.
775 Li, X., Kang, S., He, X., Qu, B., Tripathee, L., Jing, Z., Paudyal, R., Li, Y., Zhang, Y., Yan, F., Li, G. and Li, C.:
776 Light-absorbing impurities accelerate glacier melt in the Central Tibetan Plateau, Sci. Total Environ.,
777 doi:10.1016/j.scitotenv.2017.02.169, 2017.
778 Li, Y., Chen, J., Kang, S., Li, C., Qu, B., Tripathee, L., Yan, F., Zhang, Y., Guo, J., Gul, C. and Qin, X.: Impacts of
779 black carbon and mineral dust on radiative forcing and glacier melting during summer in the Qilian Mountains,
780 northeastern Tibetan Plateau, Cryosph. Discuss., (April), 1–14, doi:10.5194/tc-2016-32, 2016.
781 Lu, Z., Streets, D. G., Zhang, Q. and Wang, S.: A novel back-trajectory analysis of the origin of black carbon
782 transported to the Himalayas and Tibetan Plateau during 1996-2010, Geophys. Res. Lett., 39(1), 1–6,
783 doi:10.1029/2011GL049903, 2012.
784 Lüthi, Z. L., Škerlak, B., Kim, S. W., Lauer, A., Mues, A., Rupakheti, M. and Kang, S.: Atmospheric brown clouds
785 reach the Tibetan Plateau by crossing the Himalayas, Atmos. Chem. Phys., 15(11), 6007–6021, doi:10.5194/acp-
786 15-6007-2015, 2015.

Mahowald, N., Albani, S., Kok, J. F., Engelstaeder, S., Scanza, R., Ward, D. S. and Flanner, M. G.: The size distribution of desert dust aerosols and its impact on the Earth system, Aeolian Res., 15, 53–71, doi:10.1016/j.aeolia.2013.09.002, 2014.

Ménégoz, M., Krinner, G., Balkanski, Y., Cozic, a., Boucher, O. and Ciais, P.: Boreal and temperate snow cover variations induced by black carbon emissions in the middle of the 21st century, Cryosph., 7, 537–554, doi:10.5194/tc-7-537-2013, 2013.

Ménégoz, M., Krinner, G., Balkanski, Y., Boucher, O., Cozic, A., Lim, S., Ginot, P., Laj, P., Gallée, H., Wagnon, P., Marinoni, A. and Jacobi, H. W.: Snow cover sensitivity to black carbon deposition in the Himalayas: From atmospheric and ice core measurements to regional climate simulations, Atmos. Chem. Phys., 14(8), 4237–4249, doi:10.5194/acp-14-4237-2014, 2014.

Ming, J., Cachier, H., Xiao, C., Qin, D., Kang, S., Hou, S. and Xu, J.: Black carbon record based on a shallow Himalayan ice core and its climatic implications, Atmos. Chem. Phy., 8, 1343–1352, doi:10.5194/acpd-7-14413-2007, 2008.

Ming, J., Xiao, C., Cachier, H., Qin, D., Qin, X., Li, Z. and Pu, J.: Black Carbon (BC) in the snow of glaciers in west China and its potential effects on albedos, Atmos. Res., 92(1), 114–123, doi:10.1016/j.atmosres.2008.09.007, 2009.

Ming, J., Xiao, C., Du, Z. and Yang, X.: An overview of black carbon deposition in High Asia glaciers and its impacts on radiation balance, Adv. Water Resour., 55(May), 80–87, doi:10.1016/j.advwatres.2012.05.015, 2013a.

Ming, J., Du, Z., Xiao, C., Xu, X., and Zhang, D.: Darkening of the mid-Himalaya glaciers since 2000 and the potential causes, Environ. Res. Lett., 7, 014021, doi:10.1088/1748-9326/7/1/014021, 2012.

Ming, J., Xiao, C., Wang, F., Li, Z. and Li, Y.: Grey Tienshan Urumqi Glacier No.1 and light-absorbing impurities, Environ. Sci. Pollut. Res., 23(10), 9549–9558, doi:10.1007/s11356-016-6182-7, 2016.

Nair, V. S., Babu, S. S., Moorthy, K. K., Sharma, A. K., Marinoni, A. and Ajai: Black carbon aerosols over the Himalayas: Direct and surface albedo forcing, Tellus, Ser. B Chem. Phys. Meteorol., 65(1), doi:10.3402/tellusb.v65i0.19738, 2013.

Naoe, H., Hasegawa, S., Heintzenberg, J., Okada, K., Uchiyama, A., Zaizen, Y., Kobayashi, E., Yamazaki, A.: State of mixture of atmospheric submicrometer black carbon particles and its effect on particulate light absorption, Atmos. Environ., 43(6), 1296–1301, doi:org/10.1016/j.atmosenv.2008.11.031, 2009.

Niu, H., Kang, S., Shi, X., Paudyal, R., He, Y., Li, G. and Wang, S.: Science of the Total Environment In-situ measurements of light-absorbing impurities in snow of glacier on Mt . Yulong and implications for radiative forcing estimates, Sci. Total Environ., 581–582, 848–856, doi:10.1016/j.scitotenv.2017.01.032, 2017.

Novakov, T., Menon, S., Kirchstetter, T. W., Koch, D. and Hansen, J. E.: Aerosol organic carbon to black carbon ratios : Analysis of published data and implications for climate forcing of soot emissions maybe a useful approach to slow global warming ., , 110, 1–13, doi:10.1029/2005JD005977, 2005.

Painter, T. H., Deems, J. S., Belnap, J., Hamlet, A. F., Landry, C. C. and Udall, B.: Response of Colorado River

Formatted: Font: Times New Roman, 10 pt

runoff to dust radiative forcing in snow., Proc. Natl. Acad. Sci. U. S. A., 107(40), 17125–30, doi:10.1073/pnas.0913139107, 2010.

Painter, T. H., Barrett, A. P., Landry, C. C., Neff, J. C., Cassidy, M. P., Lawrence, C. R., McBride, K. E. and Farmer, G. L.: Impact of disturbed desert soils on duration of mountain snow cover, Geophys. Res. Lett., 34(12), 1–6, doi:10.1029/2007GL030284, 2007.

Pandolfi, M., Ripoll, A., Querol, X. and Alastuey, A.: Climatology of aerosol optical properties and black carbon mass absorption cross section at a remote high-altitude site in the western Mediterranean Basin, Atmos. Chem. Phys., 14(12), 6443–6460, doi:10.5194/acp-14-6443-2014, 2014.

Park, M., Randel, W. J., Emmons, L. K. and Livesey, N. J.: Transport pathways of carbon monoxide in the Asian summer monsoon diagnosed from Model of Ozone and Related Tracers (MOZART), , 114, 1–11, doi:10.1029/2008JD010621, 2009.

Qian Y, TJ Yasunari, SJ Doherty, MG Flanner, WK Lau, J Ming, H Wang, M Wang, SG Warren, and R Zhang. 2015. "Light-absorbing Particles in Snow and Ice: Measurement and Modeling of Climatic and Hydrological Impact." Advances in Atmospheric Sciences 32(1):64-91. doi:10.1007/s00376-014-0010-0.

Qian Y, H Wang, R Zhang, MG Flanner, and PJ Rasch. 2014. "A Sensitivity Study on Modeling Black Carbon in Snow and its Radiative Forcing over the Arctic and Northern China." Environmental Research Letters 9(6):Article No. 064001. doi:10.1088/1748-9326/9/6/064001.

Qian Y, MG Flanner, LYR Leung, and W Wang. 2011. "Sensitivity studies on the impacts of Tibetan Plateau snowpack pollution on the Asian hydrological cycleand monsoon climate." Atmospheric Chemistry and Physics 11(5):1929-1948. doi:10.5194/acp-11-1929-2011

Qu, B., Ming, J., Kang, S. C., Zhang, G. S., Li, Y. W., Li, C. D., Zhao, S. Y., Ji, Z. M. and Cao, J. J.: The decreasing albedo of the Zhadang glacier on western Nyainqentanglha and the role of light-absorbing impurities, Atmos. Chem. Phys., 14(20), 11117–11128, doi:10.5194/acp-14-11117-2014, 2014.

Venkataraman, C., Habib, G., Eiguren-Fernandez, A., Miguel, A, H., Friedlander, S, K.:Residential Biofuels in South Asia: Carbonaceous Aerosol Emissions and Climate Impacts, Science, 307 (5714), 1454-1456, doi: 10.1126/science.1104359, 2005.

Wang, J., He, X., Ye, B., and Yang, G.: Variations of Albedo on the Dongkemadi Glacier, Tanggula Range, Journal of Glaciology and Geocryology, 34, 21–28, 2012.

~~Venkataraman, C., Habib, G., Eiguren-Fernandez, A., Miguel, A, H., Friedlander, S, K.:Residential Biofuels in South Asia: Carbonaceous Aerosol Emissions and Climate Impacts, Science, 307 (5714), 1454-1456, doi: 10.1126/science.1104359, 2005.~~

Wang, M., Xu, B., Zhao, H., Cao, J., Joswiak, D., Wu, G. and Lin, S.: The Influence of Dust on Quantitative

Formatted: Indent: Left: 0", Hanging: 0.2", Line spacing: 1.5 lines, Adjust space between Latin and Asian text, Adjust space between Asian text and numbers

Measurements of Black Carbon in Ice and Snow when Using a Thermal Optical Method, Aerosol Sci. Technol., 46 (April 2017), 60–69, doi:10.1080/02786826.2011.605815, 2012.

Wang M, B Xu, J Cao, X Tie, H Wang, R Zhang, Y Qian, PJ Rasch, S Zhao, G Wu, H Zhao, DR Joswiak, J Li, and Y Xie. 2015. "Carbonaceous Aerosols Recorded in a Southeastern Tibetan Glacier: Analysis of Temporal Variations and Model Estimates of Sources and Radiative Forcing." Atmospheric Chemistry and Physics 15:1191-1204. doi:10.5194/acp-15-1191-2015.

Wang, Q., Jacob, D. J., Fisher, J. A., Mao, J., Leibensperger, E. M., Carouge, C. C., Le Sager, P., Kondo, Y., Jimenez, J. L., Cubison, M. J. and Doherty, S. J.: Sources of carbonaceous aerosols and deposited black carbon in the Arctic in winter-spring: Implications for radiative forcing, Atmos. Chem. Phys., 11(23), 12453–12473, doi:10.5194/acp-11-12453-2011, 2011.

Wang, X., Pu, W., Ren, Y., Zhang, X., Zhang, X., Shi, J., Jin, H., Dai, M. and Chen, Q.: Snow albedo reduction in seasonal snow due to anthropogenic dust and carbonaceous aerosols across northern China, Atmos. Chem. Phys. Discuss., (September), 1–52, doi:10.5194/acp-2016-667, 2016.

Warren, S. G.: Optical Properties of Snow (Paper 1R1505), Rev. Geophys. Sp. Phys., 20(1), 67 [online] Available from: http://adsabs.harvard.edu/cgi-bin/nph-data_query?bibcode=1982RvGSP..20...67W&link_type=EJOURNAL%5Cnpapers3://publication/doi/10.1029/RG020i001p00067, 1982.

Warren, S. G. and Wiscombe, W. J.: Dirty snow after nuclear war, Nature, 313, 467–470, doi:10.1038/313467a0, 1985.

Xu, B., Cao, J., Hansen, J., Yao, T., Joswia, D. R., Wang, N., Wu, G., Wang, M., Zhao, H., Yang, W., Liu, X. and He, J.: Black soot and the survival of Tibetan glaciers, Proc. Natl. Acad. Sci., 106(52), 22114–22118, doi:10.1073/pnas.0910444106, 2009a.

Xu, B., Cao, J., Joswiak, D. R., Liu, X., Zhao, H. and He, J.: Post-depositional enrichment of black soot in snow-pack and accelerated melting of Tibetan glaciers, Environ. Res. Lett., 7(1), 14022, doi:10.1088/1748-9326/7/1/014022, 2012.

Yang, S., Xu, B., Cao, J., Zender, C. S. and Wang, M.: Climate effect of black carbon aerosol in a Tibetan Plateau glacier, Atmos. Environ., 111, 71–78, doi:10.1016/j.atmosenv.2015.03.016, 2015.

Yasunari, T. J., Bonasoni, P., Laj, P., Fujita, K., Vuillermoz, E., Marinoni, A., Cristofanelli, P., Duchi, R., Tartari, G. and Lau, K. M.: Estimated impact of black carbon deposition during pre-monsoon season from Nepal Climate Observatory - Pyramid data and snow albedo changes over Himalayan glaciers, Atmos. Chem. Phys., 10(14), 6603–6615, doi:10.5194/acp-10-6603-2010, 2010.

~~Yasunari, T. J., Lau, K.-M., Mahanama, S. P. P., Colarco, P. R., Silva, A. M. Da, Aoki, T., Aoki, K., Murao, N., Yamagata, S. and Kodama, Y.: The GOddard SnoW Impurity Module (GOSWIM) for the NASA GEOS-5 Earth System Model: Preliminary Comparisons with Observations in Sapporo, Japan, Sola, 10(MAY), 50–56,~~

Formatted: Indent: Left: 0", Hanging: 0.2", Line spacing: 1.5 lines, Adjust space between Latin and Asian text, Adjust space between Asian text and numbers

~~doi:10.2151/sola.2014-011, 2014.~~

Yasunari, T. J., Lau, K.-M., Mahanama, S. P. P., Colarco, P. R., Silva, A. M. Da, Aoki, T., Aoki, K., Murao, N., Yamagata, S. and Kodama, Y.: The GOddard SnoW Impurity Module (GOSWIM) for the NASA GEOS-5 Earth System Model: Preliminary Comparisons with Observations in Sapporo, Japan, Sola, 10(MAY), 50–56, doi:10.2151/sola.2014-011, 2014.

Zhang, G., Kang, S., Fujita, K., Huintjes, E., Xu, J., Yamazaki, T., Haginoya, S., Wei, Y., Scherer, D., Schneider, C. and Yao, T.: Energy and mass balance of Zhadang glacier surface, central Tibetan Plateau, J. Glaciol., 59(213), 137–148, doi:10.3189/2013JoG12J152, 2013.

Zhang, Y., Kang, S., Xu, M., Sprenger, M., Gao, T., Cong, Z., Li, C., Guo, J., Xu, Z., Li, Y., Li, G., Li, X., Liu, Y. and Han, H.: Sciences in Cold and Arid Regions Light-absorbing impurities on Keqikaer Glacier in western Tien Shan : concentrations and potential impact on albedo reduction, , 9(2), doi:10.3724/SP.J.1226.2017.00097.Light-absorbing, 2017.

Zhang, Y., Hirabayashi, Y., Liu, Q. and Liu, S.: Glacier runoff and its impact in a highly glacierized catchment in the southeastern Tibetan Plateau: Past and future trends, J. Glaciol., 61(228), 713–730, doi:10.3189/2015JoG14J188, 2015.

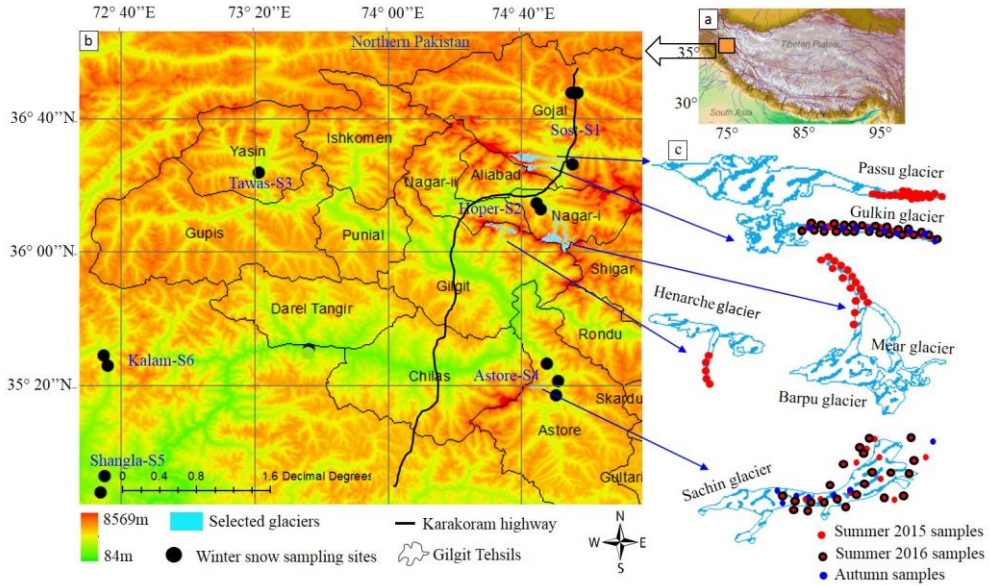

Figure 1. The study area and sampling sites: (a) Himalayan mountain range and Tibetan Plateau, (b) winter sampling sites (solid black circles), (c) glaciers selected for summer and autumn sampling

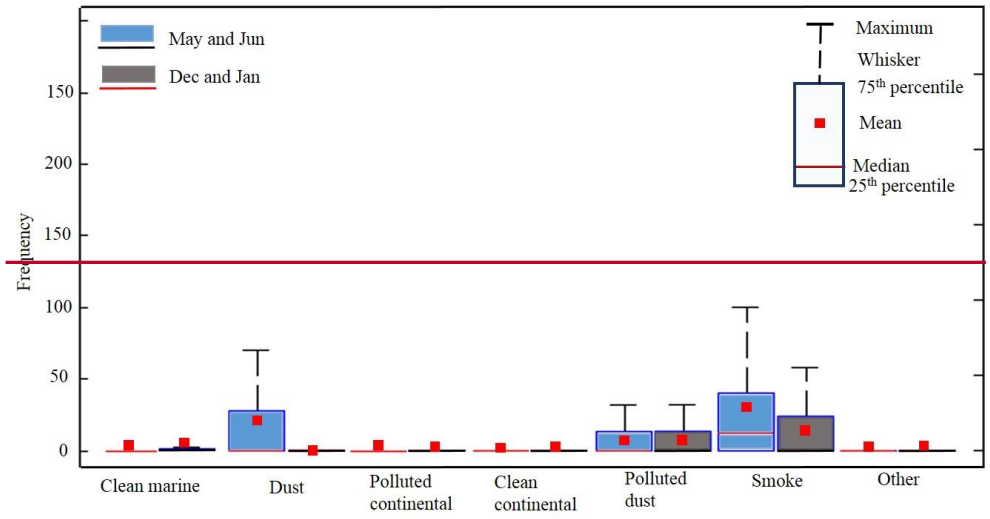
May and Jun
Dec and Jan
Maximum
Whisker
75th percentile
Mean
Median
25th percentile
Frequency
150
200
150
100
50
0
Clean marine
Dust
Polluted continental
Clean continental
Polluted dust
Smoke
Other

913

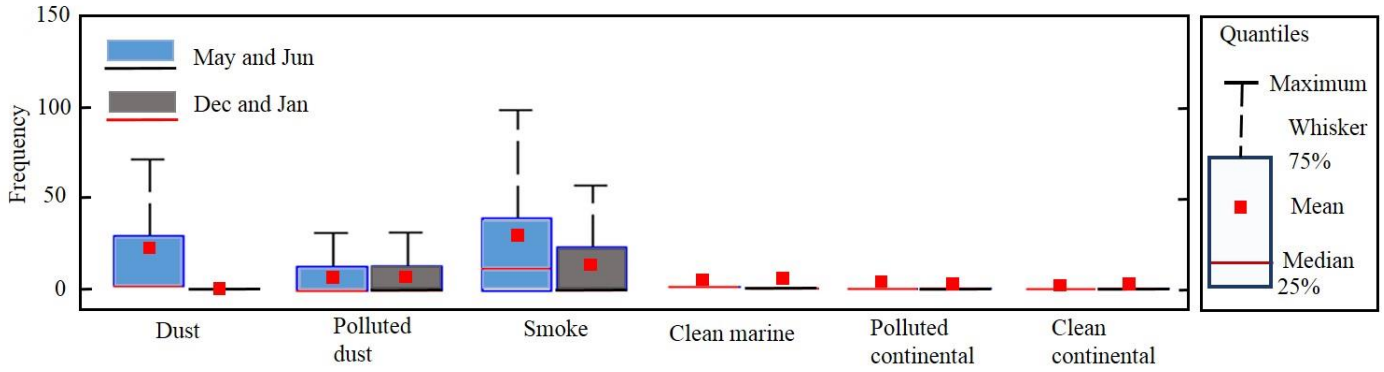

914

915 **Figure 2. Frequency distribution of aerosol subtypes in the atmosphere over the study region calculated from CALIPSO data for the months in 2006 to 2014**

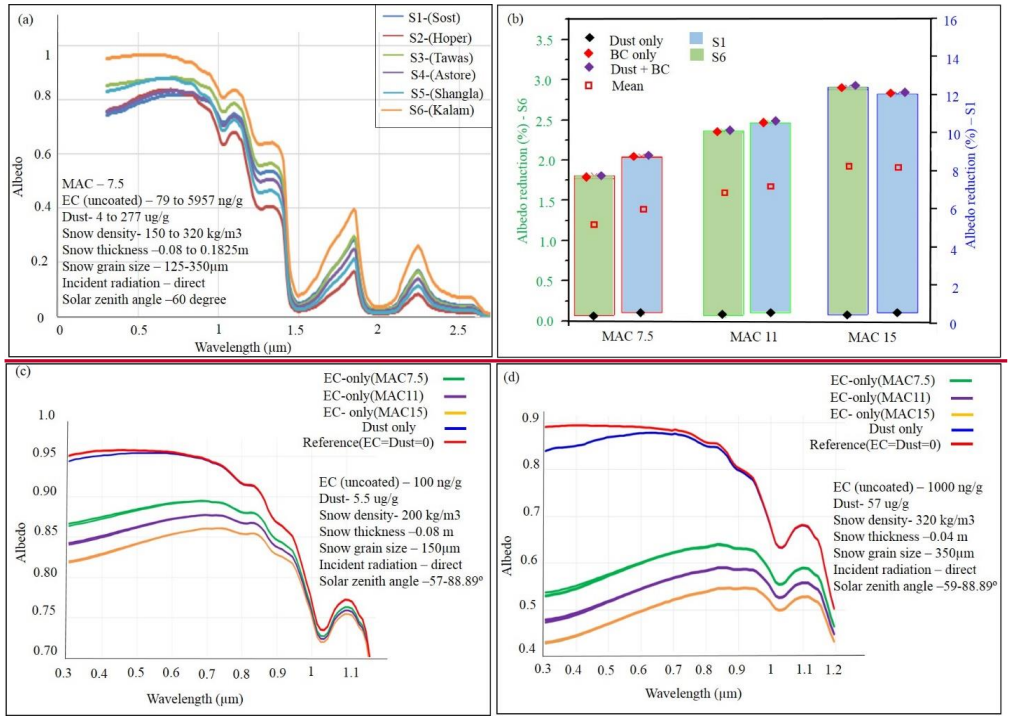
(a)
S1-(Sost)
S2-(Hoper)
S3-(Tawas)
S4-(Astore)
S5-(Shangla)
S6-(Kalam)
MAC – 7.5
EC (uncoated) – 79 to 5957 ng/g
Dust- 4 to 277 ug/g
Snow density- 150 to 320 kg/m3
Snow thickness –0.08 to 0.1825m
Snow grain size – 125-350µm
Incident radiation – direct
Solar zenith angle –60 degree
Albedo
Wavelength (µm)
(b)
Dust only
BC only
Dust + BC
Mean
S1
S6
Albedo reduction (%) - S6
Albedo reduction (%) – S1
MAC 7.5
MAC 11
MAC 15
(c)
EC-only(MAC7.5)
EC-only(MAC11)
EC- only(MAC15)
Dust only
Reference(EC=Dust=0)
EC (uncoated) – 100 ng/g
Dust- 5.5 ug/g
Snow density- 200 kg/m3
Snow thickness –0.08 m
Snow grain size – 150µm
Incident radiation – direct
Solar zenith angle –57-88.89°
Albedo
Wavelength (µm)
(d)
EC-only(MAC7.5)
EC-only(MAC11)
EC- only(MAC15)
Dust only
Reference(EC=Dust=0)
EC (uncoated) – 1000 ng/g
Dust- 57 ug/g
Snow density- 320 kg/m3
Snow thickness –0.04 m
Snow grain size – 350µm
Incident radiation – direct
Solar zenith angle –59-88.89°
Albedo
Wavelength (µm)

916

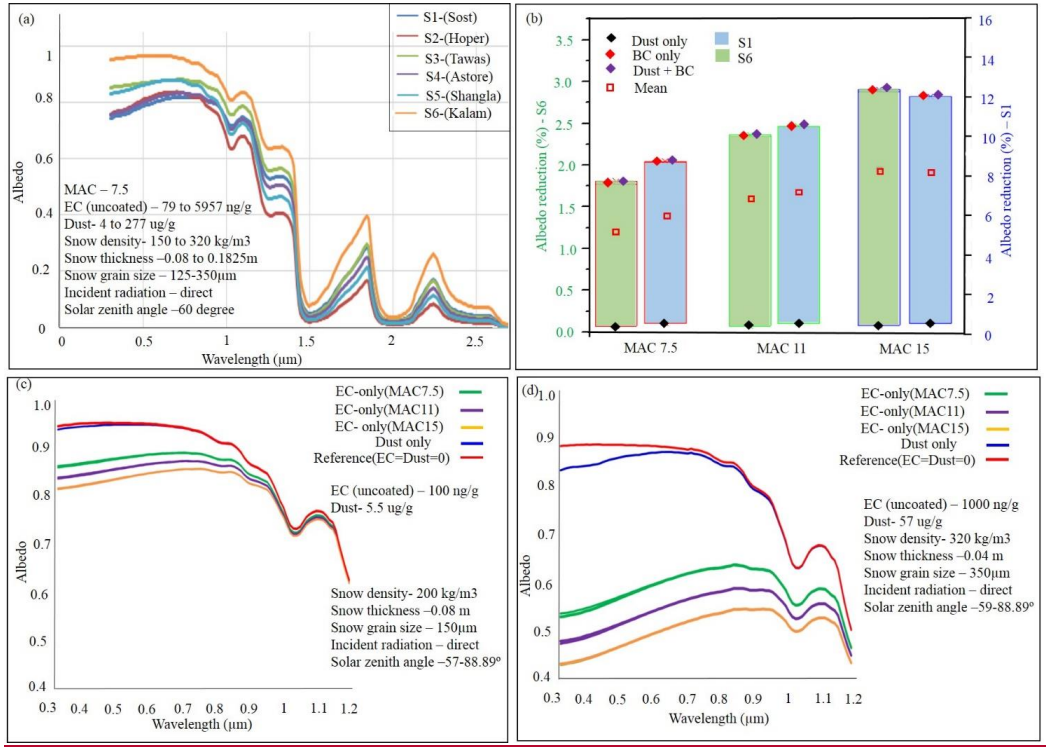

Figure 3. Spectral variation in albedo for winter sampling sites and selected ~~MAC~~ Mass Absorption Cross section (MAC) values, (a) average albedo of samples at each of the sites (b) daily mean albedo reduction of fresh snow (site S6) and aged snow (site S1) snow, (note different scales of y axis) (c) albedo of fresh snow site S6, (d) albedo of aged snow site S1.

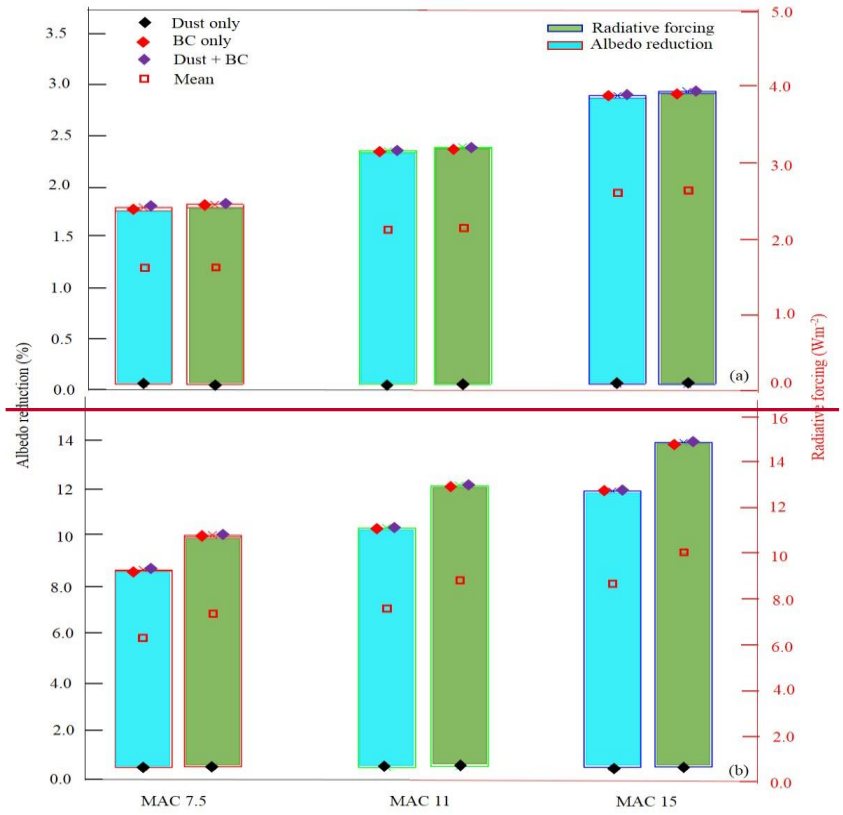
Dust only
BC only
Dust + BC
Mean
Radiative forcing
Albedo reduction
Albedo reduction (%)
Radiative forcing (Wm-2)
(a)
(b)
MAC 7.5
MAC 11
MAC 15

921
922

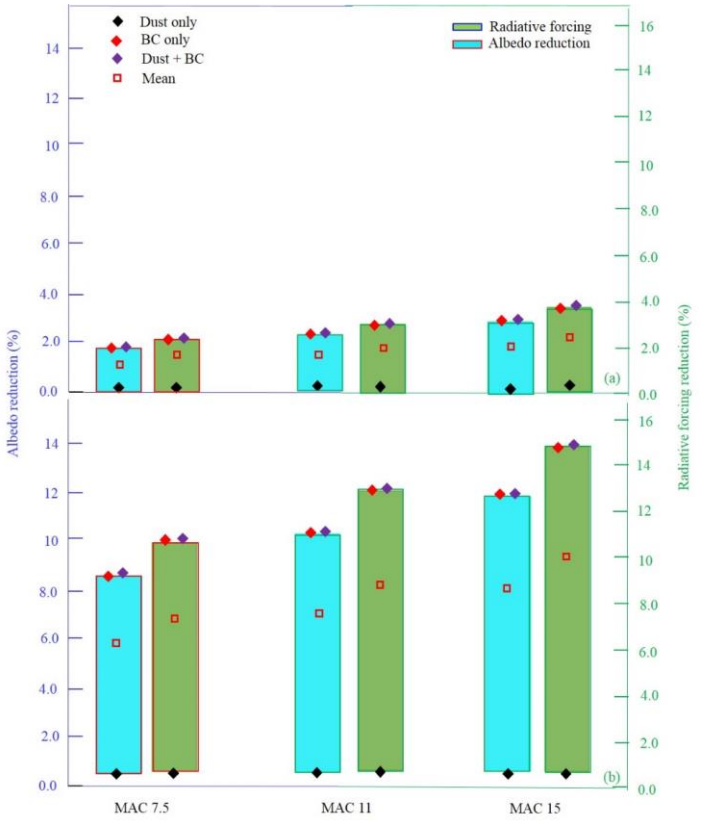

Figure 4. Daily mean radiative forcing ~~(%)~~ reduction and albedo reduction (%) caused by ~~BC~~ black carbon and dust for different Mass Absorption Cross section (MAC) in (a) fresh (low ~~BC~~black carbon) and (b) aged (high ~~BC~~black carbon) snow samples (note different scales of y axis)

926

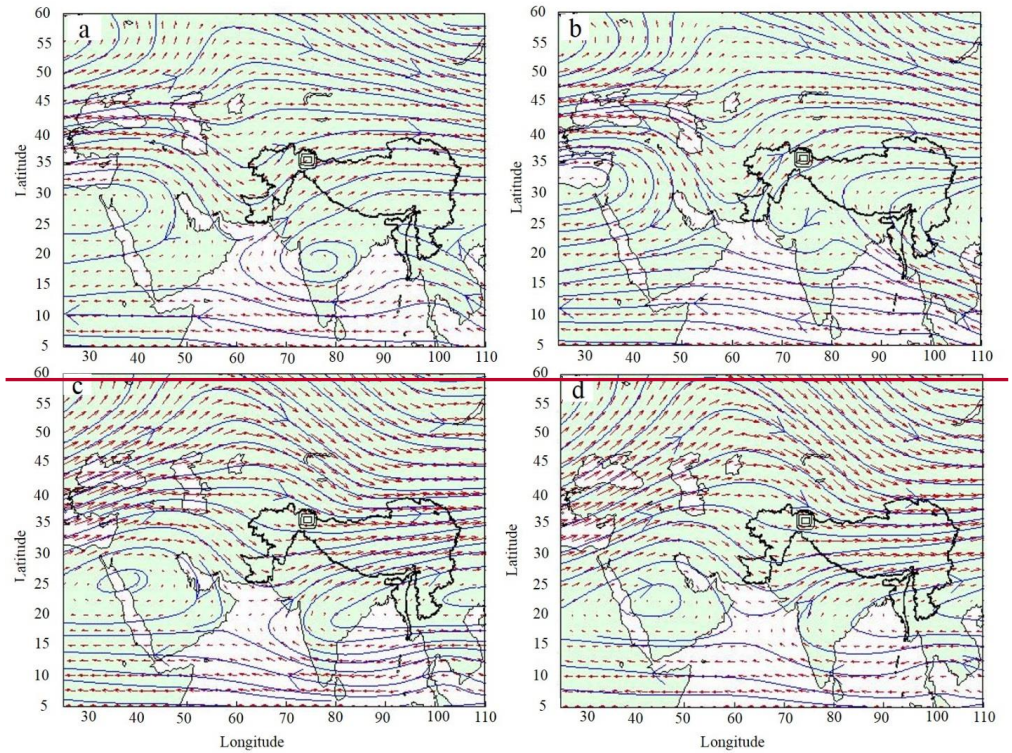
a
b
c
d
Latitude
Longitude
60
55
50
45
40
35
30
25
20
15
10
5
30
40
50
60
70
80
90
100
110

927

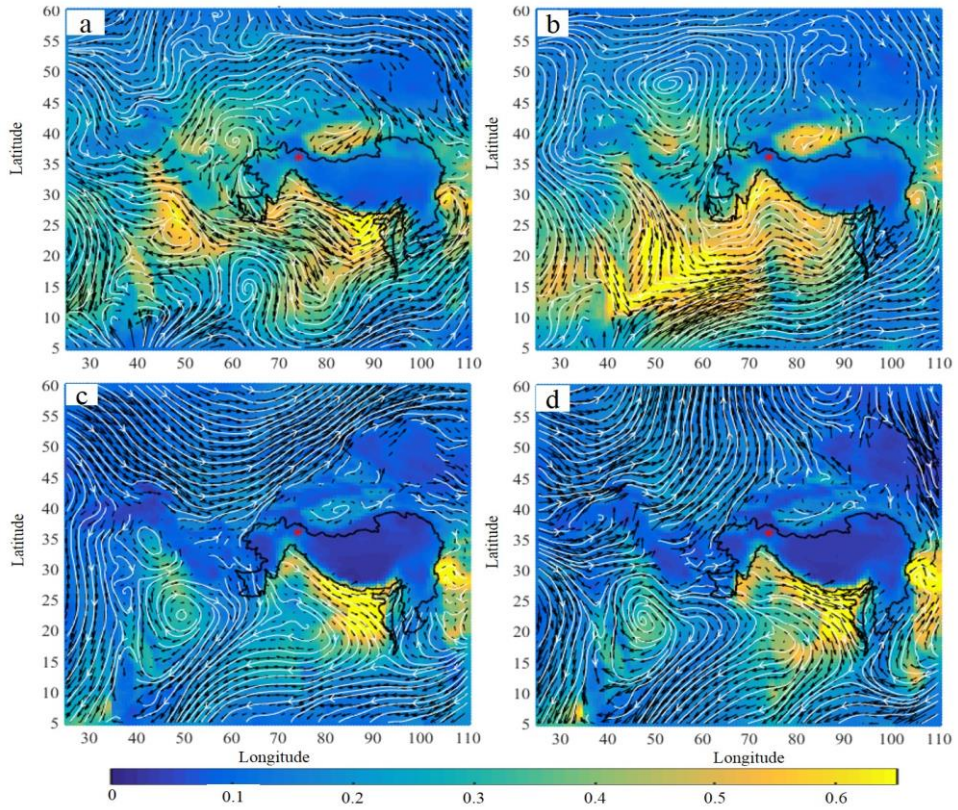

928

929 **Figure 5. ~~Fifty years m~~Monthly average horizontal wind patterns at ~~700~~ 850 hPa during a) May, b) June, c) December, and d) January, corresponding to approximately**
930 **~~3000~~ 2500 masl, from ~~NCEP NCAR~~GES DISC. ~~The study area is indicated by a square~~ Red star indicates the position of the study area, and white lines indicating**
931 **streamlines. The background colors show monthly mean aerosol optical depth.**

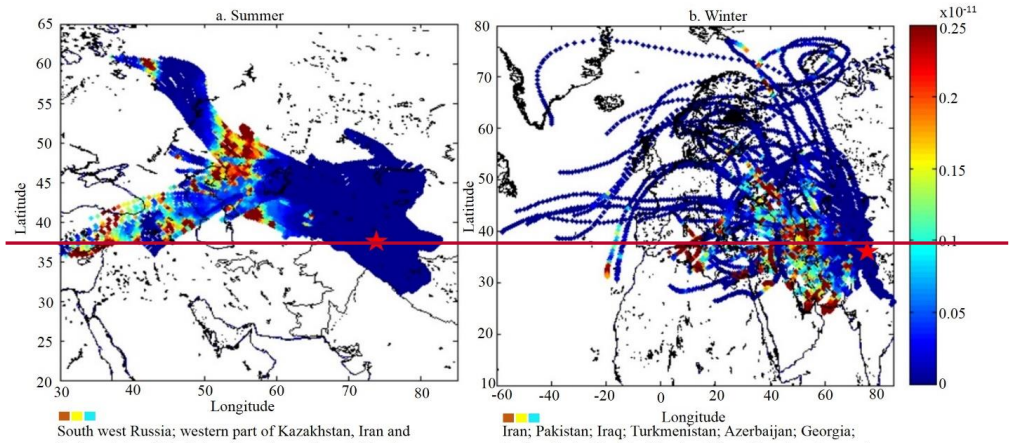
a. Summer
b. Winter
Latitude
Longitude
x10-11
0.25
0.2
0.15
0.1
0.05
0
South west Russia; western part of Kazakhstan, Iran and Turkmenistan; Uzbekistan; Georgia; north east side of Turkey; Syria; Cyprus.
Iran; Pakistan; Iraq; Turkmenistan; Azerbaijan; Georgia; Jordan; Syria; Tunisia; Ukraine; Libya; Egypt; eastern part of Turkey and south western part of Russia.

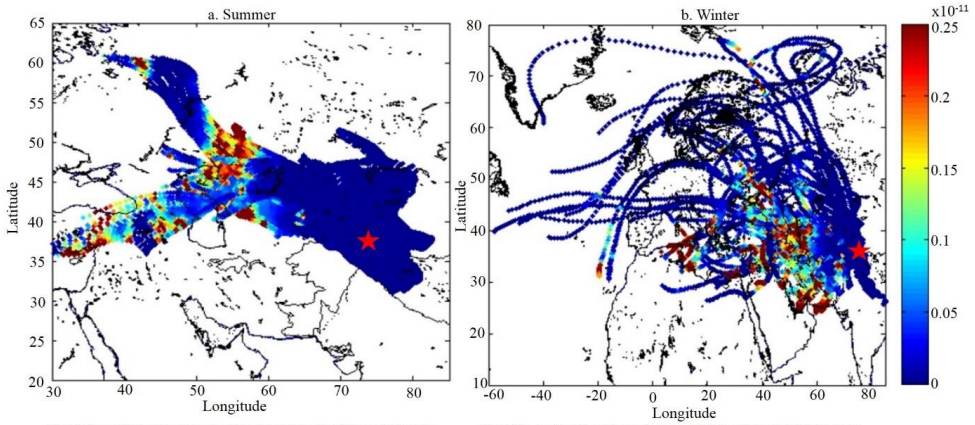

Figure 6. Source contribution regions of pollutants identified using an emissions inventory (Representative Concentration Pathways) coupled with back trajectories (a. 77 simulated days, b. 63 simulated days). Red star indicates the position of the study area.

Formatted: Font: Bold

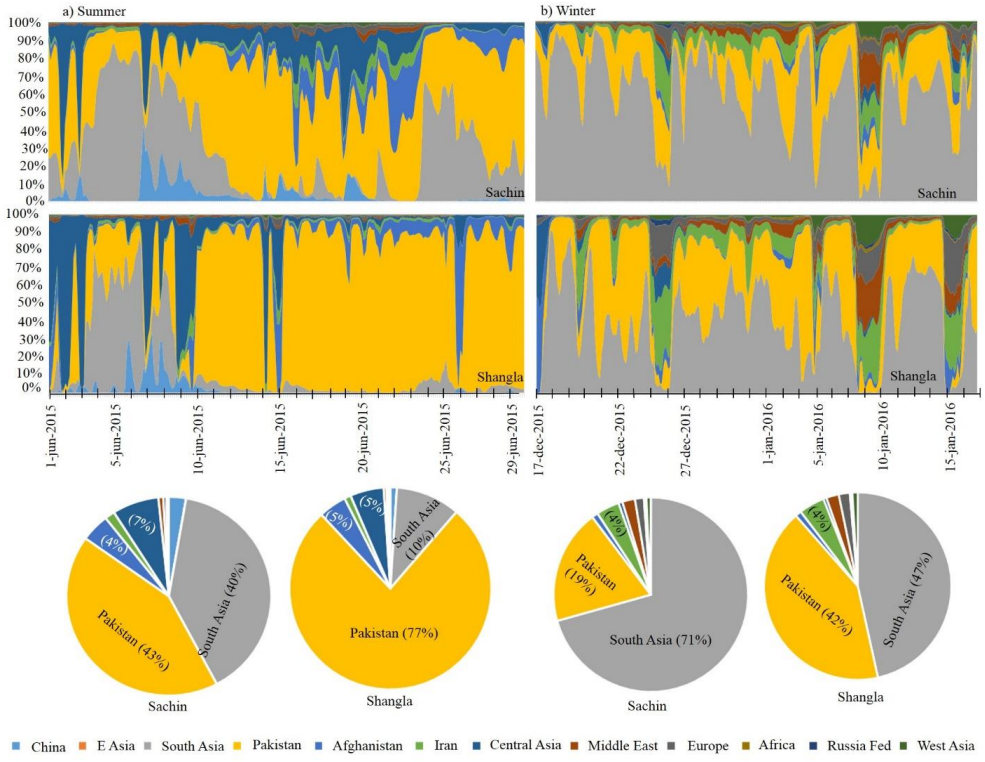

Figure 7. Source contribution regions of carbon monoxide for selected sites identified by WRF-STEM during (a) summer and (b) winter seasons.

Formatted: Font: Bold

Table 1. Concentration of black carbon~~BC~~, organic carbon~~OC~~, and dust in summer, autumn, and winter samples in 2015 and 2016.

Glacier/ Site	No.	Elevation (masl) min–max	BC min–max (avg) (ngg^{-1})	OC min–max (avg) (ngg^{-1})	Dust min–max (avg) (μgg^{-1})	Type[a] / snow age in days	OC/BC[b]	Year
Summer (May 2015/ May 2016)								
Barpu	6	2901–3405	877–5994 (2938)	244–1228 (691)	292–5250 (1998)	DCI	0.07–1.38	2015
Gulkin	31	2741–3319	82–5676 (1327)	238–8514 (1594)	31–2039 (648)	DCIS	0.169–3.76	2015/16
Henarche	4	2569–2989	778–10502 (4820)	275–4176 (1628)	225–2723 (993)	Ice	0.04–1.63	2015
Mear	8	2961–3539	222–3656 (1593)	703–6588 (2992)	33–656 (211)	DCI	0.72–4.88	2015
Passu	14	2663–3158	87–734 (346)	132–1810 (741)	28–524 (196)	DCI	1.85–4.80	2015
Sachin	35	3414–3895	257–4127 (1769)	128–7592 (3348)	5.6–2495 (314)	DCIS	0.08–0.53	2015/16
Total	98							
Autumn (October 2016)								
Gulkin	7	2741–3319	125–1028 (451)	266–3574 (1276)	60–767 (253)	DCIS	1.29–3.59	2016
Sachin	6	3414–3895	4342–6481 (5314)	543–3478 (1571)	124–1348 (546)	DCIS	0.11–0.53	2016
Total	13							
Winter (Dec 2015/ Jan 2016)								
S1-Sost	6	2873–3092	482–5957 (2506)	378–2934 (1039)	29–311 (131)	2–17 d	0.25–0.78	2015
S2-Hopar	2	2602–2794	229–1064 (646)	330–1976 (1153)	23–129 (76)	1–15 d	1.4–1.8	2016
S3-Tawas	1	2437	650	1320	16	8–17 d	2.03	2016
S4-Astore	3	2132–2396	450–2640 (1305)	914–3645 (2161)	55–171 (97)	4–7 d	1.38–2.33	2016
S5-Shangla	2	2324–2373	367–1110 (739)	1302–2856 (2079)	13–49 (31)	8–9 d	2.5–3.5	2016
S6-Kalam	4	1933–2101	79–123 (107)	214–558 (347)	4–6 (5)	1 d	2.3–5	2016
Total	18							

[a] type = snow or ice type; DCI = debris-covered ice; DCIS = debris-covered ice and aged snow

[b] range of OC/BC in individual samples

Table 2. Snow albedo reduction (%) ~~at 0.975 μm~~ by ~~BC~~black carbon, dust, and ~~BC~~ black carbon plus dust at the site with the lowest average pollutant concentration (S6) and the site with the highest average pollutant concentration (S1), under different ~~M~~mass ~~A~~absorption ~~C~~cross section values.

Pollutant	Mass ~~A~~Absorption Cross section (m^2/g)	Low concentration site (S6)			High concentration site (S1)		
		Daytime min	Daytime max	Daily mean	Daytime min	Daytime max	Daily mean
B~~C~~lack carbon	7.5	2.8	5.1	1.8	15.6	23.9	9.0
	11	3.7	6.9	2.3	19.2	28.6	10.5
	15	4.6	8.3	2.9	22.3	32.5	12.0
Dust	7.5	0.1	0.2	0.07	0.9	1.6	0.05
	11	0.1	0.2	0.07	0.9	1.6	0.05
	15	0.1	0.2	0.07	0.9	1.6	0.05
Black carbon~~C~~ and dust	7.5	2.9	5.2	1.8	15.7	24.0	8.8
	11	3.8	6.8	2.4	19.2	28.6	10.5
	15	4.6	8.3	2.9	22.3	32.5	12.0

Formatted: Centered
Formatted Table
Formatted: Centered
Formatted: Centered
Formatted: Centered
Formatted: Centered
Formatted: Centered
Formatted: Centered
Formatted: Centered
Formatted: Centered
Formatted: Centered

Concentrations and source regions of light absorbing ~~impurities~~ particles in snow/ice in northern Pakistan and their impact on snow albedo

Chaman Gul[1,2,5], Siva Praveen Puppala[2], Shichang Kang[1,3,5], Bhupesh Adhikary[2], Yulan Zhang[1], Shaukat Ali[4], Yang Li[3], Xiaofei Li[1]

[1]State Key Laboratory of Cryosphere Science, Northwest Institute of Eco-Environment and Resources, Chinese Academy of Sciences, Lanzhou 73000, China

[2]International Centre for Integrated Mountain Development (ICIMOD), G.P.O. Box 3226, Kathmandu, Nepal

[3]CAS Center for Excellence in Tibetan Plateau Earth Sciences, Beijing, 100101, China

[4]Global Change Impact Studies Centre (GCISC), Ministry of Climate Change, Islamabad, Pakistan

[5]University of Chinese Academy of Sciences, Beijing, China

Correspondence to: Chaman Gul (chaman.gul@icimod.org; chaman@lzb.ac.cn)

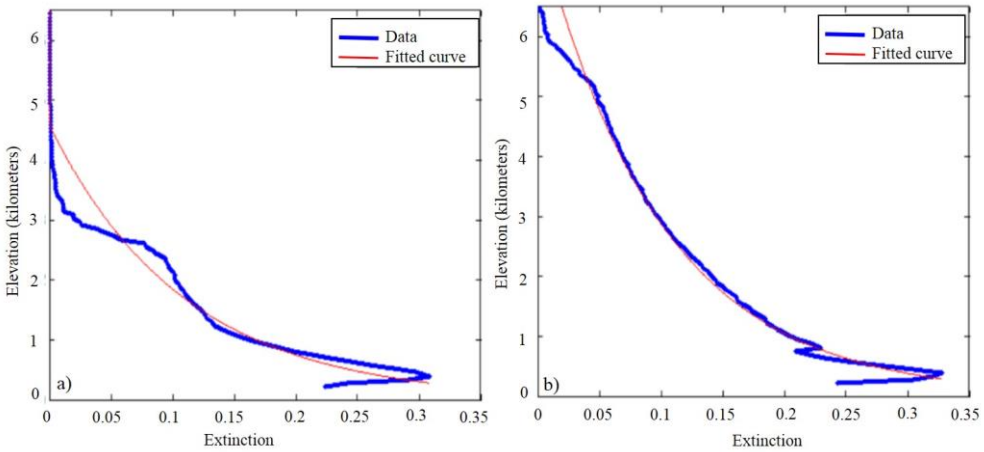

Figure S1. CALPISO extinction profile for a) winter (December, January), and b) summer (May, June)

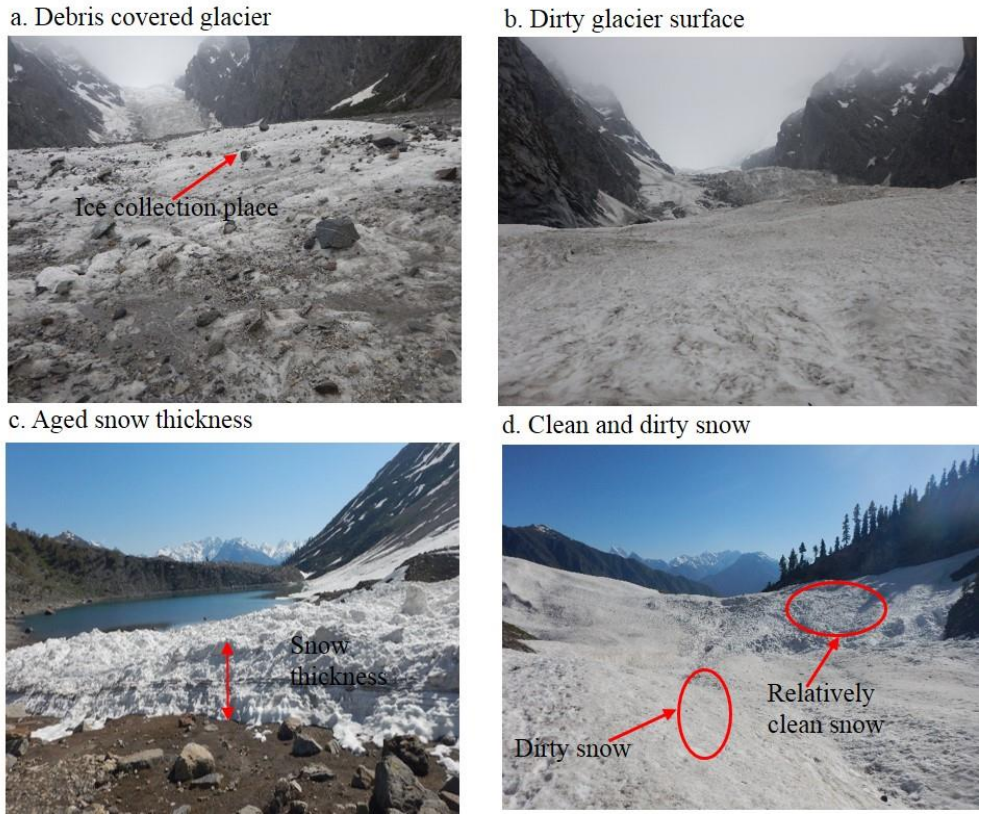

Figure S2. Appearance of different summer snow/ice sampling sites on a) b) Gulkin glacier, c) near Sachin glacier, and d) Sachin glacier

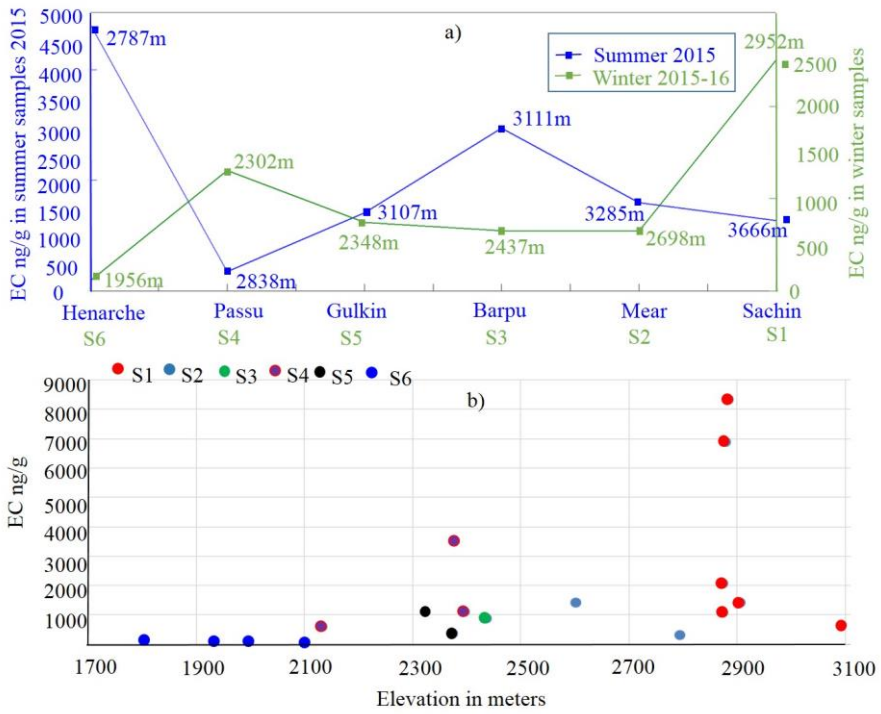

Figure S3. a) Average concentration of ~~EC~~ black carbon at sites S1 to S6 sampled in winter and glaciers sampled in summer; b) individual sample concentration in winter samples.

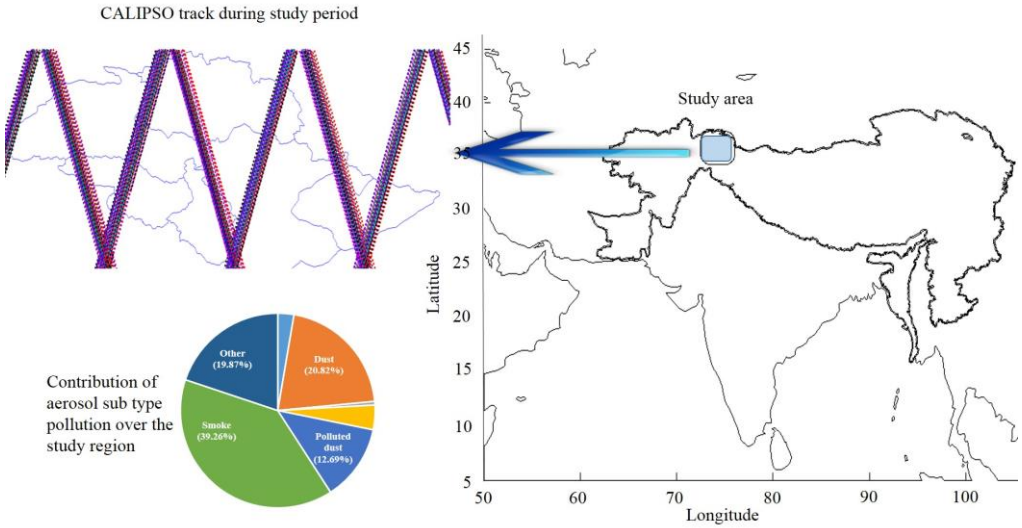

Figure S4. Contribution of subtype aerosols (%) in the atmosphere along the track of CALIPSO during the selected month June in 2006-2014

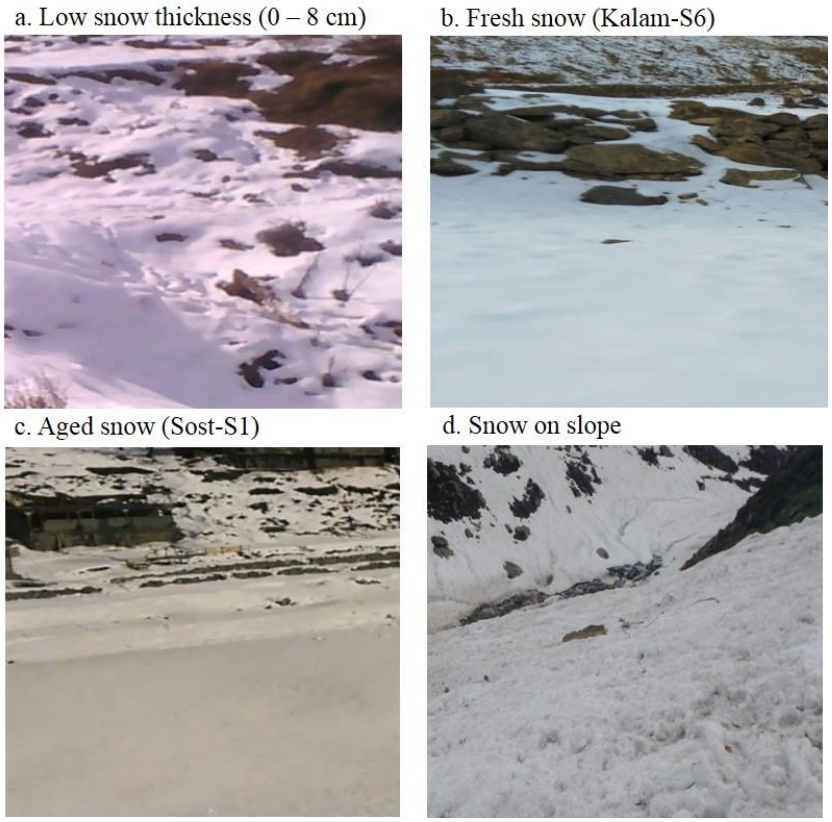

Figure S5. Appearance of different snow areas sampled in winter

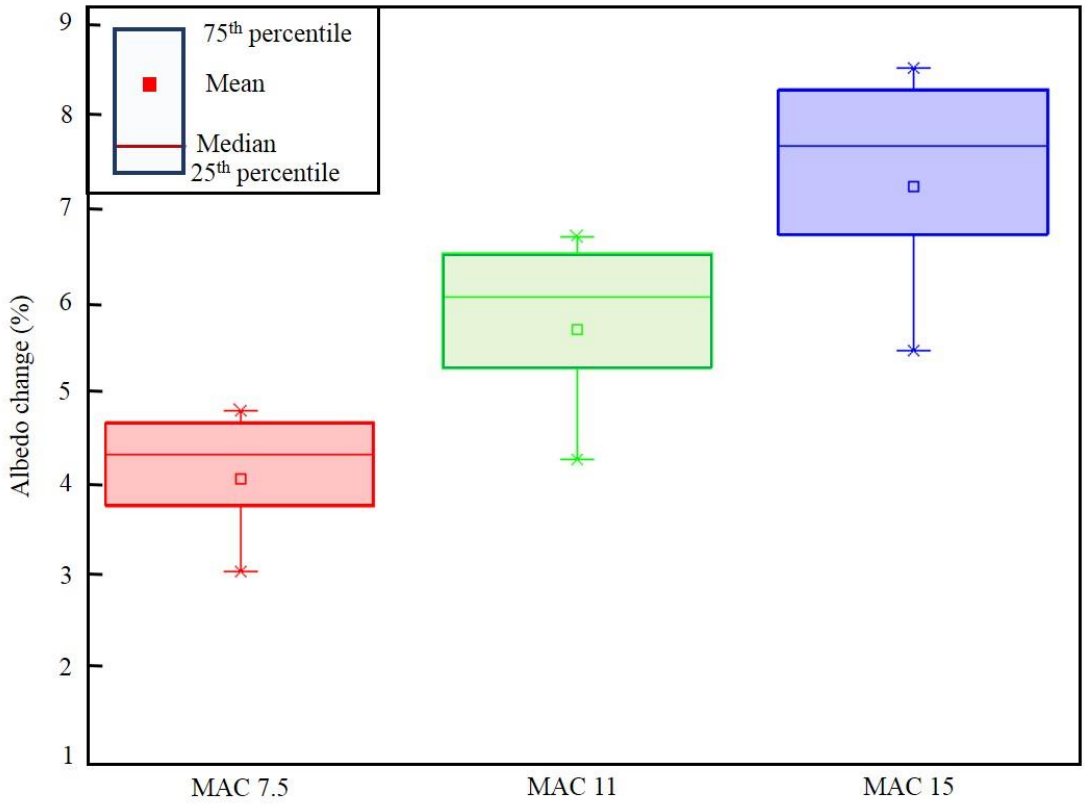
75th percentile
Mean
Median
25th percentile
Albedo change (%)
9
8
7
6
5
4
3
2
1
MAC 7.5
MAC 11
MAC 15

32

Figure S6. Albedo reduction (%) range between sulfate coated and uncoated black carbon calculated for different Mass Absorption Cross section (MAS) and the low concentration site S6.

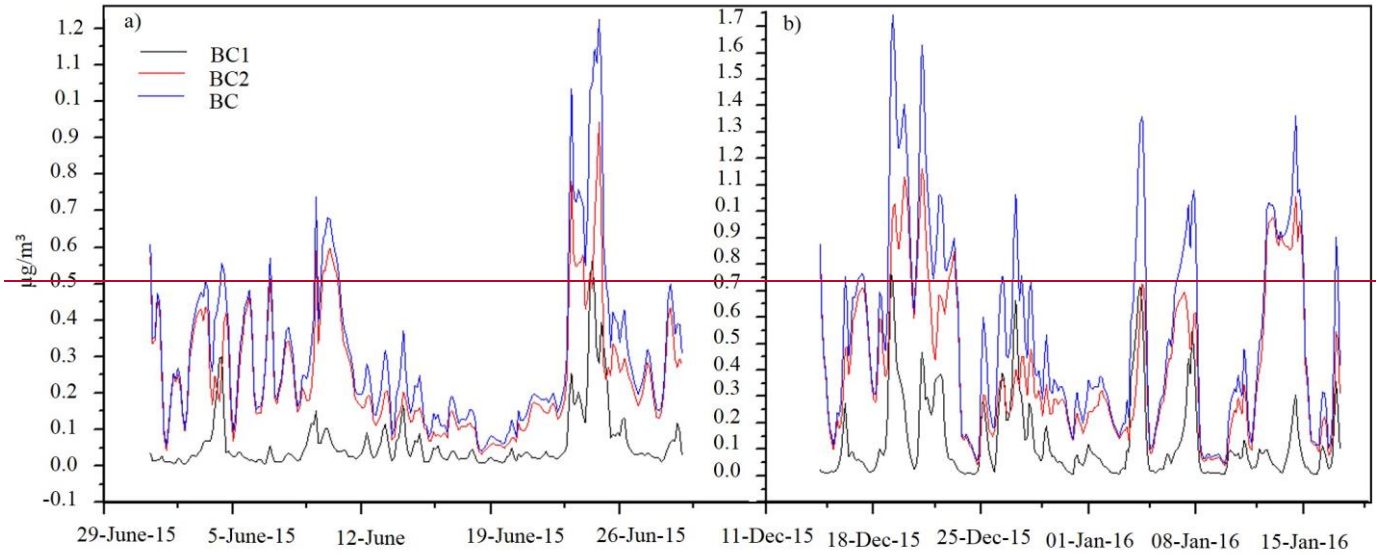

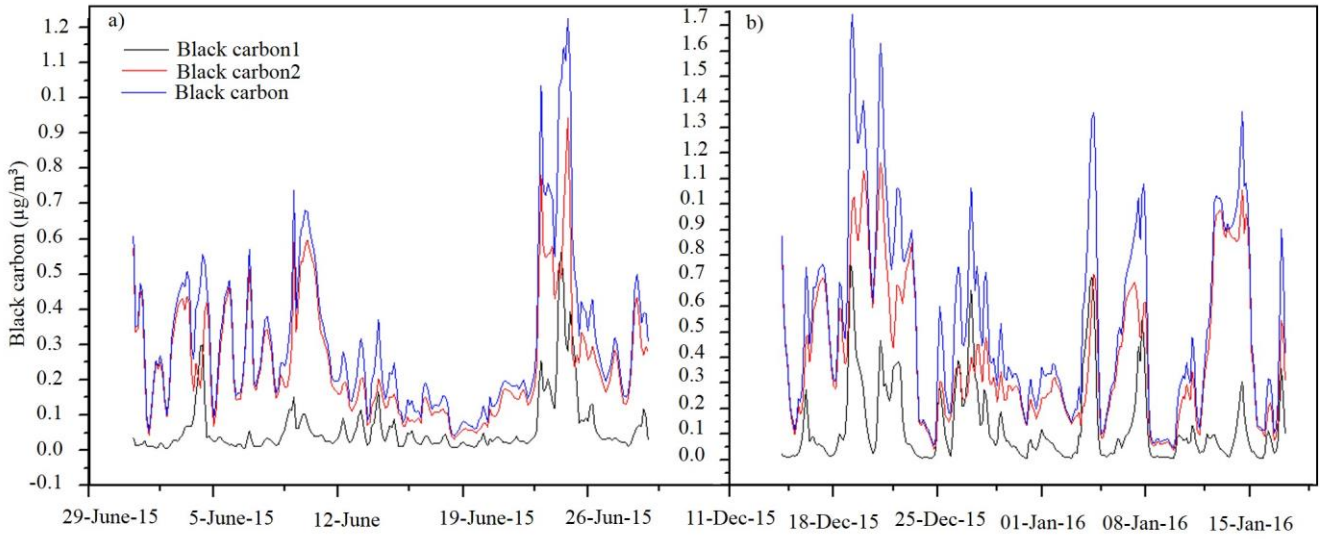

Figure S7. Concentration of ~~black carbon (BC1~~black carbon1, ~~B~~black carbon~~C~~2 and ~~BC~~black carbon~~)~~ on the Sachin glacier calculated using the WRF-STEM model: a) summer, b) winter.

Tables

Table S1 Parameters used for sensitivity analysis with SNICAR model for winter snow samples under the input parameters of direct incident radiation and mid-latitude winter, clear-sky conditions.

1 = solar zenith angle

2 = snow grain effective radius (µm)

3 = snowpack thickness (m)

4 = snowpack density (kg m^{-3})

5 = albedo of underlying ground (a. visible, 0.3-0.7µm, b. near-infrared, 0.7-5.0µm)

6 = ~~MAC~~ Mass Absorption Cross section scaling factor (experimental) for ~~BC~~black carbon

7= BC concentration (ppb, uncoated)

8 = dust concentration (ppm, 5.0–10.0 µm diameter)

9 = volcanic ash concentration (ppm)

10 = experimental particle 1 concentration (ppb)

Site	1	2	3	4	5a	5b	6	7	8	9	10
Kalam-S6	80.34	150	0.08	200	0.2	0.4	7.5/11/15	100	5.5	0	0
Kalam-S6	71.25	150	0.08	200	0.2	0.4	7.5/11/15	100	5.5	0	0
Kalam-S6	63.96	150	0.08	200	0.2	0.4	7.5/11/15	100	5.5	0	0
Kalam-S6	59.21	150	0.08	200	0.2	0.4	7.5/11/15	100	5.5	0	0
Kalam-S6	57.66	150	0.08	200	0.2	0.4	7.5/11/15	100	5.5	0	0
Kalam-S6	59.54	150	0.08	200	0.2	0.4	7.5/11/15	100	5.5	0	0
Kalam-S6	64.57	150	0.08	200	0.2	0.4	7.5/11/15	100	5.5	0	0

Formatted: Font: 10 pt, Check spelling and grammar

Kalam-S6	72.07	150	0.08	200	0.2	0.4	7.5/11/15	100	5.5	0	0
Kalam-S6	81.31	150	0.08	200	0.2	0.4	7.5/11/15	100	5.5	0	0
Kalam-S6	88.95	150	0.08	200	0.2	0.4	7.5/11/15	100	5.5	0	0
Sost-S1	82.61	350	0.04	320	0.19	0.35	7.5/11/15	1000	57	0	0
Sost-S1	73.66	350	0.04	320	0.19	0.35	7.5/11/15	1000	57	0	0
Sost-S1	66.45	350	0.04	320	0.19	0.35	7.5/11/15	1000	57	0	0
Sost-S1	61.64	350	0.04	320	0.19	0.35	7.5/11/15	1000	57	0	0
Sost-S1	59.66	350	0.04	320	0.19	0.35	7.5/11/15	1000	57	0	0
Sost-S1	61.36	350	0.04	320	0.19	0.35	7.5/11/15	1000	57	0	0
Sost-S1	65.93	350	0.04	320	0.19	0.35	7.5/11/15	1000	57	0	0
Sost-S1	72.98	350	0.04	320	0.19	0.35	7.5/11/15	1000	57	0	0
Sost-S1	81.80	350	0.04	320	0.19	0.35	7.5/11/15	1000	57	0	0
Sost-S1	88.95	350	0.04	320	0.19	0.35	7.5/11/15	1000	57	0	0

54

Table S2. EC concentrations in glacier ice and snow and plains snow in north Pakistan, and other regions

Location	Lat/long	Elevation (masl)	Min. EC (ngg^{-1})	Max. EC (ngg^{-1})	Time period (years)	Sample type/snow age	Reference
Mera Glacier, Nepal	27.72°N 86.8°E	6376	3	13	1999–2010	Ice core (rBC)	Ginot et al., 2014
Numanani, China	30.45°N 81.27°E	5900	4	14	Annual mean 2004	Ss (EC)	Xu et al., 2006
Greenland	72.6°N, 38.5°W	3209	4.2	30.1	1994 – 1996		Slater et al., 2002
NCO-P, Nepal	27.95°N, 86.82°E	5079	26	68.2	March – May 2006		Yasunari et al., 2010
Kangwure, China	28.47°N 85.82°E	6000	22	122	Annual mean 2001	Ss (EC)	Xu et al., 2007
Qiangyong, China	28.83°N 90.25°E	5400	43	143	Annual mean 2001	Ss (EC)	Xu et al., 2008
Zhadang, China	30.47°N 90.50°E	5802	334	473	2001–2010		Qu et al., 2014
Muji glacier, China	39.19°N 73.74° E	5062	25	731	2012		Yang et al., 2015
Zhadang, China	30.47°N 90.5°E	5802	114	1114	2005–2006		Ming et al., 2009
Tien Shan, China	43.1°N 86.82°E	4050		3000	2011	bottom firn-pack	Xu et al., 2012
Mera glacier, Nepal	27.72°N 86.8°E	5400		3535	2009		Kaspari et al., 2014
Northern China			60	4020	Jan-14		Wang et al., 2016
Urumqi glacier, China	43.10°N 86.80°E	4040	16	4093	2013		Ming et al., 2016
LHG glacier, China	39.17°N 96.17°E	5480		28,636	summer 2013-14	superimposed ice	Li et al., 2016
Present study							
Passu glacier	36.45°N 74.85°E	2838	87	734	May-June 2015	DCI (EC)	This study
Sachin glacier	35.32°N 74.76°E	3666	492	1789	May-June 2015	DCI & snow (EC)	This study
Sachin glacier	35.32°N 74.76°E	3666	543	3478	Oct-16	DCI & snow	This study
Gulkin glacier	36.42°N 74.77°E	3066	266	3574	Oct-16	DCI	This study
Mear glacier	36.15°N 74.82°E	3281	222	3656	May-June 2015	DCI (EC)	This study

Gulkin glacier	36.42°N 74.77°E	3066	81	5676	May-June 2015	DCI (EC)	This study
Barpu glacier	36.18°N 74.08°E	3055	877	5994	May-June 2015	DCI (EC)	This study
Henarche glacier	36.05°N 74.57°E	2941	778	10,502	May-June 2015	Surface ice (EC)	This study
S6-Kalam	35.43°N 72.6°E	1958	79	123	8-Jan-16	1–2 days	This study
S3-Tawas	36.39°N 73.36°E	2437		650	2-Jan-16	8–17 days	This study
S2- Hopar	36.22°N 74.75°E	2698	229	1064	1-Jan-16	1–15 days	This study
S5-Shangla	34.83°N 74.82°E	2348	367	1111	6–7 Jan 2016	8–9 days	This study
S4-Astore	35.37°N 74.80°E	2302	450	2640	3–4 Jan 2016	4–7 days	This study
S1- Sost	36.78°N 74.93°E	2951	482	5957	30–31 Dec 2015	2–17 days	This study

Table S3. Broadband albedo values ~~at 0.975 µm wavelength~~ for selected solar zenith angles, and daily mean albedo reduction (%)

Pollutant		Site S6 (low ~~EC~~ BC and dust)				Site S1 (high ~~EC~~ BC and dust)		
	SZA	MAC 7.5	MAC 11	MAC 15	SZA	MAC 7.5	MAC 11	MAC 15
~~EC~~ BC only	80.34	0.79	0.78	0.77	82.61	0.59	0.56	0.52
	71.25	0.77	0.75	0.74	73.66	0.54	0.50	0.46
	63.96	0.75	0.74	0.72	66.45	0.50	0.46	0.42
	59.21	0.74	0.72	0.71	61.64	0.48	0.43	0.40
	57.66	0.74	0.72	0.71	59.66	0.47	0.43	0.39
	59.54	0.74	0.72	0.71	61.36	0.48	0.43	0.39
	64.57	0.75	0.74	0.72	65.93	0.50	0.46	0.42
	72.07	0.77	0.76	0.74	72.98	0.54	0.49	0.46
	81.31	0.80	0.78	0.77	81.80	0.59	0.55	0.51
	88.95	0.82	0.81	0.80	88.95	0.64	0.60	0.57
	Daily mean reduction (%)	1.77	2.35	2.87		8.70	10.49	12.03
Dust only	80.34	0.83	0.83	0.83	82.61	0.76	0.76	0.76
	71.25	0.81	0.81	0.81	73.66	0.73	0.73	0.73
	63.96	0.80	0.80	0.80	66.45	0.71	0.71	0.71
	59.21	0.79	0.79	0.79	61.64	0.70	0.70	0.70
	57.66	0.79	0.79	0.79	59.66	0.70	0.70	0.70
	59.54	0.79	0.79	0.79	61.36	0.70	0.70	0.70
	64.57	0.80	0.80	0.80	65.93	0.71	0.71	0.71
	72.07	0.81	0.81	0.81	72.98	0.73	0.73	0.73

	81.31	0.83	0.83	0.83	81.80	0.76	0.76	0.76
	88.95	0.85	0.85	0.85	88.95	0.78	0.78	0.78
	Daily mean reduction (%)	0.07	0.07	0.07		0.05	0.05	0.05
	80.34	0.79	0.78	0.77	82.61	0.59	0.55	0.52
	71.25	0.77	0.75	0.74	73.66	0.54	0.50	0.46
	63.96	0.75	0.73	0.72	66.45	0.50	0.46	0.42
	59.21	0.74	0.72	0.71	61.64	0.48	0.43	0.40
	57.66	0.74	0.72	0.70	59.66	0.47	0.42	0.39
~~EC~~ BC and dust	59.54	0.74	0.72	0.71	61.36	0.48	0.43	0.39
	64.57	0.75	0.74	0.72	65.93	0.50	0.45	0.42
	72.07	0.77	0.76	0.74	72.98	0.54	0.49	0.46
	81.31	0.79	0.78	0.77	81.80	0.59	0.55	0.51
	88.95	0.82	0.81	0.80	88.95	0.64	0.60	0.57
	Daily mean reduction (%)	1.80	2.36	2.90		8.75	10.51	12.03
	80.34	0.83	0.83	0.83	82.61	0.77	0.77	0.77
	71.25	0.81	0.81	0.81	73.66	0.75	0.75	0.75
	63.96	0.80	0.80	0.80	66.45	0.73	0.73	0.73
	59.21	0.79	0.79	0.79	61.64	0.72	0.72	0.72
	57.66	0.79	0.79	0.79	59.66	0.71	0.71	0.71
No ~~EC~~BC/ no dust	59.54	0.79	0.79	0.79	61.36	0.72	0.72	0.72
	64.57	0.79	0.80	0.80	65.93	0.73	0.73	0.73
	72.07	0.81	0.81	0.81	72.98	0.75	0.75	0.75
	81.31	0.83	0.83	0.83	81.80	0.77	0.77	0.77

	88.95	0.85	0.85	0.85	88.95	0.79	0.79	0.79

MAC = Mass Absorption Cross section, SZA = Solar Zenith Angle

Formatted: Font: 9 pt

Table S4. Radiative forcing for selected solar zenith angles (Wm^{-2}) and daily mean (%)

Pollutant	Site S6 (low EC and dust)				Site S1 (high EC and dust)			
	SZA	MAC 7.5	MAC 11	MAC 15	SZA	MAC 7.5	MAC 11	MAC 15
	80.34	4.90	6.47	8.00	82.61	23.87	29.10	33.71
	71.25	5.86	7.72	9.53	73.66	27.50	33.25	38.21
	63.96	6.57	8.65	10.65	66.45	29.96	36.01	41.16
	59.21	7.00	9.70	11.33	61.64	31.39	37.58	42.82
~~**EC**~~ **BC**	57.66	7.14	9.38	11.54	59.66	31.93	38.18	43.44
only	59.54	6.97	9.16	11.29	61.36	31.47	37.67	42.91
	64.57	6.51	8.58	10.56	65.93	30.13	36.19	41.35
	72.07	5.78	7.61	9.40	72.98	27.75	33.53	38.52
	81.31	4.79	6.33	7.83	81.80	24.23	29.51	34.16
	88.95	3.93	5.20	6.44	88.95	20.88	25.62	29.86
	Daily mean	2.40	3.18	3.90	-	10.74	12.95	14.85
	80.34	0.20	0.20	0.20	82.61	1.43	1.43	1.43
	71.25	0.24	0.24	0.24	73.66	1.71	1.71	1.71
	63.96	0.27	0.27	0.27	66.45	1.91	1.91	1.91
Dust	59.21	0.29	0.29	0.29	61.64	2.03	2.03	2.03
only	57.66	0.30	0.30	0.30	59.66	2.08	2.08	2.08
	59.54	0.29	0.29	0.29	61.36	2.04	2.04	2.04
	64.57	0.27	0.27	0.27	65.93	1.93	1.93	1.93
	72.07	0.24	0.24	0.24	72.98	1.73	1.73	1.73

	81.31	0.20	0.20	0.20	81.80	1.38	1.38	1.38
	88.95	0.16	0.16	0.16	88.95	1.21	1.21	1.21
	Daily mean	0.10	0.10	0.10	-	0.67	0.67	0.67
~~EC~~ BC and dust	80.34	5.00	6.55	8.07	82.61	24.03	29.16	33.71
	71.25	5.98	7.82	9.61	73.66	27.70	33.33	38.22
	63.96	6.70	8.75	10.75	66.45	30.17	36.09	41.17
	59.21	7.14	9.32	11.43	61.64	31.61	37.68	42.83
	57.66	7.28	9.49	11.64	59.66	32.15	38.27	43.45
	59.54	7.11	9.28	11.38	61.36	31.69	37.76	42.92
	64.57	6.65	8.68	10.66	65.93	30.34	36.27	41.36
	72.07	5.89	7.71	9.48	72.98	27.95	33.61	38.52
	81.31	4.89	6.41	7.90	81.80	24.39	29.58	34.16
	88.95	4.01	5.26	6.49	88.95	21.01	25.67	29.85
	Daily mean	2.45	3.20	3.93	-	10.81	12.98	14.86

MAC = Mass Absorption Cross section, SZA = Solar Zenith Angle

Table S5. Potential source countries for pollutants: a) identified using wind vector analysis; b) identified using trajectory analysis; and c) identified using the WRF-STEM model

Method	Region	Countries
a) Wind vector	East Asia	~~Thailand, Myanmar~~South west China.
	Central Asia	Tajikistan, Kyrgyzstan, Uzbekistan, Azerbaijan, Turkmenistan
	South Asia	~~Bay of Bengal,~~ India, Pakistan, Afghanistan
	Middle East	Syria, Iraq, Lebanon, Armenia.
	West Asia	Iran, Turkey
	Europe	Western parts of Russia.
b) Trajectory analysis	Central Asia	Uzbekistan, Western part Turkmenistan, Kazakhstan, Azerbaijan
	South Asia	Pakistan
	Middle East	Iraq, Armenia, Syria, United Arab Emirates, Jordan
	West Asia	Iran, Georgia, Turkey, Cyprus
	Russian Federation	Western Russia.
	Europe	Ukraine
	Africa	Egypt, Libya, Tunisia
c) WRF-STEM	East Asia	Indonesia, Singapore, Malaysia, Thailand, Myanmar, Sri Lanka
	Central Asia	Mongolia, Tajikistan, Kyrgyzstan, Kazakhstan, Uzbekistan, Turkmenistan
	South Asia	Bangladesh, India, Bhutan, Nepal
	Middle East	Oman, United Arab Emirates, Qatar, Bahrain, Kuwait, Iraq, Syria, Lebanon, Palestinian Territory, Israel, Jordan, Saudi Arabia, Yemen

Russian Federation	Russia
West Asia	Azerbaijan, Armenia, Georgia, Turkey and Cyprus
Europe	Europe
Africa	Kenia, Somalia, Egypt, Congo
Other	China, Pakistan, Afghanistan, Iran

66

Concentrations and source regions of light absorbing ~~impurities~~ particles in snow/ice in northern Pakistan and their impact on snow albedo

Chaman Gul[1,2,5], Siva Praveen Puppala[2], Shichang Kang[1,3,5], Bhupesh Adhikary[2], Yulan Zhang[1], Shaukat Ali[4], Yang Li[3], Xiaofei Li[1]

[1]State Key Laboratory of Cryosphere Science, Northwest Institute of Eco-Environment and Resources, Chinese Academy of Sciences, Lanzhou 73000, China
[2]International Centre for Integrated Mountain Development (ICIMOD), G.P.O. Box 3226, Kathmandu, Nepal
[3]CAS Center for Excellence in Tibetan Plateau Earth Sciences, Beijing, 100101, China
[4]Global Change Impact Studies Centre (GCISC), Ministry of Climate Change, Islamabad, Pakistan
[5]University of Chinese Academy of Sciences, Beijing, China

Correspondence to: Chaman Gul (chaman.gul@icimod.org; chaman@lzb.ac.cn), SivaPraveen.Puppala@icimod.org.

Abstract. Black carbon (BC), water-insoluble organic carbon (OC), and mineral dust are important ~~particulate impurities~~particles in snow and ice, which significantly reduce albedo and accelerate melting. Surface snow and ice samples were collected from the Karakoram-Himalayan region of northern Pakistan during 2015 and 2016 in summer (six glaciers), autumn (two glaciers), and winter (six mountain valleys). The average BC concentration overall was 2130 ± 1560 ngg^{-1} in summer samples, 2883±3439 ngg^{-1} in autumn samples, and 992 ± 883 ngg^{-1} in winter samples. The average water insoluble OC concentration overall was 1839 ± 1108 ngg^{-1} in summer samples, 1423 ± 208 ngg^{-1} in autumn samples, and 1342 ± 672 ngg^{-1} in winter samples. The overall concentration of BC, OC, and dust in aged snow samples collected during the summer campaign was higher than the concentration in ice samples. The values are relatively high compared to reports by others for the Himalayas and Tibetan Plateau. This is probably the result of taking more representative samples at lower elevation where deposition is higher and the effects of ageing and enrichment more marked. A reduction in snow albedo of 0.1–8.3% for fresh snow and 0.9–32.5% for aged snow was calculated for selected solar zenith angles during day time using the Snow, Ice, and Aerosol Radiation (SNICAR) model. Daily mean albedo was reduced by 0.07–12.0%. The calculated radiative forcing ranged from 0.16 to 43.45 Wm^{-2} depending on snow type, solar zenith angle, and location. The potential source regions of the deposited pollutants were identified using spatial variance in wind vector maps, emission inventories coupled with backward air trajectories, and simple region tagged chemical transport modelling. Central, South, and West Asia were the major sources of pollutants during the sampling months, with only a small contribution from East Asia. Analysis based on the Weather Research and Forecasting (WRF-STEM) chemical transport model identified a significant contribution (more than 70%) from South Asia at selected sites. Research into the presence and effect of pollutants in the glaciated areas of Pakistan is economically significant because the surface water resources in the country mainly depend on the rivers (the Indus and its tributaries) that flow from this glaciated area.

1 Introduction

Carbon is an essential component of atmospheric aerosols, where it appears in the form of black carbon (BC, or elemental carbon EC), and organic carbon (OC). BC is emitted into the atmosphere from incomplete combustion of carbon-based fuels (mainly fossil fuels and biomass) (Jacobson, 2004) while OC can be directly emitted into or formed in the atmosphere. After deposition on snow and ice surfaces, BC particles significantly reduce the snow albedo (hemispheric reflectance) in the visible part of the electromagnetic spectrum, cause snow albedo feedback (Doherty et al., 2013), enhance solar radiation absorption (Warren and Wiscombe, 1980), and accelerate snow melting (Hansen and Nazarenko, 2004). BC, both in air and deposited on snow, is important in net positive forcing of the climate. Clean snow is one of the most reflective natural surfaces on Earth at the ultraviolet and visible wavelengths, while BC is the most efficient light-absorbing species in the visible spectral range (Horvarth, 1993). One ngg^{-1} of BC has almost the same effect on albedo reduction as 100 ngg^{-1} mineral dust at 500 nm wavelength (Warren et al., 1982). However, the exact amount of albedo reduction also depends on the refractive index, ~~snow age,~~ grain size, solar zenith angle (SZA), snow density, dust particle size and concentration, particle morphology, surface roughness, snow depth, liquid water content, snow shape and topography ~~and dust particle size~~(Wiscombe and Warren 1985). Albedo reduction usually results in amplification of the energy absorbed by dirty snow (Painter et al., 2010). An albedo feedback is triggered and amplified by deposition of impurities on the snow surface which reduces snow albedo thus accelerating melting and further reducing albedo (Doherty et al., 2013; Flanner et al., 2009). Albedo feedback is amplified by the presence of light-absorbing ~~impurities~~ particles (Doherty et al., 2013). Studies conducted in Greenland showed that at visible wavelengths 10 ngg^{-1} coarse-grained BC particles in aged snow and 40 ngg^{-1} BC particles in new snow could reduce snow albedo by around 1 to 3% (Warren and Wiscombe, 1985).

Increased BC mass concentration and deposition on the Tibetan glaciers over the last 20 years (Xu et al., 2009a) has played a significant role in rapid glacier melting in the region (Xu et al., 2012; Yao et al., 2012). A high concentration of aerosol has deposited on the snow surface and increased the BC content in snow over the southern edge of the Tibetan Plateau to the north of the Himalayas (Gertler et al., 2016). The southern slope of the Himalayas is relatively even more exposed to BC due to emissions from India and transport through southwesterly and westerly winds (Xu et al., 2009; Yasunari et al., 2010). BC deposited on snow in the Himalayan region induces an increase in net shortwave radiation at the snow surface with an annual mean of about 1 to 3 Wm^{-2}, producing an estimated 0.05–0.3°C warming (Ménégoz et al., 2014). Deposition of anthropogenic BC has been observed to contribute significantly to the decrease in snow cover extent over recent decades (Dery et al., 2007), and shortening the duration of the snow cover season by several days (Ménégoz et al., 2013a). The climate warming efficiency of BC in snow is greater than the warming efficiency of other anthropogenic pollutants, including carbon dioxide (Hansen et al., 2005). Besides warming efficiency, another important characteristic of BC is its higher snowmelt efficiency. The snowmelt efficacy induced by BC in snow is larger for snow cover fraction and snow water equivalent than induced by carbon dioxide increase (Qian et al., 2011). The annual snow albedo reduction effect due to BC outweighs the

aerosol dimming effect (reduction in solar radiation reaching the surface) by a factor of about six over the global snow cover (Flanner et al., 2009).

At present, South and East Asia are considered to be the two largest BC emission regions in the world and likely to remain so (Menon et al., 2010). BC transported from East Asia can be lifted high and moved towards the northeast during the summer monsoon season (Zhang et al., 2015; Cong et al., 2015; Lüthi et al., 2015), affecting the life of glaciers and snow-covered areas.

Research into the glaciers of the extended Himalayan region and Tibetan Plateau has prime importance because these glaciers act as a water storage tower for South and East Asia, and shrinking could affect water resources for up to a billion people (Immerzeel et al., 2010). The glaciated area in northern Pakistan may be more exposed to BC effects than that in other regions because potentially it can receive emissions generated from both South and Central Asia as well as from the Middle East. Meltwater coming from these glaciers flows into the river Indus, which has major economic importance for the people of Pakistan.

A number of authors have described the concentration and impacts of light absorbing ~~impurities~~ particles in the Tibetan glaciers (for example Qian et al., 2015; Wang et al., 2015; Que et al., 2016; Zhang et al., 2017; Li et al., 2017; Niu et al., 2017~~;~~). However, until now, no studies have been published related to the concentration of light absorbing aerosols in the surface snow and ice of northern Pakistan, and although several authors have investigated transport pathways over the Himalayan region (e.g. Babu et al., 2011 for the western trans-Himalayas; Lu et al., 2012~~, and Kopacz et al., 2011~~ for the Tibetan Plateau and Himalayas) little is known about the potential sources and transport pathways of pollutants affecting the Pakistan area.

In this study, we looked at the concentration of light absorbing ~~impurities~~ particles (BC, OC, dust) in snow and ice in northern Pakistan, their impact on snow albedo and radiative forcing, and the likely source regions. Albedo was estimated from the BC and dust concentrations identified in collected samples of snow and ice using the online snow albedo simulation SNICAR model (Flanner et al., 2009). Radiative forcing was calculated from the albedo reduction obtained from the SNICAR model together with the incident short-wave solar radiation obtained from the SBDART (Santa Barbara DISORT Atmospheric Radiative Transfer) model. The frequency distribution of aerosol subtypes (smoke, continental polluted, dust, and others) in the atmosphere over the study area was calculated for the snow and ice sampling periods using Cloud-Aerosol Lidar and Infrared Pathfinder Satellite Observations (CALIPSO) satellite data from 2006 to 2014 as a further indication of the types of aerosol contributing to the observed deposition. The potential source regions of pollutants were identified using spatial variance in wind vector maps prepared using ~~50 years of~~MERRA-2 reanalysis data, calculation of back air trajectories using the HYSPLIT-4 (Hybrid Single Particle Lagrangian Integrated Trajectory) model, and a simple region tagged chemical transport model (WRF-STEM). The back air trajectories approach has been used in many studies to identify possible source regions for atmospheric and deposited BC (Zhang et al., 2013). Pollutant source regions identified using the different approaches were compared and the most likely source regions of the pollutants identified.

2 Methodology

2.1 Study area

The study area was located around 35.40°N 74.38°E in the mountains and adjacent mountain valleys of the Karakoram and Himalayan region in northern Pakistan (Figure 1). Snow and ice samples were collected in summer from six glaciers – Passu, Gulkin, Barpu, Mear, Sachin, and Henarche – and in autumn from Gulkin and Sachin (Figure 1). The Passu and Gulkin glaciers are located very near to the Karakoram highway connecting Pakistan with China, and there are a number of small villages (Passu, Hussaini, Gulmit, and others) close by. The Barpu and Mear glaciers are located very close to each other and around ~~2~~ 3 km away from the residential area of the Hopar and Nagar valleys. There is a small city (Astore) near the Sachin glacier and some restaurants near its terminus. Winter snow samples were collected from mountain valleys near to Passu, Barpu and Sachin glaciers, and three other areas to the west with a number of small villages (Figure 1). The average elevation of the selected glaciers was quite low comparted to the elevation of the glaciers studied for BC, OC and dust on the Tibetan plateau by previous researchers. The mountains around the selected glaciers are mostly dry and rocky. ~~The mean annual precipitation (rain) at Gilgit was approximately 0.412 ± 2 mm during the period 1980–2013 (Gul et al., 2017)~~ According to the 10 years record (1999–2008) of the two nearby climatic stations, the mean total annual precipitation was 170 mm at Khunjerab (36.83°N, 75.40°E, 4730 m) station, and 680 mm at Naltar (36.29°N, 74.12°E,2858 m) station, while the daily average temperature during winter and pre-monsoon showed an increasing trend between 1980 and 2014 (Gul et al., 2017).The study area is mostly exposed to the westerlies and emission from South Asia. Most of the people in the region use wood for cooking and heating.

2.2 Sample collection

A total of 50 surface ice and 49 snow samples were collected from the glaciers in summer 2015 and 2016 (Passu 15, Gulkin 31, Barpu 6, Mear 8, Sachin 35, Henarche 4), and 13 in autumn 2016 (Gulkin 7, Sachin 6) at elevations ranging from 2,569 to 3,895 masl (Figure 1). Eighteen snow samples were collected in winter 2015 and 2016 from nearby mountain valleys at elevations of 1,958 to 2,698 masl; the winter sampling region was divided into six sites (S1 to S6) based on geographical location and elevation (Figure 1). Samples were collected using the "clean hands – dirty hands" principle (Fitzgerald, 1999). Ice samples were collected from the surface (5 cm depth) at different points on the glaciers. The elevation difference between collection points on the same glacier ranged from 30 to 100 meters.

The samples were preserved in ultra clean plastic bags, allowed to melt in a temporary laboratory near the sampling location, and filtered through quartz-filters immediately after melting. An electric vacuum pump was used to accelerate filtration. The melted snow/ice volume of the samples was measured using a graduated cylinder. Sampled filters were carefully packed inside petri-slides marked with a unique code representing the sample.

The snow density of winter snow samples was measured using a balance; snow/ice grain sizes were observed with a hand lens (25×) with an accuracy of 0.02 mm (Aoki et al., 2011) and snow shape were estimated through

snow card. We assumed external mixing of snow and aerosol particles and considered spherical snow grains. Qian et al., 2015 summarized sample methods for light absorbing particles in snow and ice from different region including Arctic, Tibetan Plateau and mid-latitude regions. Snow grain size and snow texture were larger sources of uncertainty in the albedo reduction mentioned in section 3.3.

2.3 Dust, OC, and BC analysis

Before analysis, sampled filters were allowed to dry in an oven for 24 hours and then weighed using a microbalance. The dust mass on the filters was calculated from the mass difference in weight before and after sampling (Kaspari et al., 2014; Li et al., 2017).

There are many methods available for analyzing BC and OC. The three methods considered most effective for measuring BC and water insoluble OC concentrations in snow are thermal optical analysis, filter-based analysis, and single particle soot photometer analysis (Ming et al., 2008). The thermal optical analysis method has been used by many researchers (e.g., Li et al., 2017) and was chosen for the study. This is an indirect method for measuring BC and OC on sampled filters; it follows Beer's law and uses stepwise combustion of the ~~impurities~~ particles deposited on quartz filters (Boparai et al., 2008), followed by measurement of light transmission and/or reflectance of the filters. The BC and OC content present in the collected samples was measured using a thermal optical DRI carbon analyzer, similar to the IMPROVE protocol (Cao et al., 2003). The temperature threshold that was applied to separate the two species is mentioned in Wang et al., 2012. A few (less than ten) filters had higher dust loads; for these the method was slightly modified using a 100% helium atmosphere and temperature plateau (550°C). A very few (less than 5) samples with very dense dust concentrations were not properly analyzed by the instrument and were excluded from the results. The extremely high dust value of one sample from Passu (15 times the level in the next highest sample) which had low values of other pollutants was excluded as a probable error. In some cases, a single sample was analyzed two or three times to ensure accurate results were obtained. Beside this filter based BC, OC and dust analysis

~~2.3.1 Frequency of different aerosol subtypes in the atmosphere~~

the CALIPSO models define multiple aerosol sub-types, with 532-nm (1064 nm) extinction-to-backscatter ratio. The frequency of different aerosol subtypes – clean marine, dust, polluted continental, clean continental, polluted dust, smoke, and other – present in the atmosphere over the study region was investigated using CALIPSO data for the same months in which ice and snow samples were collected i.e. January, May, June, and December – over the period June 2006 to December 2014. ~~The Level 2 aerosol profile data products were downloaded from https://eosweb.larc.nasa.gov/project/calipso/aerosol_profile_table. A set of feature classification flags (including aerosol subtype) detected in different layers of the CALIPSO backscatter data were derived.~~ The CALIPSO Level 2 lidar vertical feature mask data product describes the vertical and horizontal distribution of clouds and aerosol layers (downloaded from https://eosweb.larc.nasa.gov/project/calipso/aerosol_profile_table). On the basis of observed

Formatted: Normal

Formatted: Left, Adjust space between Latin and Asian text, Adjust space between Asian text and numbers

backscatter strength and depolarization, aerosol subtypes have been pre classified in the downloaded data. The details of algorithm used for the classification have been presented in Omar et al., 2009. Percentage contribution of individual aerosol subtypes were plotted using matlab.

The frequencies of different subtypes were calculated along the specific paths followed by CALIPSO over the study region.

2.4 Albedo simulations and estimation of radiative forcing

~~Light absorbing impurities (BC and dust particles) present on surface snow can reduce the snow surface albedo in the visible portion of the electromagnetic spectrum, increase solar radiation absorption, and accelerate melting (Yasunari et al., 2014). SZA, snow grain size, BC and dust concentration in snow, the presence of other light absorbing impurities, particle morphology, surface roughness, snow depth, liquid water content, snow shape, and topography are all important factors in reducing snow albedo (Wiscombe and Warren 1985).~~

Snow albedo was estimated for each of the 18 winter samples and the average calculated for samples at each of the sites (1 to 6). Albedo from two sites – S1 (Sost), which had the highest average concentration of BC and dust, and S6 (Kalam), which had the lowest average concentration of BC and dust – were further explored using the SNICAR model (Flanner et al., 2007). The aim was to quantify the effect of BC, dust, and Mass Absorption Cross section (MAC) on albedo reduction. Sensitivity model experiments were carried out using various combinations of BC, dust, and MAC values, while other parameters were kept constant (parameters for sites 1 and 6 shown in supplementary materials, Table S1). Snow albedo was simulated for different daylight times, with the SZA set in the range 57.0–88.9° based on the position of the sun in the sky for the sampling date and locations. The daily mean was calculated from the mean of the albedo values simulated for 24 different SZA values (one per hour), and the daytime mean from the mean of the albedo values simulated for 10 SZA values (one per hour during daylight). The mid-latitude winter clear-sky option was selected for surface spectral distribution. The parameters used for sensitivity analysis are shown in Table S1. MAC values of 7.5, 11, and 15 m^2/g were selected based on a literature review (Que et al., 2014; Pandolfi et al., 2014). In order to reduce the uncertainty, the dust concentration in the samples was divided into four diameter classes (as per the model requirements): size 1 (0.1–1.0 µm) was taken to be 2%, size 2 (1–2.5 µm) to be 13%, size 3 (2.5–5 µm) to be 31%, and size 4 (5–10 µm) to be 54% of total dust mass present in the sample, based on results published by others (Gillette et al., 1974; Mahowald et al., 2014). Radiative forcing (RF) was estimated for the same samples following Eq. (1):

$$RF_x = R_{in-short} * \Delta \boldsymbol{\alpha}_x \quad (1)$$

where $R_{in\text{-}short}$ denotes incident short-wave solar radiation (daily mean), as measured by the SBDART (Santa Barbara DISORT Atmospheric Radiative Transfer) model, and $\Delta\alpha_x$ denotes the daily mean reduction in albedo, as simulated by the SNICAR model.

Formatted: Justified

2.5 Source regions of pollutants

~~Black carbon particles have a residence time of days to weeks in the atmosphere (Cape et al., 2012) and may be transported a long way away from the source location (Kopacz et al., 2011; Aruna et al., 2013).~~ Three methods were used to identify the potential source regions of pollutants found at the study site: wind maps, emissions inventory coupled with back trajectories, and a region-tagged chemical transport modeling analysis.

~~2.5.1 Wind maps~~

~~Wind speed and direction were represented using the two perpendicular vectors U (the zonal velocity towards the east) and V (the meridional velocity towards the north).~~ Wind vector maps were prepared using ~~50 years of~~MERRA-2 reanalysis data ~~from the joint National Centers for Environmental Prediction and the National Center for Atmospheric Research (NCEP/NCAR) Reanalysis Project~~ (available from the National Aeronautics and Space Administration~~National Oceanic and Atmospheric Administration~~ [N~~O~~AASA] https://gmao.gsfc.nasa.gov/reanalysis/MERRA-2/docs/~~https://www.esrl.noaa.gov/psd/data/gridded/data.ncep.reanalysis.html~~). The U and V wind components were combined into a matrix around the study area for each individual month and then plotted against latitude/longitude values to show the spatial variance of monthly wind stress at ~~700~~ 850 mb using arrows to indicate the direction and intensity of wind.

~~2.5.2 Back air trajectories~~

Air trajectories were calculated backwards from the sampling sites (S1: 36.40°N 74.50°E; S6: 35.46°N 72.54°E) to identify potential source regions for the pollutants using the web version of the Hybrid Single Particle Lagrangian Integrated Trajectory (HYSPLIT-4) model (Draxler and Hess, 1998). The HYSPLIT-4 model has been used by others to compute air mass trajectories to identify possible source regions (Ming et al., 2009; Zhang et al., 2013). Reanalysis meteorological data from the same source as the wind data (https://www.esrl.noaa.gov/psd/data) were used as input data in the HYSPLIT model for May, June, and December 2015, and January 2016. HYSPLIT was run in a seven-day backward trajectory mode with trajectories initiating every six hours (0, 6, 12, and 18) on a daily basis from 4 May to 19 June 2015 (77 days during summer) and from 1 December 2015 to 31 January 2016 (62 during winter). The HYSPLIT model results were combined with Representative Concentration Pathways (RCPs) emission data for 2010 (available from http://sedac.ipcc-data.org/ddc/ar5_scenario_process/RCPs.html) to identify the source location. The data file used as a RCP emission inventory was "RCPs_anthro_BC_2005-2100_95371.nc". This comprises emission~~s~~ pathways starting from identical base year (2000) for multiple pollutants including black carbon and organic carbon. According to the description of the file, biomass burning sources were included in the RCP emission inventory that were utilized with the back-trajectory analysis. RCP had the same emissions sectors as for Hemispheric Transport Air Pollution (HTAP) emission inventory used in the molding part. The emission sectors include~~s~~ fuel combustion, industries, agriculture and livestock. The difference in HTAP and RCP inventories is the

Formatted: Justified

resolution. HTAP had relatively high resolution (0.1 x 0.1 degree) as compared to RCP (0.5 x 0.5 degree). Some discussion related to the inventory and the sectorial detail (12 sectors), which was used for the base year calibration of the RCPs is given in Lamarque et al., 2010.

Monthly CALIPSO satellite based extinction data from 2006 to 2014 were used to calculate the vertical profile for aerosol extinction over the study region. The CALIPSO extinction profile was constructed for selected months – May and June for summer and December and January for winter – in 2006 to 2014 (Figure S1). The exponential equation $X = (\log(10.46) - \log(Y))/10.29$ was used to calculate the extinction profile for the trajectory heights, where Y is the vertical height in kilometers and X indicates the extinction against the height of trajectories. Height of individual trajectory points ~~were~~ was put in the above equation and got a normalized extinction profile by assuming surface extinction =1(Figure S1).

~~2.5.3 WRF-STEM model~~

The WRF-STEM model was used as a third approach for identifying the origin (source regions) of air masses carrying pollutants. Region tagged CO tracer is a standard air quality modeling tool used by other regional and global chemical transport models to identify pollution source regions (Chen et al., 2009; Park et al., 2009; Lamarque and Hess, 2003). The WRF-STEM model uses region tagged carbon monoxide (CO) tracers for many regions in the world to identify geographical areas contributing to observed pollutants (Adhikary et al., 2010). The model domain centered on 50.377° E longitude and 29.917° N latitude. The model horizontal grid resolution was 45x45 km with 200 grids in the east-west direction and 125 north-south. The meteorological variables needed for the chemical transport were derived from the Weather Research and Forecast (WRF) meteorological model (Grell et al., 2005) using FNL data (ds083.2) available from the UCAR website as input data. The main aim of the simulation was to identify the geographic locations contributing to the observed pollutants at the field sites. ~~, thus emissions from open biomass burning were not included in the simulation. The simulations used the anthropogenic emissions from HTAPv2 (available from http://edgar.jrc.ec.europa.eu/htap_v2/), thus the results indicate the amount of pollutants reaching the study area from day-to-day planned and recurring activities in domestic, transport, industrial, and other sectors.~~ The HTAP version 2 emission inventory was used in our WRF-STEM modeling. The HTAP version 2 dataset consists of multiple pollutants including black carbon and organic carbon. This emission inventory include major sectors such as energy, industry, transport, and residential are included except large scale open agricultural and open forest fire burning). The simulations applied in our study used the anthropogenic emissions from HTAP inventory (available from http://edgar.jrc.ec.europa.eu/htap_v2/). So the results indicate the amount of pollutants reaching the study area from day-to-day planned and recurring activities in domestic, transport, industrial, and other sectors.

The model was run for a month prior to the field campaign dates to allow for model spin up (normal practice for a regional chemical transport model), and then for the months of December, January, and June, to match the field campaign dates.

3. Results and discussion

3.1 BC, OC and dust concentrations

Reported concentrations of OC and BC have been field blank subtracted. Total carbon (TC), OC and BC concentration values were blank corrected by subtracting an average of the field blanks. Blank concentrations were used to calculate detection limits as mean ± standard deviation. The minimum, maximum, and average concentrations of BC, OC, and dust in the ice and snow samples are given in Table 1. We represent water insoluble organic carbon as OC in this manuscript. The average BC concentration overall was 2130 ± 1560 ngg^{-1} in summer samples, 2883 ± 3439 ngg^{-1} in autumn samples (both from glaciers), and 992 ± 883 ngg^{-1} in winter samples. The average water insoluble OC concentration overall was 1839 ± 1108 ngg^{-1} in summer samples, 1423 ± 208 ngg^{-1} in autumn samples, and 1342 ± 672 ngg^{-1} in winter samples. There was considerable variation in individual samples, with summer values of BC ranging from 82 ngg^{-1} (Gulkin glacier) to 10,502 ngg^{-1} (Henarche glacier), autumn values from 125 ngg^{-1} (Gulkin glacier) to 6481 ngg^{-1} (Sachin glacier), and winter samples from 79 ngg^{-1} (Kalam) to 5957 ngg^{-1} (Sost).

The lowest BC (82 ngg^{-1}) and OC (128 ngg^{-1}) concentrations were observed in summer samples collected from the Gulkin and Sachin glaciers, respectively. The average values of BC and OC were low in all samples from the Passu glacier, even though it lies close to the Karakoram highway which links Pakistan with China. The low concentrations of BC may have been due to the east facing aspect of the glacier shielding it from pollutants transported from west to east. Slope aspect of a glacier is important for snow cover dynamics (Gul et al., 2017). Dust concentrations are known to vary with slope aspect due to the effects of wind direction on deposition.

The highest average concentration of BC was found in autumn samples from the Sachin glacier, and highest average concentration of OC in summer samples from the same glacier. The average concentration of BC was much greater in autumn than in summer on the Sachin glacier, but somewhat greater in summer than in autumn on the Gulkin glacier, indicating highly spatiotemporal patterns in the deposition of ~~impurities~~particles. The marked difference on the Sachin glacier may have reflected the difference in the direction of air, which comes from Iran and Afghanistan in summer and the Bay of Bengal via India in autumn, with the generally lower deposition on the Gulkin glacier more affected by other factors (such as slope aspect of the glacier and status of local emission near the glacier).

Most summer samples were collected from surface ice (Figure S2a), but a few samples for Gulkin and Sachin were collected from aged snow on the glacier surface (Figure S2 b,c). Dust was visible on the relatively aged snow, and the BC and OC concentrations in these snow samples were much higher than those in ice. The highest average BC values in winter were also observed in aged snow (from Sost) and the lowest in fresh snow (from Kalam) (Table 1). Generally, snow samples collected within 24hours after snowfall event ~~is considering~~considered as a fresh snow.

There was no clear correlation between average BC concentration of glacier samples and glacier elevation, while the winter snow samples showed a weak increasing trend in average BC with site elevation (Table 1, Figure S3). In most cases the concentration of OC was greater than the concentration of BC. In few cases the concentration of BC

Formatted: Normal

was greater than the concentration of OC, which might indicates the contribution of coal combustion and/or biomass burning to the emissions. The reported OC concentration was water insoluble OC. Including the water soluble OC could dominate the temporal variation of the OC/BC ratio. One important factor was post-deposition process, melt water can bring dissolved organic carbon away but not for BC. Low OC/BC ratio may also possible due to the fact that OC and BC had redistributed primarily under the control of strong melt water rather than sublimation and/or dry/wet deposition. The spatio-temporal variability of OC/BC ratio may also indicate the contribution of various sources, seasonal variation and frequent change in wind directions. The OC vs BC correlation in snow and ice samples depend on OC vs BC ratio/concentrations in the atmosphere, post deposition process and then scavenging, enrichment and melt rate of snow/snow after deposition. According to our understanding the analysis method and amount of dust loading on the sample can also alter OC/BC ratio. Further details about OC and BC splitting in thermal optical method are available in Wang et al., 2012.

We analyzed the ratios of OC to BC in the different samples as in atmospheric fractions this can be used as an indicator of the emission source, although apportionment is not simple and only indicative. The BC fraction is emitted during combustion of fossil fuels, especially biomass burning in rural areas in winter, and urban emissions from road transport. The OC fraction can be directly emitted to the atmosphere as particulate matter (primary OC) from fossil fuel emissions, biomass burning, or in the form of biological particles or plant debris; it can also be generated in the atmosphere as gases are converted to particles (secondary OC). In general, lower OC/BC ratios are associated with fossil fuel emissions and higher OC/BC ratios with biomass burning. The lowest OC/BC ratio of 0.041 was observed in a summer sample from Henarche glacier, and the highest ratio of 5 in a winter sample from Kalam. The higher value at Kalam may indicate greater contributions from biomass burning than from fossil fuel combustion in the region. There was no clear correlation between BC and OC concentrations. In summer samples, the average concentration of OC was greater than the average concentration of BC in samples from four of the six glaciers, but it was much lower in Barpu and Henarche. In winter, individual snow samples indicated that concentration of OC was greater than BC at low elevation sites and vice versa; the average OC was greater than average BC at all except the highest elevation site (Table 1).

In deposited samples, low OC/BC ratios can result from a reduction in OC (Niu et al., 2017), greater contributions from BC enrichment and OC scavenging, and/or the contribution of different emission sectors (including quantity, combustion conditions, and fuel type). Often, the OC/BC ratio reflects the impact of dilution of dissolved organic carbon and enrichment of primary organic carbon during snow/ice melting, and differences in OC/BC ratios may reflect differences in the enrichment process. The low OC/BC ratio in the samples from Henarche, the glacier at the lowest elevation, could, for example, be due to preferential washing out of OC particles with meltwater. Overall, there was a higher positive correlation between BC and dust compared to OC suggesting that for BC and dust particle precipitation and enrichment processes were similar.

A wide range of values has been reported by different authors for BC concentrations in snow and ice samples

Formatted: Justified

from different regions (Table S2). The concentrations of BC in our samples were higher than those reported by many authors (Table S2), but were comparable with the results reported by Xu et al. (2012) in the Tien Shan Mountains, Li et al. (2016) in the northeast of the Tibetan plateau, and Wang et al. (2016) in northern China and Zhang et al. (2017) in western Tien Shan, Central Asia. High concentrations indicate high deposition rates on the snow and ice surface, but there are several possible reasons for a wide variation in values apart from differences in deposition rates, including differences in sampling protocols, geographical/sampling location (Qu et al., 2014) and elevation of sampling site, and year/season of sampling. Majority of samples were from the ablation zone of the glaciers. Strong melting of surface snow and ice in the glacier ablation zone could also lead BC enrichment which causes high BC concentrations as Li et al., 2017 observed in the Southern Tibetan Plateau glacier. ~~T~~ The sampling season (May to September in our case) is an important factor because during the melting season rapid enrichment occurs immediately as snow melts. The peak melting period is May to August/September, thus the concentration of BC, OC, and dust in our samples would have been increased as melting progressed due to the enrichment in melting snow and scavenging by the melting water. In most cases snow and ice samples were collected quite a long time after snow fall, and the concentration of pollutants would also have increased in the surface snow and ice due to dry deposition. It seems likely that the pollutants in surface samples would be affected by sublimation and deposition until the next melt season (Yang et al., 2015). In some of the cases in our study, the average concentration of BC, OC, and/or dust for a particular glacier/site was increased as a result of a single highly concentrated sample, reflecting the wide variation that results from the interplay of many factors.

Enrichment is more marked at lower elevations as the temperatures are higher which enhances melting and ageing of surface snow, while deposition also tends to be higher because the pollutant concentrations in the air are higher (~~Wang et al., 2012~~ Wang et al., 2012; Nair et al., 2013). Previous studies have tended to focus on the accumulation area of glaciers (e.g. ice cores and snow pits) where enrichment influences are less marked, and on high elevation areas, where deposition is expected to be lower, in both cases leading to lower values. In our study, the majority of samples collected in summer and autumn were collected from the ablation area of debris-covered glaciers where enrichment influences are marked due to the relatively high temperature, and this is reflected in the relatively high values of BC, OC, and dust. Li et al. (2017) showed a strong negative relationship between the elevation of glacier sampling locations and the concentration of light absorbing ~~impurities~~particles. Stronger melt at lower elevations leads to higher pollutant concentrations in the exposed snow. Equally, BC may be enriched in the lower elevation areas of glaciers as a result of the proximity to source areas, as well as by the higher temperatures causing greater melting. Thus the main reason for the high concentrations of BC, OC, and dust in our samples may have been that the samples were taken from relatively low elevation sites. Human activities near the sampling sites in association with the summer pilgrimage season probably also contributed to an increase in pollutant concentrations. According to our understanding all the glaciers of the whole Karakoram region, may not substantially darkened by BC. Ablation zones of the debris covered glaciers which are relatively at low elevation and near to pollution source may be quite polluted.

3.2 Frequency distribution of aerosol sub types in the atmosphere

~~The frequency of different aerosol subtypes present in the atmosphere over the study region was investigated using CALIPSO subtype aerosol data (clean marine, dust, polluted continental, clean continental, polluted dust, smoke, and other) for January, May, June, and December (the months in which samples were collected) from June 2006 to December 2014. The frequency was calculated along the tracks followed by the CALIPSO satellite.~~ The CALIPSO aerosol type identifications analysis indicated that "smoke" was the most frequent-occurring type of aerosol over the study region during both summer and winter seasons.~~-~~ This result indicate that biomass burning sources may be the dominant contributor in this region. Frequency of sub type aerosol for the month of June in 2006 to 2014 is shown in Figure S4. Figure 2 shows the seasonal results for month of May, June (summer) and December, January (winter) in the form of a box plot. During June smoke had the highest frequency (39%), followed by dust (21%), polluted dust (12%), and others (20%) Figure S4. Overall Smoke, dust and or polluted dust were the dominant subtype aerosols in selected months over the study region. This type of aerosol measurement in the atmosphere is important for our current study because it provides observation based data over the study region. Other approaches used (such as modeling) were based on interpolation not observation. Pollutant deposition depends on the concentration of pollutants in the atmosphere, the results are consistent with the high concentration of BC (from smoke) and dust particles in the glacier and snow surface samples.

3.3 Snow albedo reduction

The albedo of individual winter snow samples was calculated using the SNICAR model and then averaged for each site (S1 to S6). Figure 3a shows the average for each site across the visible and infrared spectrum. Two sites were chosen for further analysis: S1 (Sost) which had the highest average concentration of BC, and S6 (Kalam) which had the lowest average concentration of BC. The albedo was simulated for different MAC values and SZA for samples at the two sites as described in the methods. The values for average albedo of samples from the two sites simulated ~~at a wavelength of 0.975 µm~~ for MAC values of 7.5, 11, and 15 m^2/g and SZA of 57.0–88.9° (day time) under a clear sky ranged from 0.39 (site S1, BC only, midday, MAC 15 m^2/g) to 0.85 (site S6, dust only, early evening, MAC 7.5–15 m^2/g). The albedo reduction values presented here are relative, indicating the difference of albedo with having certain pollutants (BC or dust or both) and a reference albedo (with zero pollutants i.e. zero BC and zero dust concentration). The detailed values are shown in Table S3.

Table 2 show the calculated percentage reduction (compared to a reference value with zero BC, OC, and dust) in daily minimum, maximum, and mean broadband snow albedo at different MAC values (7.5, 11, 15 m^2/g) resulting from the average BC, dust, and combined BC and dust concentrations found in samples at each of the sites. The reduction was strongly dependent on BC concentration and almost independent of dust concentration, and increased with increasing MAC value. The results suggest that BC was the dominant forcing factor, rather than dust, ~~as a result of the rapid snowmelt~~which influence glacial surface albedo and accelerate glacier melt.~~-~~ BC was found to play an important role in forcing in the northern Tibetan plateau (Li et al., 2016), whereas in the central Tibetan plateau and

Himalayas, dust played a more important role (Qu et al., 2014; Kaspari et al., 2014). The MAC value affected the albedo more in the visible range than at 1.2 µm (near infrared) wavelength (Fig 3c, d). The combined concentration of BC and dust, or BC alone, strongly reduced the snow albedo for a given combination of other input parameters. The effect at the low pollutant site (S6) was small: the values for day time snow albedo at 0.975 µm due to BC, or BC plus dust with different MAC and SZA, ranged from 0.70 to 0.83, with a reduction in daily mean albedo of 1.8 to 2.9%, and those for dust alone from 0.79 to 0.85, with a reduction in daily mean albedo of less than 0.1%. The effect at the high pollutant site (S1) was much more marked: BC or BC and dust reduced day time snow albedo to values ranging from 0.39 to 0.64, a reduction in daily mean albedo of 8.8 to 12.0%, but the effect of dust alone was still low with values of 0.70 to 0.78, again a reduction in daily mean albedo of less than 0.1%.

Both the snow albedo and the impact of ~~impurities~~ light absorbing particles depend on a range of factors including the SZA, snow depth, snow grain size, and ~~snow age~~snow density. For example, the snow albedo reduction due to BC is known to be less in the presence of other light absorbing ~~impurities~~ particles as these will absorb some of the available solar radiation (Kaspari et al., 2011). The snow albedo calculated for our samples was strongly dependent on the SZA with albedo increasing with decreasing SZA, especially at near infrared wavelengths (Table S3).

The impact of snow ageing was also investigated. The winter samples from S1 (Sost) were aged snow, whereas those from S6 (Kalam) were fresh snow (Table 1, Figure S5 b,c). Not only was dust clearly visible on the surface of the aged snow, the grain size was large and the snow was dense. The aged snow had a much higher concentration of BC and dust, which reduced the albedo, but the extent of reduction is also affected by other factors. Albedo reduction by BC and dust particles is known to be greater for aged snow than for fresh snow (Warren and Wiscombe, 1985). In our samples, the calculated reduction in snow albedo for high MAC values (15) compared to low MAC values (7.5) was greater in aged snow than in fresh snow (Figure 3b). The effective grain size of snow increases with time as water surrounds the grains. Snow with larger grain size absorbs more radiation because the light can penetrate deeper into the snowpack, thus decreasing surface albedo (Flanner et al., 2006). In the melting season, the snowpack becomes optically thin and more ~~impurities~~ particles are concentrated near the surface layer, which further increases the effect on albedo.

The estimated reduction in snow albedo by dust and BC ~~compounded by the age of snow~~ (up to 29% of daytime maximum value, Table 2) was higher than that reported by others for High Asia based on farmers' recordings (e.g 1.5 to 4.6% reported by Nair et al., 2013) and in the Himalayas (Ming et al., 2008; Kaspari et al., 2014; Gertler et al., 2016). However, although the values were relatively high, they were at the same level or lower than the estimates for albedo reduction of 28% by BC and 56% by dust in clean ice samples, and of 36% by BC and 29% by dust in aged snow samples, reported by Qu et al. (2014) for surface samples from the Zhadang glacier, China. Simulation results by Ming et al. (2013a) showed BC, dust, and grain growth to reduce broadband albedo by 11%, 28%, and 61%, respectively, in a snowpack in central Tibet. Dust was the most significant contributor to albedo reduction when mixed inside the snow and ice, or when the glacier was covered in bare ice. In our case BC was a more influential

445 factor than dust during a similar study period to that reported by Li et al. (2017), indicating that BC plays a major
446 role in albedo reduction.
447 The possible reasons for the relatively high values for albedo reduction in our samples include the lower
448 elevation of the sampling locations, relatively high concentrations of BC and dust, high MAC values, low snow
449 thickness, underlying ground quality, presence of small and large towns near the sampling sites, and predominance
450 of aged snow samples. Most of the samples collected in winter were from places with snow depth less than 50 cm
451 (Figure S5a), thus mud, stones, and clay below the snow layer would be expected to increase the absorption of solar
452 radiation and reduce the albedo.
453 The high albedo reduction in the visible range of the electromagnetic spectrum could be due to the relatively
454 high concentration of surface (~1cm) snow impurities. The total amount of deposited ~~impurities~~ particles in the
455 surface layer of aged snow was relatively high, indicating a high deposition rate of atmospheric pollutants.
456 Flanner et al. (2007) reported that BC emission and snow ageing are the two largest sources of uncertainty in
457 albedo estimates. The uncertainties in our estimated albedo reduction include the BC type (uncoated or sulfate
458 coated), ~~exact snow age,~~ the size distribution of dust concentration, the accuracy of snow grain size, snow texture,
459 snow density, and albedo of the underlying ground. Sulfate-coated particles have an absorbing sulfate shell
460 surrounding the carbon; recent studies confirm that coated BC has a larger absorbing power than non-coated BC
461 (Naoe et al., 2009). We used uncoated black carbon concentration in the SNICAR model, but the pollutants at the
462 remote site are presumed to be mainly from long range transport, thus the BC may have gained some coating. The
463 albedo reduction for sulfate-coated black carbon was calculated to be 3–8.5% higher, depending on the MAC and
464 SZA values, than for uncoated black carbon at low concentrated site S6 (Figure S6). According to our
465 understanding, snow grain size (snow aging) and snow texture are larger sources of uncertainty. The effect of snow
466 grain size is generally larger than the uncertainty in light absorbing particles which varies with the snow type
467 (Schmale et al., 2017). For an effective snow grain radius of 80 μm, 100 μm, 120 μm, the albedo reduction caused
468 by 100 ng g−1 of BC was 0.017, 0.019 and 0.021 respectively. As snow grain size was measured with a hand lens
469 (with reported accuracy of 20 μm), so at least 0.002 uncertainty is present in our albedo results. Snow grain shape
470 was measured with the help of snow card, however grain shape was not used in the online SNICAR albedo
471 simulation model and assumed a spherical shape for the snow grains. Albedo of non-spherical grain is higher than
472 the albedo of spherical grains (Dang et al., 2016). The shapes of snow grains and/or ice crystals is significantly
473 changing with snow age and meteorological conditions during and after snowfall (LaChapelle 1969). Besides this, a
474 number of recent studies (e.g., Flanner et al., 2012; Liou et al., 2014; He et al., 2014, 2017) have shown that both
475 snow grain shape and aerosol-snow internal mixing play important roles in snow albedo calculations.
476

477 **3.4 Radiative forcing (RF)**

478 Radiative forcing (RF) is a measure of the capacity of a forcing agent to affect the energy balance in the

Formatted: Justified

Formatted: Font: 10 pt

atmosphere – the difference between sunlight absorbed by the Earth and energy radiated back to space – thereby contributing to climate change. Changes in albedo contribute directly to radiative forcing: a decrease in albedo means that more radiation will be absorbed and the temperature will rise. In snow and ice, the additional energy absorbed by any pollutants present also increases and accelerates the melting rate.

Various authors have described the impact of albedo change in snow and ice on radiative forcing. Zhang et al. (2017) reported that a reduction in albedo by 9% to 64% can increase the instantaneous radiative forcing by as much as 24.05–323.18 Wm^{-2}. Nair et al. (2013) estimated that in aged snow a BC concentration of 10–200 ngg^{-1} can increase radiative forcing by 2.6 to 28.1 Wm^{-2}; while Yang et al. (2015) reported radiative forcing of 18–21 Wm^{-2} for aged snow in samples from the westernmost Tibetan Plateau. To estimate these radiative forcing measurements, mid-latitude winter with clear sky and cloudy environment was used by Zhang et al. 2017; mid-latitude winter atmospheric conditions was used by Nair et al., 2013; while clear-sky and cloudy conditions environment was used by Yang et al., 2015.

We calculated the radiative forcing in the samples assessed for day time albedo and daily (24h) mean albedo. The radiative forcing at different daylight times caused by BC deposition varied from 3.93 to 43.44 Wm^{-2} (3.93–11.54 Wm^{-2} at the low BC site and 20.88–43.45 Wm^{-2} at the high BC site), and that by dust from 0.16 to 2.08 Wm^{-2} (0.16–0.30 Wm^{-2} at the low BC site and 1.38–2.08 Wm^{-2} at the high BC site) (detailed values given in Table S4), indicating that BC was the dominant factor. The RF due to combined BC and dust was very similar to that for BC alone. Based on optical properties and size distribution of dust particles some studies in past showed higher forcing due to dust as compared to BC (Qu et al., 2014). The increase in daily mean radiative forcing ranged from 0.1% for dust only at the low pollutant site to 14.9% for BC at the high pollutant site. It is important to mention here that dust forcing varies strongly with dust optical properties, source material and particle size distribution. Properties for dust are unique for each of four size bins used in SNICAR online model. These size bins represent partitions of a lognormal size distribution. We used the estimated size of dust particles with generic property of dust in the model. Some dust particles can have a larger impact on snow albedo than the dust applied here (e.g., Aoki et al., 2006; Painter et al., 2007).

Both radiative forcing and albedo reduction increased with decreasing daytime SZA, indicating higher melting at midday compared to morning and evening. Figure 4 shows the daily mean albedo reduction and corresponding radiative forcing caused by BC for fresh (low BC) and aged (high BC) snow with different MAC values. Snow aging (snow grain size) plays an important role in albedo reduction and radiative forcing. Schmale et al., (2017) stating that the effect of snow grain size is generally larger than the uncertainty in light absorbing particles which varies with the snow type. The impact of snow aging factor on BC in snow and induced forcing are complex and had spatial and seasonal variation (Qian et al., 2014). Increase of snow aging factor reduces snow albedo and accelerate the snow melting.

An increase in MAC value from 7.5 to 15 led to an increase in radiative forcing by 1.48 Wm^{-2} in fresh snow and 4.04 Wm^{-2} in aged snow. This suggests that when the surface of snow, ice, and glaciers experience strong melting,

Formatted: Justified, Don't adjust space between Latin and Asian text, Don't adjust space between Asian text and numbers

enrichment with BC and dust could cause more forcing. Previous studies of ice cores and snow pits probably underestimated the albedo reduction and radiative forcing in glacier regions as samples were taken from high elevation areas where there is less ageing and melting and thus lower surface enrichment of BC and dust than at lower elevation. Our results are higher than those reported in other studies on the northern slope of the Himalayas (Ming et al., 2012), western Tibetan Plateau (Yang et al., 2015b), and Tien Shan mountains (Ming et al., 2016). However, they are comparable to values for radiative forcing reported more recently by others, for example for the Muji glacier (Yang et al., 2015), Zhadang glacier (Qu et al., 2014), in high Asia (Flanner et al., 2007; Nair et al., 2013), and in the Arctic (Wang et al., 2011; Flanner, 2013). The results suggest that enrichment of black carbon (in our case) and mineral dust (other authors) can lead to increased absorption of solar radiation, exerting a stronger effect on climate and accelerating glacier melt.

3.5 Potential source regions

3.5.1 Wind vector maps

Figure 5 shows the spatial variance of wind vector maps (U and V) at ~~700~~ 850 mb in May, June, January, and December prepared using ~~50 years of~~MERRA-2 reanalysis data for the year 2015 and 2016. The wind blows primarily from west to east but there were variations over the year. Central ~~and South~~ Asia contributed ~~a large~~ some part of the air in ~~December, January, and~~ May and June. In winter (December and January), the wind blew from Azerbaijan and northwest Iran, reaching the study site via Syria, Iraq, Turkmenistan, and Afghanistan. In May, the prevailing air masses were from Syria, Turkey, Turkmenistan, Iraq, Azerbaijan, northwest Iran, Afghanistan, Nepal, South west China and southern Pakistan. In June, the trend ~~shifted gradually towards~~was almost same as in May ~~air arriving from the east (Myanmar and Thailand) through the Bay of Bengal, India, the Arabian Sea, and southeast Pakistan, especially to lower elevation areas,~~with relatively less contribution from Nepal ~~and~~ and South west China~~becoming dominated by these easterlies in autumn~~. In ~~November~~ January and December, the western trade winds ~~again became~~were stronger than the easterlies.

3.5.2 Coupled emissions inventory with back air trajectory

Trajectory analysis using the HYSPLIT model showed that in May and June 2015 air parcels reached the study site along three different pathways: one from north Asia (Russia) via Central Asia (Kazakhstan), one from western Asia (Cyprus and Syria) via Central and Southern Asia (Georgia), and one via India, which was more local (Figure 6). The trajectories in summer had distinct pathways, while those in winter were dispersed in all directions, partially covering West, East, and South Asia, and completely covering Central Asia. Figure 6 shows the product of extinction and emission calculated along the pathways of trajectories calculated using the vertical profile for aerosol extinction over the study region obtained from the monthly CALIPSO satellite-based extinction data. Scattering and absorption decreased exponentially with increasing elevation (Figure S1) but was still visible at elevations above 5 km in summer.

The RCP emission data combined with back trajectories and extinction data showed that the hotspot regions of pollution that affected the study sites during winter were mainly to the southwest rather than very distant (Figure 6b). Iran, Turkmenistan, Azerbaijan, Georgia, the eastern part of Turkey, and the southwestern part of Russia all showed comparatively high pollutant emissions in winter which moved towards northern Pakistan. The western part of Kazakhstan, Uzbekistan, and northeastern Turkey emitted particularly high concentrations of pollutants.

Combination of the back-trajectory results and surface-wind direction analysis indicated that during the sampling months, aerosols were significantly influenced by the long-range transport of pollutants coming from Central and South Asia, with a small contribution from West and East Asia. This differs somewhat from previous reports which suggested that the Tibetan Plateau and Himalayan region are mainly effected by pollutants from East and South Asia (Zhang et al., 2015). An increasing trend has been reported for black carbon emissions in Central and South Asia over the past 150 years (Bond et al., 2007), and a significant increase has been found in black carbon concentrations in glacier snow in west China in the last 20 years, especially during the summer and monsoon seasons (Ming et al., 2008). In South Asia, the largest source of atmospheric black carbon is emission from biomass and biofuels used for cooking and heating (dung, crop residues, wood) (Venkataraman et al., 2005).

~~BC from East Asia can potentially be lifted up high and transported to the northeast during the summer monsoon season (Zhang et al., 2015). Nevertheless, t~~The results indicate that only a low level of pollutants (minor contribution) reached the study area from ~~this source~~Northwest China. BC particles emitted from distant low latitude source regions such as ~~South~~ tropical Africa barely reach the Tibetan Plateau and Himalayan regions because their ~~weak~~ emissions are removed along the transport pathways during the summer monsoon season (Zhang et al., 2015).

3.5.3 Chemical transport modelling

The contribution of pollutants from potential source regions was also investigated using the WRF-STEM model with tagged carbon monoxide tracers and source regions of East Asia, South Asia, Central Asia, the Middle East, Europe, the Russian Federation, and West Asia. (The individual countries in the regions are listed in Table S5).

Figure 7 shows the results of the model simulations for summer (1 June to 4 July 2015) and winter (15 December 2015 to 17 January 2016) at two glacier sites (Sachin and Shangla) where the model terrain elevation was close to the observation terrain elevation. The model simulations showed Pakistan to be the major contributor of pollutants in summer (77% at Shangla and 43% at Sachin) followed by the South Asian countries; and the south Asian countries in winter (47% at Shangla and 71% at Sachin) followed by Pakistan, which is in line with the findings by Lu et al. (2012) that South Asia contributed 67% black carbon in the Himalayas. There were minor contributions of 2–7% of pollutants from Afghanistan, Iran, Central Asia, and the Middle East, and extremely small amounts from East Asia, Europe, Africa, West Asia, and China. The contribution from Iran, the Middle East, and Europe was greater in winter than in summer, while the contribution from Central Asia and China was greater in summer than in winter. The proportion of daily contributions fluctuated ~~considerable~~considerably: with higher contributions from Iran, the Middle East, and Europe on individual days in winter, ranging for example from 2–30%

for the Middle East.

The concentration of hydrophobic BC (BC1), hydrophilic BC (BC2), and total black carbon (BC = BC1 + BC2) given by the model for Sachin glacier grid point in the summer and winter seasons is shown in supplemental material (Figure S7). Freshly emitted BC particles are hydrophobic and gradually acquire a hygroscopic coating over time in the model. Time series analysis of BC1 and BC2 concentration show influence of both freshly emitted BC as well as aged BC reaching the observation location. The highest concentration of BC1 was observed on 20th December 2015 followed by 25th June 2015, indicating influence of freshly emitted air mass both in the summer as well as winter months. Future study (BC tracer) will evaluate the details of the different source region of BC reaching the glaciers as compared to region tagged CO tracers.

3.5.4 Comparison of the different approaches used to identify potential source regions

The high BC concentration in the atmosphere over the study region was attributed to long-range transport from urban source regions. Potential source regions of the pollutants deposited on glaciers and snow were identified using wind vector mapping with ~~50 years~~ MERRA-2 ~~of~~ reanalyzed data, calculation of back air trajectories using the HYSPLIT-4 model, and chemical transport pathways using the WRF-STEM tagged chemical transport model. The back trajectory results indicated that the majority of pollutants in summer were from Central and South Asia, and in winter from Iran, Pakistan, Iraq, Turkmenistan, Azerbaijan, Georgia, Jordan, Syria, Tunisia, Ukraine, Libya and Egypt. The WRF-STEM model indicated that most anthropogenic pollutants were from Pakistan and South Asia during both summer and winter. However, both approaches showed a reasonable contribution from Central Asian countries and limited contribution from East Asian countries in summer. The wind vector maps also indicated that the study site was mostly effected by westerly winds. All three approaches showed a reasonable contribution from neighboring countries such as Afghanistan, Pakistan, Iran, and India in specific months. Overall, the results indicate that South, Central, and West Asia were the major sources of the pollutants detected at the sampling sites.

There was some mismatching in source regions among the three approaches. The WRF-STEM model and wind vector maps both identified a small contribution from East Asia, but this was not identified in the back trajectories approach. Similarly, the wind vector maps and back air trajectories showed a dominant contribution from the west, while the WRF-STEM model showed a major contribution from Pakistan and South Asia. The differences in the results obtained by the different methods may be due in part to the complex topography of the region and the different altitudes used by the methods; the coarse resolution of the WRF-STEM model; and differences in the emission source inventories and meteorological parameters used by the WRF-STEM and HYSPLIT-4 models. Limitation of using back trajectories to identify source region is explained further in a paper by (Jaffe et al., 1999).

Furthermore, the atmospheric BC concentration over the Himalayas has significant temporal variations associated with synoptic and meso scale changes in the advection pattern (Babu et al., 2011) which can affect pollutant transport and deposition. The large uncertainty among different emission inventories can also affect the results, especially in the Himalayan region.

4 Summary and conclusion

Black carbon (BC) and organic carbon (OC) concentrations were measured using thermal optical analysis of snow and ice surface samples collected from glacier and mountain valleys in northern Pakistan in summer, autumn, and winter. The samples contained high concentrations of BC, OC, and dust in low elevation glaciers and surface snow in mountain valleys. The samples from Sost contained the highest average concentration of BC in mountain valleys snow (winter) and those from Kalam the lowest, probably due to the impact of snow age, increased concentration of black carbon and dust (the Sost samples were aged snow and Kalam samples fresh snow), ~~and increased grain size and density~~. The average concentration of BC in surface samples from Sachin glacier was higher in autumn than in summer; the BC values in summer snow samples collected from Sachin and Gulkin glaciers (aged snow from the glacier surface) were much higher than those in ice. The average BC concentration in summer samples collected from glaciers was 2130 ± 1560 ngg^{-1} and that in autumn samples 2883± 3439ngg^{-1}. The average concentration of OC was 1839 ± 1108 ngg^{-1} in summer samples, 1423 ± 208 ngg^{-1} in autumn samples, and 1342 ± 672 ngg^{-1} in winter samples, with the highest variability in summer samples. The individual lowest BC (82 ngg^{-1}) and OC (129 ngg^{-1}) concentrations were observed in summer samples collected from the Gulkin and Sachin glaciers, respectively. Dust and other pollutants were clearly visible on aged snow and ice surfaces; the results indicate considerable enrichment during ageing. The pollutant concentrations in our samples were relatively higher than those reported by others in earlier studies, which tended to focus on the accumulation area of glaciers (e.g. ice cores and snow pits), where enrichment influences are less marked and measured values are likely to be lower, and high elevation areas, where deposition of pollutants is expected to be lower. It is likely that pollutant concentrations were underestimated in these earlier studies, particularly when there was strong surface melting.

Snow albedo was calculated for winter samples using the SNICAR model with various combinations of BC and dust concentrations, three values for MAC, and a range of values for SZA (57 – 88.89º during daytime), with other parameters kept constant. BC was the major component responsible for albedo reduction, dust had little effect. The reduction by BC ranged from 2.8 to 32.5% during daytime, which is quite high, with albedo reduced to below 0.6. The reduction was greater for higher concentrations of BC and greater MAC. The reduction in 24 h average albedo ranged from <0.07–2.9% for fresh snow samples and <0.05–12.0% for aged snow. Changes in albedo contribute directly to radiative forcing: a decrease in albedo means that more radiation will be absorbed and the temperature will rise. The radiative forcing by BC was also higher than that caused by dust, indicating that BC was the dominant factor. The day time albedo values in winter snow samples ranged from 0.39 to 0.82 with BC alone or BC plus dust, and from 0.70 to 0.85 with dust alone; the corresponding radiative forcing was 3.93–43.44 Wm^{-2} for BC alone, 4.01–43.45 Wm^{-2} for BC and dust, and 0.16–2.08 Wm^{-2} with dust alone. The radiative forcing calculated from the daily mean albedo reduction ranged from 0.1% for dust only at the low pollutant site to 14.9% for BC at the high pollutant site.

The potential source regions of the pollutants deposited on glaciers and snow were identified using spatial variance in wind vector maps, emission inventories coupled with back air trajectories, and region tagged chemical

transport modelling. The wind vector maps identified Central Asian and South Asian countries (such as Azerbaijan, Turkmenistan, Pakistan, Afghanistan, Syria, Iraq, Turkey) as more important. The trajectory analysis coupled with emission inventories showed that air parcels reached northern Pakistan along three pathways, one from north Asia (Russia) via Central Asia (Kazakhstan), one from western Asia (Cyprus and Syria) via Central and Southern Asia (Georgia), and one via India. Combination of the back-trajectory results and surface-wind direction analysis indicated that aerosols were significantly influenced by the long-range transport of pollutants from Central and South Asia. The region tagged chemical transport model indicated that Pakistan and South Asia were the main contributors of pollutants. Analysis based on the WRF-STEM model identified a significant contribution from Pakistan (up to 77%) and South Asia (up to 71%) at selected sites. Overall, the results indicate that Central, South, and West Asia were the major sources of the pollutants detected at the sampling sites, with only a small contribution from East Asia.

The overall precision in the BC, OC and TC concentrations was estimated considering the analytical precision of concentration measurements and mass contributions from field blanks. Uncertainty of the BC and OC mass concentrations was measured through the standard deviation of the field blanks, experimentally determined analytical uncertainty, and projected uncertainty associated with filter extraction. According to our understanding the major uncertainty in our study was the dust effect on BC/OC measurement. Warming role of OC was also not included in the current research which was low, but significant in several regions (Yasunari et al. 2015). Beside this we think snow grain size (snow aging) and snow texture were larger sources of uncertainty in the albedo reduction / radiative forcing calculations ~~than indicated~~. The measured grain size was usually different from the effective optical grain size used in the SNICAR modeling. Snow grain shape was measured with the help of snow card, but was not used in the online SNICAR albedo simulation model and assumed a spherical shape for the snow grains which may slightly affect the results, because albedo of non-spherical grain is higher than the albedo of spherical grains (Dang et al., 2016). On modeling side the possible uncertainties are related to using CO as a tracer for light absorbing particles source region. Uncertainties are also attributed to errors in emissions inventories, simulated meteorology and removal processes built in the model. The physics and chemistry of removal for BC and CO are different from each other especially during wet seasons. We analyze the model during pre-monsoon and relatively dry periods, so we are expecting relatively good correlation in transport between CO and BC. While using global emission inventories we were unable to capture emissions at local scale. Contributions of local sources may be underestimated by coarse-resolution models. Therefore high resolution models and emission inventories at local scale are required to capture local emissions. Better-constrained measurements are required in the future for more robust results. High resolution satellite imagery, high resolution models and continuous monitoring can help us to reduce the present uncertainty.

Acknowledgments

This study was supported by the National Natural Science Foundation of China (41630754, 41671067, and 41501063), the Chinese Academy of Sciences (KJZD-EW-G03-04), the State Key Laboratory of Cryosphere Science (SKLCS-ZZ-2015), program funding to ICIMOD from the Governments of Sweden and Norway, and ICIMOD core funds contributed by the Governments of Afghanistan, Australia, Austria, Bangladesh, Bhutan, China, India, Myanmar, Nepal, Norway, Pakistan, Switzerland, and the United Kingdom. The authors wish to thank the unknown reviewers for their invaluable comments and advice on an earlier draft.

References

Adhikary, B., Carmichael, G. R., Kulkarni, S., Wei, C., Tang, Y., D'Allura, a., Mena-Carrasco, M., Streets, D. G., Zhang, Q., Pierce, R. B., Al-Saadi, J. a., Emmons, L. K., Pfister, G. G., Avery, M. a., Barrick, J. D., Blake, D. R., Brune, W. H., Cohen, R. C., Dibb, J. E., Fried, a., Heikes, B. G., Huey, L. G., O'Sullivan, D. W., Sachse, G. W., Shetter, R. E., Singh, H. B., Campos, T. L., Cantrell, C. a., Flocke, F. M., Dunlea, E. J., Jimenez, J. L., Weinheimer, a. J., Crounse, J. D., Wennberg, P. O., Schauer, J. J., Stone, E. a., Jaffe, D. a. and Reidmiller, D. R.: A regional scale modeling analysis of aerosol and trace gas distributions over the eastern Pacific during the INTEX-B field campaign, Atmos. Chem. Phys., 10(5), 2091–2115, doi:10.5194/acp-10-2091-2010, 2010.

Aoki, T., Kuchiki, K., Niwano, M., Kodama, Y., Hosaka, M. and Tanaka, T.: Physically based snow albedo model for calculating broadband albedos and the solar heating profile in snowpack for general circulation models, J. Geophys. Res. Atmos., 116(11), 1–22, doi:10.1029/2010JD015507, 2011.

~~Aruna, K., Kumar, T. V. L., Rao, D. N., Murthy, B. V. K., Babu, S. S. and Moorthy, K. K.: Black carbon aerosols in a tropical semi-urban coastal environment: Effects of boundary layer dynamics and long range transport, J. Atmos. Solar-Terrestrial Phys., 104(March), 116–125, doi:10.1016/j.jastp.2013.08.020, 2013.~~

Babu, S. S., Chaubey, J. P., Krishna Moorthy, K., Gogoi, M. M., Kompalli, S. K., Sreekanth, V., Bagare, S. P., Bhatt, B. C., Gaur, V. K., Prabhu, T. P. and Singh, N. S.: High altitude (~4520 m amsl) measurements of black carbon aerosols over western trans-Himalayas: Seasonal heterogeneity and source apportionment, J. Geophys. Res. Atmos., 116(24), 1–15, doi:10.1029/2011JD016722, 2011.

Bond, T. C., Bhardwaj, E., Dong, R., Jogani, R., Jung, S., Roden, C., Streets, D. G. and Trautmann, N. M.: Historical emissions of black and organic carbon aerosol from energy-related combustion, 1850-2000, Global Biogeochem. Cycles, 21(2), 1–16, doi:10.1029/2006GB002840, 2007.

Boparai, P., Lee, J. and Bond, T. C.: Revisiting Thermal-Optical Analyses of Carbonaceous Aerosol Using a Physical Model, Aerosol Sci. Technol., 42(11), 930–948, doi:10.1080/02786820802360690, 2008.

Cao, J. J., Lee, S. C., Ho, K. F., Zhang, X. Y., Zou, S. C., Fung, K., Chow, J. C. and Watson, J. G.: Characteristics of carbonaceous aerosol in Pearl River Delta Region, China during 2001 winter period, Atmos. Environ., 37(11), 1451–1460, doi:10.1016/S1352-2310(02)01002-6, 2003.

~~Cape J. N., Coyle. M., Dumitrean, P.: The atmospheric lifetime of black carbon, J. Atmospheric Environment, Volume 59, doi.org/10.1016/j.atmosenv.2012.05.030, 2012.~~

Chen, D., Wang, Y., Mcelroy, M. B., He, K., Yantosca, R. M. and Sager, P. Le: and Physics Regional CO pollution and export in China simulated by the high-resolution nested-grid GEOS-Chem model, , (2008), 3825–3839, 2009.

Cong, Z., Kawamura, K., Kang, S., Fu, P., River, G., River, Y. and River, Y.: Penetration of biomass-burning emissions from South Asia through the Himalayas : new insights from, , 1–7, doi:10.1038/srep09580, 2015.

Dang, C., et al. (2016), Effect of Snow Grain Shape on Snow Albedo. J. Atmos. Sci., 73, 3573–3583, doi:10.1175/JAS-D-15-0276.1

Déry, S. J. and Brown, R. D.: Recent Northern Hemisphere snow cover extent trends and implications for the snow-albedo feedback, Geophys. Res. Lett., 34(22), 2–7, doi:10.1029/2007GL031474, 2007.

Doherty, S. J., Grenfell, T. C., Forsström, S., Hegg, D. L., Brandt, R. E. and Warren, S. G.: Observed vertical redistribution of black carbon and other insoluble light-absorbing particles in melting snow, J. Geophys. Res. Atmos., 118(11), 5553–5569, doi:10.1002/jgrd.50235, 2013.

Draxler, R. R. and Hess, G. D.: An Overview of the HYSPLIT_4 Modelling System for Trajectories, Dispersion, and Deposition, Aust. Meteorol. Mag., 47(February), 295–308, 1998.

Fitzgerald, W. F.: Clean hands, dirty hands: Clair Patterson and the aquatic biogeochemistry of mercury, Clean Hands, Clair Patterson's Crusade Against Environmental Lead Contamination, 119–137, 1999.

Flanner, M. G.: Arctic climate sensitivity to local black carbon, J. Geophys. Res. Atmos., 118(4), 1840–1851, doi:10.1002/jgrd.50176, 2013.

Flanner, M. G. and Zender, C. S.: Linking snowpack microphysics and albedo evolution, J. Geophys. Res. Atmos., 111(12), 1–12, doi:10.1029/2005JD006834, 2006.

Flanner, M. G., Zender, C. S., Randerson, J. T. and Rasch, P. J.: Present-day climate forcing and response from black carbon in snow, J. Geophys. Res. Atmos., 112(11), 1–17, doi:10.1029/2006JD008003, 2007.

Flanner, M. G., Zender, C. S., Hess, P. G., Mahowald, N. M., Painter, T. H., Ramanathan, V. and Rasch, P. J.: Springtime warming and reduced snow cover from carbonaceous particles, Atmos. Chem. Phys. Discuss., 8(6), 19819–19859, doi:10.5194/acpd-8-19819-2008, 2009.

Gertler, C. G., Puppala, S. P., Panday, A., Stumm, D. and Shea, J.: Black carbon and the Himalayan cryosphere: A review, Atmos. Environ., 125(SEPTEMBER), 404–417, doi:10.1016/j.atmosenv.2015.08.078, 2016.

Gillette, D.A., Blifford, I.H., Fryrear, D.W.: Influence of wind velocity on size distributions of aerosols generated by wind erosion of soils. J. Geophys. Res. 79, 4068–4075, doi: 10.1029/JC079i027p04068, 1974.

Grell, G. A., Peckham, S. E., Schmitz, R., McKeen, S. A., Frost, G., Skamarock, W. C. and Eder, B.: Fully coupled chemistry within the WRF model, Atmos. Environ., 39(37), 6957–6975, doi:DOI: 10.1016/j.atmosenv.2005.04.027, 2005.

Gul, C., Kang, S. et al.: Using Landsat images to monitor changes in the snow-covered area of selected glaciers in

Formatted: Font color: Auto

752 northern Pakistan, Journal of Mountain Science, DOI：10.1007/s11629-016-4097-x.2017.
753 Hansen, J. and Nazarenko, L.: Soot climate forcing via snow and ice albedos, Proc. Natl. Acad. Sci. U. S. A., 101(2),
754 423–428, doi:10.1073/pnas.2237157100, 2004.
755 Hansen, J., Sato, M., Ruedy, R., Nazarenko, L., Lacis, A., Schmidt, G. A., Bell, N.:Climate and Dynamics-D18104-
756 Efficacy of climate forcings, J. Geophys. Res., Part D-Atmospheres, 110(18), doi: 10.
757 1029/2005JD005776, 2005.
758 Immerzeel, W. W., van Beek, L. P. H. and Bierkens, M. F. P.: Climate change will affect the Asian water towers.,
759 Science, 328(5984), 1382–5, doi:10.1126/science.1183188, 2010.
760 Jacobson, M. Z.: Climate response of fossil fuel and biofuel soot, accounting for soot's feedback to snow and sea ice
761 albedo and emissivity, J. Geophys. Res., 109, D21201, doi:10.1029/2004JD004945, 2004
762 Jaffe, D., Anderson, T., Covert, D., Kotchenruther, R., Trost, B., Danielson, J., Simpson, W., Blake, D., Harris, J. and
763 Carmichael, G.: Transport of Asian Air Pollution to North America, , 26(6), 711–714, 1999.
764 Kaspari, S., Painter, T. H., Gysel, M., Skiles, S. M. and Schwikowski, M.: Seasonal and elevational variations of
765 black carbon and dust in snow and ice in the Solu-Khumbu, Nepal and estimated radiative forcings, Atmos.
766 Chem. Phys., 14(15), 8089–8103, doi:10.5194/acp-14-8089-2014, 2014.
767 Kaspari, S. D., Schwikowski, M., Gysel, M., Flanner, M. G., Kang, S., Hou, S. and Mayewski, P. A.: Recent
768 increase in black carbon concentrations from a Mt. Everest ice core spanning 1860-2000 AD, Geophys. Res.
769 Lett., 38(4), 11–16, doi:10.1029/2010GL046096, 2011.
770 Lamarque, J. and Hess, P. G.: Model analysis of the temporal and geographical origin of the CO distribution during
771 the TOPSE campaign, , 108, 1–12, doi:10.1029/2002JD002077, 2003.
772 Lamarque, J.-F., Bond, T.C., Eyring, V., Granier, C., et al.: Historical (1850–2000) gridded anthropogenic and
773 biomass burning emissions of reactive gases and aerosols: methodology and application, Atmos. Chem. Phys.,
774 10, 7017–7039, doi:10.5194/acp-10-7017-2010.
775 Li, X., Kang, S., He, X., Qu, B., Tripathee, L., Jing, Z., Paudyal, R., Li, Y., Zhang, Y., Yan, F., Li, G. and Li, C.:
776 Light-absorbing impurities accelerate glacier melt in the Central Tibetan Plateau, Sci. Total Environ.,
777 doi:10.1016/j.scitotenv.2017.02.169, 2017.
778 Li, Y., Chen, J., Kang, S., Li, C., Qu, B., Tripathee, L., Yan, F., Zhang, Y., Guo, J., Gul, C. and Qin, X.: Impacts of
779 black carbon and mineral dust on radiative forcing and glacier melting during summer in the Qilian Mountains,
780 northeastern Tibetan Plateau, Cryosph. Discuss., (April), 1–14, doi:10.5194/tc-2016-32, 2016.
781 Lu, Z., Streets, D. G., Zhang, Q. and Wang, S.: A novel back-trajectory analysis of the origin of black carbon
782 transported to the Himalayas and Tibetan Plateau during 1996-2010, Geophys. Res. Lett., 39(1), 1–6,
783 doi:10.1029/2011GL049903, 2012.
784 Lüthi, Z. L., Škerlak, B., Kim, S. W., Lauer, A., Mues, A., Rupakheti, M. and Kang, S.: Atmospheric brown clouds
785 reach the Tibetan Plateau by crossing the Himalayas, Atmos. Chem. Phys., 15(11), 6007–6021, doi:10.5194/acp-
786 15-6007-2015, 2015.

Mahowald, N., Albani, S., Kok, J. F., Engelstaeder, S., Scanza, R., Ward, D. S. and Flanner, M. G.: The size distribution of desert dust aerosols and its impact on the Earth system, Aeolian Res., 15, 53–71, doi:10.1016/j.aeolia.2013.09.002, 2014.

Ménégoz, M., Krinner, G., Balkanski, Y., Cozic, a., Boucher, O. and Ciais, P.: Boreal and temperate snow cover variations induced by black carbon emissions in the middle of the 21st century, Cryosph., 7, 537–554, doi:10.5194/tc-7-537-2013, 2013.

Ménégoz, M., Krinner, G., Balkanski, Y., Boucher, O., Cozic, A., Lim, S., Ginot, P., Laj, P., Gallée, H., Wagnon, P., Marinoni, A. and Jacobi, H. W.: Snow cover sensitivity to black carbon deposition in the Himalayas: From atmospheric and ice core measurements to regional climate simulations, Atmos. Chem. Phys., 14(8), 4237–4249, doi:10.5194/acp-14-4237-2014, 2014.

Ming, J., Cachier, H., Xiao, C., Qin, D., Kang, S., Hou, S. and Xu, J.: Black carbon record based on a shallow Himalayan ice core and its climatic implications, Atmos. Chem. Phy., 8, 1343–1352, doi:10.5194/acpd-7-14413-2007, 2008.

Ming, J., Xiao, C., Cachier, H., Qin, D., Qin, X., Li, Z. and Pu, J.: Black Carbon (BC) in the snow of glaciers in west China and its potential effects on albedos, Atmos. Res., 92(1), 114–123, doi:10.1016/j.atmosres.2008.09.007, 2009.

Ming, J., Xiao, C., Du, Z. and Yang, X.: An overview of black carbon deposition in High Asia glaciers and its impacts on radiation balance, Adv. Water Resour., 55(May), 80–87, doi:10.1016/j.advwatres.2012.05.015, 2013a.

Ming, J., Du, Z., Xiao, C., Xu, X., and Zhang, D.: Darkening of the mid-Himalaya glaciers since 2000 and the potential causes, Environ. Res. Lett., 7, 014021, doi:10.1088/1748-9326/7/1/014021, 2012.

Ming, J., Xiao, C., Wang, F., Li, Z. and Li, Y.: Grey Tienshan Urumqi Glacier No.1 and light-absorbing impurities, Environ. Sci. Pollut. Res., 23(10), 9549–9558, doi:10.1007/s11356-016-6182-7, 2016.

Nair, V. S., Babu, S. S., Moorthy, K. K., Sharma, A. K., Marinoni, A. and Ajai: Black carbon aerosols over the Himalayas: Direct and surface albedo forcing, Tellus, Ser. B Chem. Phys. Meteorol., 65(1), doi:10.3402/tellusb.v65i0.19738, 2013.

Naoe, H., Hasegawa, S., Heintzenberg, J., Okada, K., Uchiyama, A., Zaizen, Y., Kobayashi, E., Yamazaki, A.: State of mixture of atmospheric submicrometer black carbon particles and its effect on particulate light absorption, Atmos. Environ., 43(6), 1296–1301, doi:org/10.1016/j.atmosenv.2008.11.031, 2009.

Niu, H., Kang, S., Shi, X., Paudyal, R., He, Y., Li, G. and Wang, S.: Science of the Total Environment In-situ measurements of light-absorbing impurities in snow of glacier on Mt . Yulong and implications for radiative forcing estimates, Sci. Total Environ., 581–582, 848–856, doi:10.1016/j.scitotenv.2017.01.032, 2017.

Novakov, T., Menon, S., Kirchstetter, T. W., Koch, D. and Hansen, J. E.: Aerosol organic carbon to black carbon ratios : Analysis of published data and implications for climate forcing of soot emissions maybe a useful approach to slow global warming ., , 110, 1–13, doi:10.1029/2005JD005977, 2005.

Painter, T. H., Deems, J. S., Belnap, J., Hamlet, A. F., Landry, C. C. and Udall, B.: Response of Colorado River

Formatted: Font: Times New Roman, 10 pt

runoff to dust radiative forcing in snow., Proc. Natl. Acad. Sci. U. S. A., 107(40), 17125–30, doi:10.1073/pnas.0913139107, 2010.

Painter, T. H., Barrett, A. P., Landry, C. C., Neff, J. C., Cassidy, M. P., Lawrence, C. R., McBride, K. E. and Farmer, G. L.: Impact of disturbed desert soils on duration of mountain snow cover, Geophys. Res. Lett., 34(12), 1–6, doi:10.1029/2007GL030284, 2007.

Pandolfi, M., Ripoll, A., Querol, X. and Alastuey, A.: Climatology of aerosol optical properties and black carbon mass absorption cross section at a remote high-altitude site in the western Mediterranean Basin, Atmos. Chem. Phys., 14(12), 6443–6460, doi:10.5194/acp-14-6443-2014, 2014.

Park, M., Randel, W. J., Emmons, L. K. and Livesey, N. J.: Transport pathways of carbon monoxide in the Asian summer monsoon diagnosed from Model of Ozone and Related Tracers (MOZART), , 114, 1–11, doi:10.1029/2008JD010621, 2009.

Qian Y, TJ Yasunari, SJ Doherty, MG Flanner, WK Lau, J Ming, H Wang, M Wang, SG Warren, and R Zhang. 2015. "Light-absorbing Particles in Snow and Ice: Measurement and Modeling of Climatic and Hydrological Impact." Advances in Atmospheric Sciences 32(1):64-91. doi:10.1007/s00376-014-0010-0.

Qian Y, H Wang, R Zhang, MG Flanner, and PJ Rasch. 2014. "A Sensitivity Study on Modeling Black Carbon in Snow and its Radiative Forcing over the Arctic and Northern China." Environmental Research Letters 9(6):Article No. 064001. doi:10.1088/1748-9326/9/6/064001.

Qian Y, MG Flanner, LYR Leung, and W Wang. 2011. "Sensitivity studies on the impacts of Tibetan Plateau snowpack pollution on the Asian hydrological cycleand monsoon climate." Atmospheric Chemistry and Physics 11(5):1929-1948. doi:10.5194/acp-11-1929-2011

Qu, B., Ming, J., Kang, S. C., Zhang, G. S., Li, Y. W., Li, C. D., Zhao, S. Y., Ji, Z. M. and Cao, J. J.: The decreasing albedo of the Zhadang glacier on western Nyainqentanglha and the role of light-absorbing impurities, Atmos. Chem. Phys., 14(20), 11117–11128, doi:10.5194/acp-14-11117-2014, 2014.

Venkataraman, C., Habib, G., Eiguren-Fernandez, A., Miguel, A, H., Friedlander, S, K.:Residential Biofuels in South Asia: Carbonaceous Aerosol Emissions and Climate Impacts, Science, 307 (5714), 1454-1456, doi: 10.1126/science.1104359, 2005.

Wang, J., He, X., Ye, B., and Yang, G.: Variations of Albedo on the Dongkemadi Glacier, Tanggula Range, Journal of Glaciology and Geocryology, 34, 21–28, 2012.

~~Venkataraman, C., Habib, G., Eiguren-Fernandez, A., Miguel, A, H., Friedlander, S, K.:Residential Biofuels in South Asia: Carbonaceous Aerosol Emissions and Climate Impacts, Science, 307 (5714), 1454-1456, doi: 10.1126/science.1104359, 2005.~~

Wang, M., Xu, B., Zhao, H., Cao, J., Joswiak, D., Wu, G. and Lin, S.: The Influence of Dust on Quantitative

Formatted: Indent: Left: 0", Hanging: 0.2", Line spacing: 1.5 lines, Adjust space between Latin and Asian text, Adjust space between Asian text and numbers

Measurements of Black Carbon in Ice and Snow when Using a Thermal Optical Method, Aerosol Sci. Technol., 46 (April 2017), 60–69, doi:10.1080/02786826.2011.605815, 2012.

Wang M, B Xu, J Cao, X Tie, H Wang, R Zhang, Y Qian, PJ Rasch, S Zhao, G Wu, H Zhao, DR Joswiak, J Li, and Y Xie. 2015. "Carbonaceous Aerosols Recorded in a Southeastern Tibetan Glacier: Analysis of Temporal Variations and Model Estimates of Sources and Radiative Forcing." Atmospheric Chemistry and Physics 15:1191-1204. doi:10.5194/acp-15-1191-2015.

Wang, Q., Jacob, D. J., Fisher, J. A., Mao, J., Leibensperger, E. M., Carouge, C. C., Le Sager, P., Kondo, Y., Jimenez, J. L., Cubison, M. J. and Doherty, S. J.: Sources of carbonaceous aerosols and deposited black carbon in the Arctic in winter-spring: Implications for radiative forcing, Atmos. Chem. Phys., 11(23), 12453–12473, doi:10.5194/acp-11-12453-2011, 2011.

Wang, X., Pu, W., Ren, Y., Zhang, X., Zhang, X., Shi, J., Jin, H., Dai, M. and Chen, Q.: Snow albedo reduction in seasonal snow due to anthropogenic dust and carbonaceous aerosols across northern China, Atmos. Chem. Phys. Discuss., (September), 1–52, doi:10.5194/acp-2016-667, 2016.

Warren, S. G.: Optical Properties of Snow (Paper 1R1505), Rev. Geophys. Sp. Phys., 20(1), 67 [online] Available from: http://adsabs.harvard.edu/cgi-bin/nph-data_query?bibcode=1982RvGSP..20...67W&link_type=EJOURNAL%5Cnpapers3://publication/doi/10.1029/RG020i001p00067, 1982.

Warren, S. G. and Wiscombe, W. J.: Dirty snow after nuclear war, Nature, 313, 467–470, doi:10.1038/313467a0, 1985.

Xu, B., Cao, J., Hansen, J., Yao, T., Joswia, D. R., Wang, N., Wu, G., Wang, M., Zhao, H., Yang, W., Liu, X. and He, J.: Black soot and the survival of Tibetan glaciers, Proc. Natl. Acad. Sci., 106(52), 22114–22118, doi:10.1073/pnas.0910444106, 2009a.

Xu, B., Cao, J., Joswiak, D. R., Liu, X., Zhao, H. and He, J.: Post-depositional enrichment of black soot in snow-pack and accelerated melting of Tibetan glaciers, Environ. Res. Lett., 7(1), 14022, doi:10.1088/1748-9326/7/1/014022, 2012.

Yang, S., Xu, B., Cao, J., Zender, C. S. and Wang, M.: Climate effect of black carbon aerosol in a Tibetan Plateau glacier, Atmos. Environ., 111, 71–78, doi:10.1016/j.atmosenv.2015.03.016, 2015.

Yasunari, T. J., Bonasoni, P., Laj, P., Fujita, K., Vuillermoz, E., Marinoni, A., Cristofanelli, P., Duchi, R., Tartari, G. and Lau, K. M.: Estimated impact of black carbon deposition during pre-monsoon season from Nepal Climate Observatory - Pyramid data and snow albedo changes over Himalayan glaciers, Atmos. Chem. Phys., 10(14), 6603–6615, doi:10.5194/acp-10-6603-2010, 2010.

~~Yasunari, T. J., Lau, K.-M., Mahanama, S. P. P., Colarco, P. R., Silva, A. M. Da, Aoki, T., Aoki, K., Murao, N., Yamagata, S. and Kodama, Y.: The GOddard SnoW Impurity Module (GOSWIM) for the NASA GEOS-5 Earth System Model: Preliminary Comparisons with Observations in Sapporo, Japan, Sola, 10(MAY), 50–56,~~

Formatted: Indent: Left: 0", Hanging: 0.2", Line spacing: 1.5 lines, Adjust space between Latin and Asian text, Adjust space between Asian text and numbers

~~doi:10.2151/sola.2014-011, 2014.~~

Yasunari, T. J., Lau, K.-M., Mahanama, S. P. P., Colarco, P. R., Silva, A. M. Da, Aoki, T., Aoki, K., Murao, N., Yamagata, S. and Kodama, Y.: The GOddard SnoW Impurity Module (GOSWIM) for the NASA GEOS-5 Earth System Model: Preliminary Comparisons with Observations in Sapporo, Japan, Sola, 10(MAY), 50–56, doi:10.2151/sola.2014-011, 2014.

Zhang, G., Kang, S., Fujita, K., Huintjes, E., Xu, J., Yamazaki, T., Haginoya, S., Wei, Y., Scherer, D., Schneider, C. and Yao, T.: Energy and mass balance of Zhadang glacier surface, central Tibetan Plateau, J. Glaciol., 59(213), 137–148, doi:10.3189/2013JoG12J152, 2013.

Zhang, Y., Kang, S., Xu, M., Sprenger, M., Gao, T., Cong, Z., Li, C., Guo, J., Xu, Z., Li, Y., Li, G., Li, X., Liu, Y. and Han, H.: Sciences in Cold and Arid Regions Light-absorbing impurities on Keqikaer Glacier in western Tien Shan : concentrations and potential impact on albedo reduction, , 9(2), doi:10.3724/SP.J.1226.2017.00097.Light-absorbing, 2017.

Zhang, Y., Hirabayashi, Y., Liu, Q. and Liu, S.: Glacier runoff and its impact in a highly glacierized catchment in the southeastern Tibetan Plateau: Past and future trends, J. Glaciol., 61(228), 713–730, doi:10.3189/2015JoG14J188, 2015.

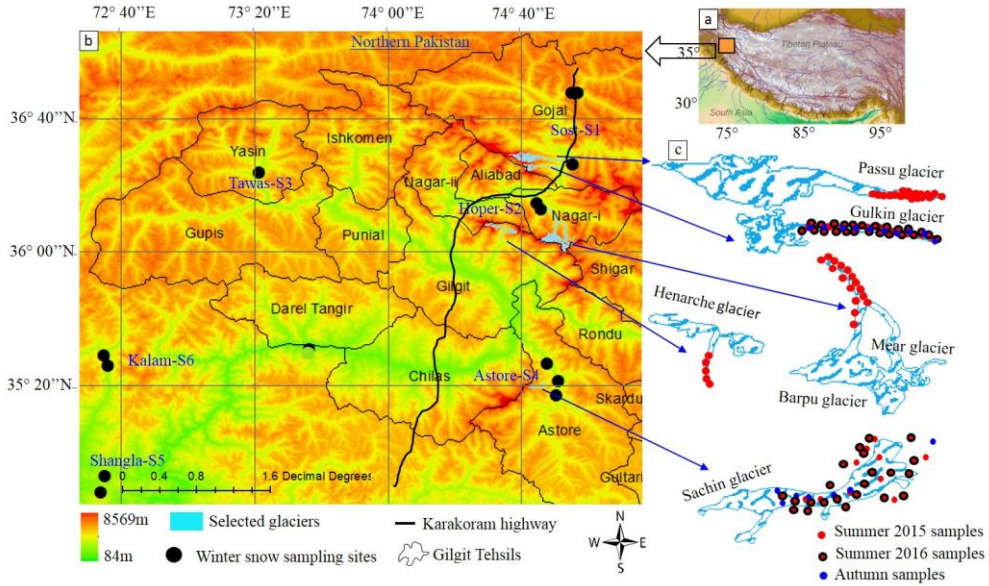

Figure 1. The study area and sampling sites: (a) Himalayan mountain range and Tibetan Plateau, (b) winter sampling sites (solid black circles), (c) glaciers selected for summer and autumn sampling

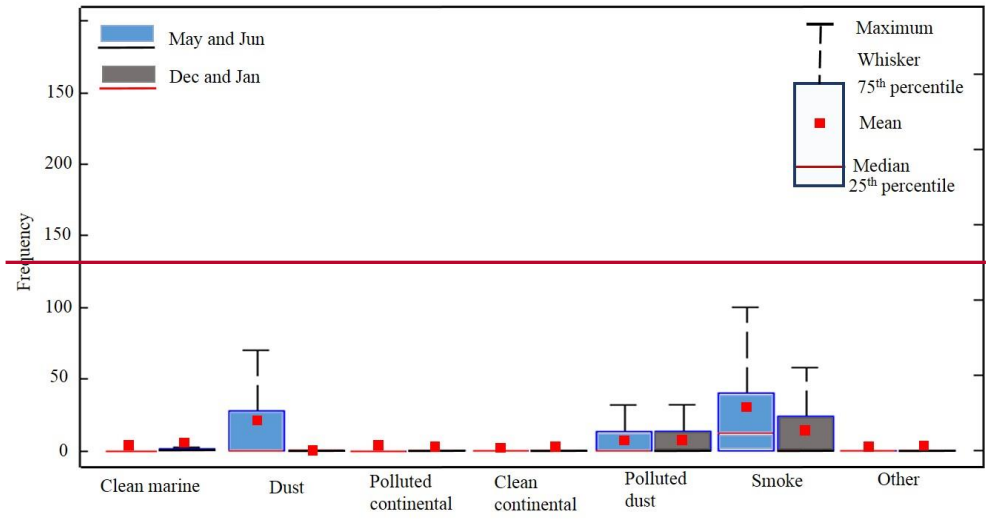
May and Jun
Dec and Jan
Maximum
Whisker
75th percentile
Mean
Median
25th percentile
Frequency
150
200
150
100
50
0
Clean marine
Dust
Polluted continental
Clean continental
Polluted dust
Smoke
Other

913

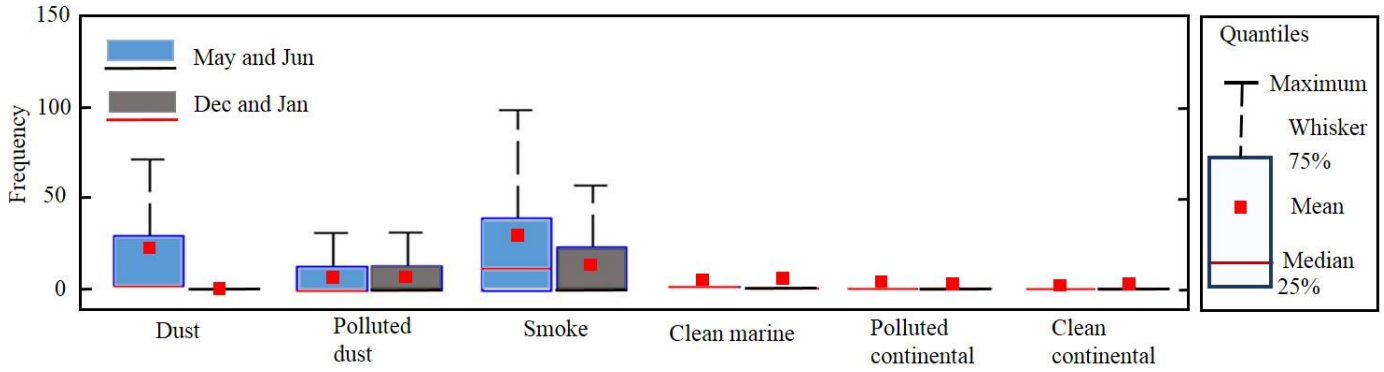

914

915 **Figure 2. Frequency distribution of aerosol subtypes in the atmosphere over the study region calculated from CALIPSO data for the months in 2006 to 2014**

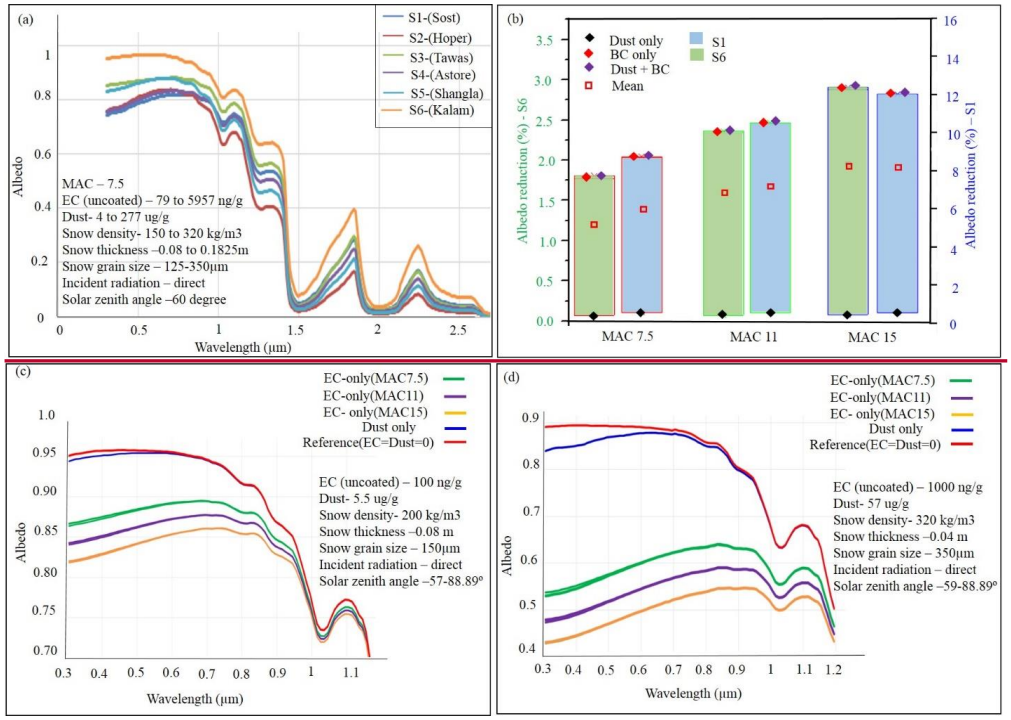
(a)
S1-(Sost)
S2-(Hoper)
S3-(Tawas)
S4-(Astore)
S5-(Shangla)
S6-(Kalam)
MAC – 7.5
EC (uncoated) – 79 to 5957 ng/g
Dust- 4 to 277 ug/g
Snow density- 150 to 320 kg/m3
Snow thickness –0.08 to 0.1825m
Snow grain size – 125-350µm
Incident radiation – direct
Solar zenith angle –60 degree
Albedo
Wavelength (µm)
(b)
Dust only
BC only
Dust + BC
Mean
S1
S6
Albedo reduction (%) - S6
Albedo reduction (%) – S1
MAC 7.5
MAC 11
MAC 15
(c)
EC-only(MAC7.5)
EC-only(MAC11)
EC- only(MAC15)
Dust only
Reference(EC=Dust=0)
EC (uncoated) – 100 ng/g
Dust- 5.5 ug/g
Snow density- 200 kg/m3
Snow thickness –0.08 m
Snow grain size – 150µm
Incident radiation – direct
Solar zenith angle –57-88.89°
Albedo
Wavelength (µm)
(d)
EC-only(MAC7.5)
EC-only(MAC11)
EC- only(MAC15)
Dust only
Reference(EC=Dust=0)
EC (uncoated) – 1000 ng/g
Dust- 57 ug/g
Snow density- 320 kg/m3
Snow thickness –0.04 m
Snow grain size – 350µm
Incident radiation – direct
Solar zenith angle –59-88.89°
Albedo
Wavelength (µm)

916

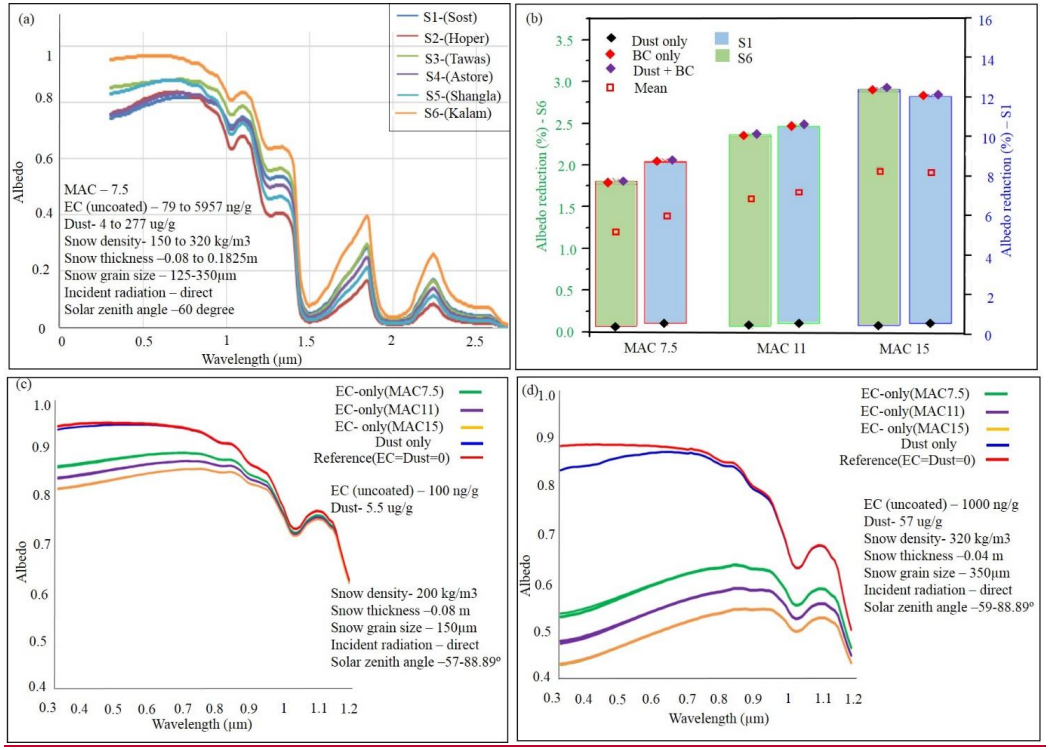

Figure 3. Spectral variation in albedo for winter sampling sites and selected ~~MAC~~ Mass Absorption Cross section (MAC) values, (a) average albedo of samples at each of the sites (b) daily mean albedo reduction of fresh snow (site S6) and aged snow (site S1) snow, (note different scales of y axis) (c) albedo of fresh snow site S6, (d) albedo of aged snow site S1.

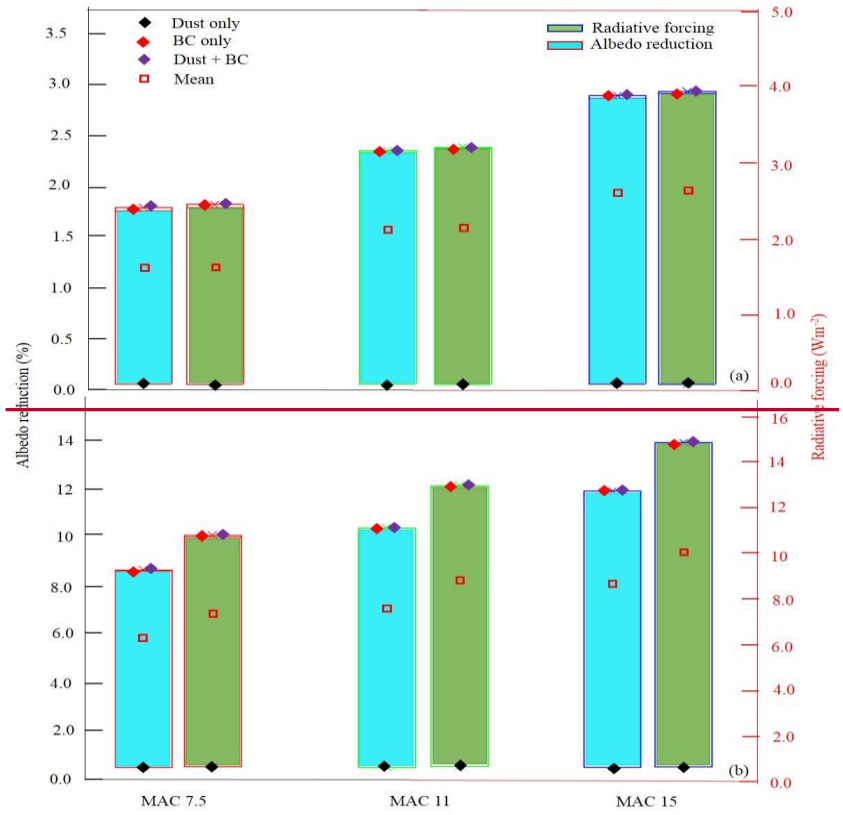
Dust only
BC only
Dust + BC
Mean
Radiative forcing
Albedo reduction
Albedo reduction (%)
Radiative forcing (Wm-2)
(a)
(b)
MAC 7.5
MAC 11
MAC 15

921
922

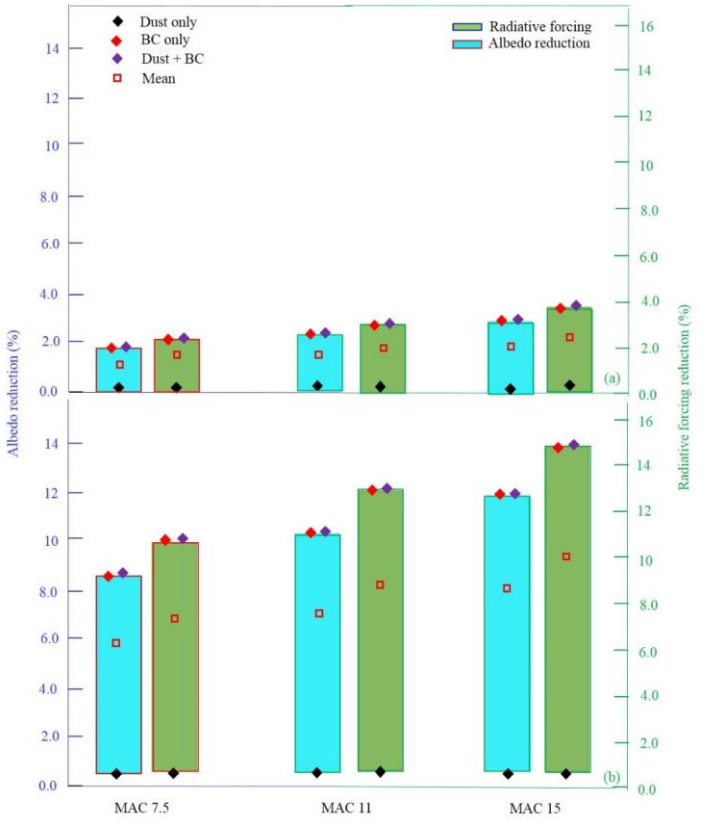

Figure 4. Daily mean radiative forcing ~~(%)~~ reduction and albedo reduction (%) caused by ~~BC~~ black carbon and dust for different Mass Absorption Cross section (MAC) in (a) fresh (low ~~BC~~black carbon) and (b) aged (high ~~BC~~black carbon) snow samples (note different scales of y axis)

926

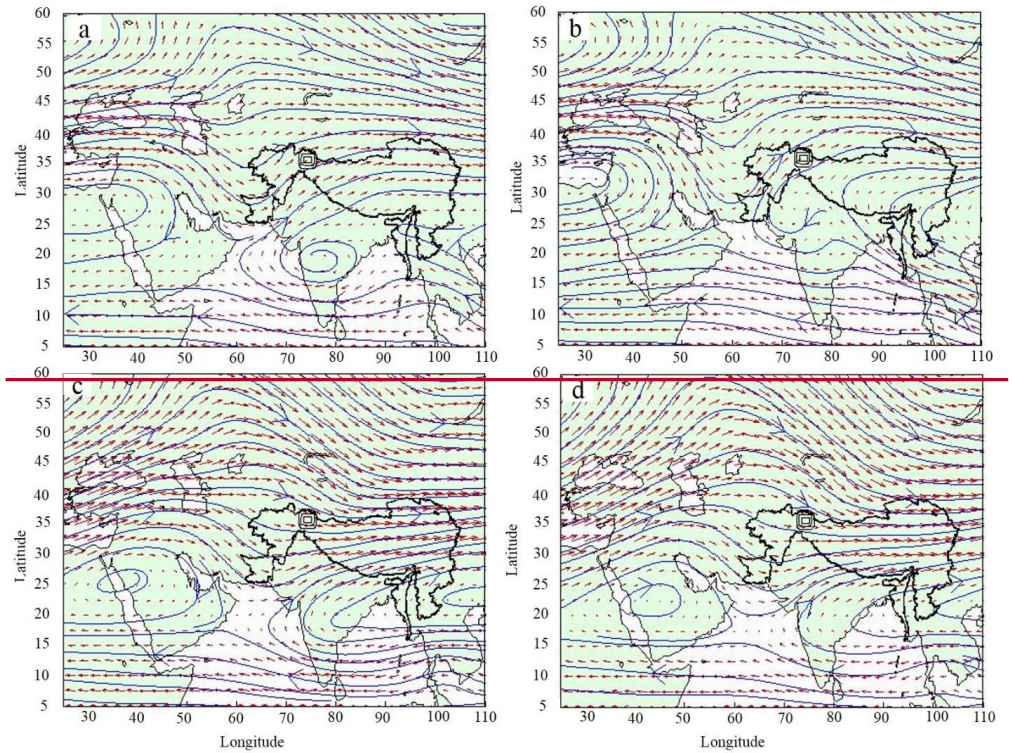
a
b
c
d
Latitude
Longitude
60
55
50
45
40
35
30
25
20
15
10
5
30
40
50
60
70
80
90
100
110

927

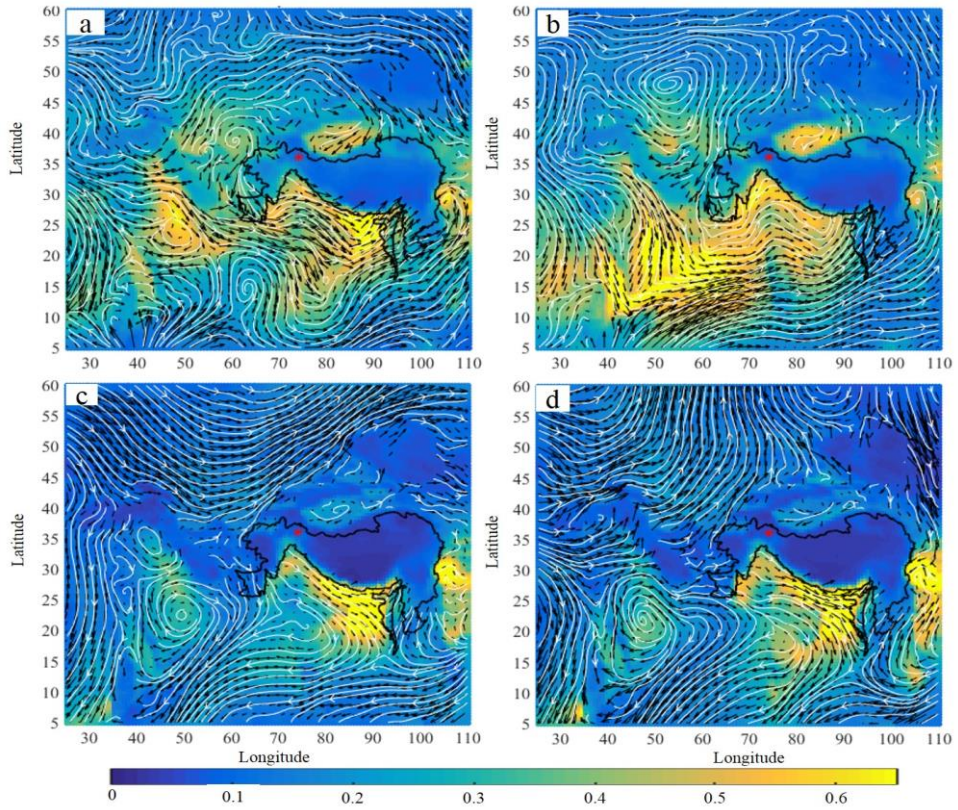

928

929 **Figure 5. ~~Fifty years m~~Monthly average horizontal wind patterns at ~~700~~ 850 hPa during a) May, b) June, c) December, and d) January, corresponding to approximately**
930 **~~3000~~ 2500 masl, from ~~NCEP NCAR~~GES DISC. ~~The study area is indicated by a square~~ Red star indicates the position of the study area, and white lines indicating**
931 **streamlines. The background colors show monthly mean aerosol optical depth.**

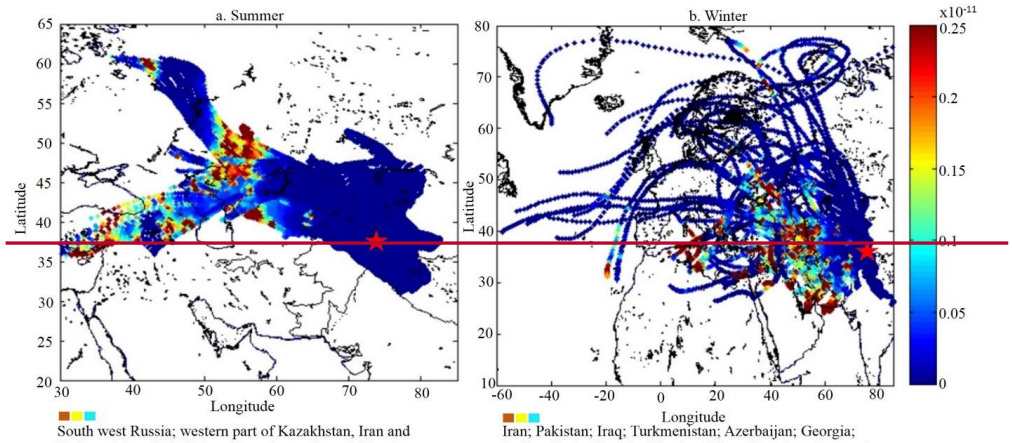
a. Summer
b. Winter
Latitude
Longitude
x10-11
0.25
0.2
0.15
0.1
0.05
0
South west Russia; western part of Kazakhstan, Iran and Turkmenistan; Uzbekistan; Georgia; north east side of Turkey; Syria; Cyprus.
Iran; Pakistan; Iraq; Turkmenistan; Azerbaijan; Georgia; Jordan; Syria; Tunisia; Ukraine; Libya; Egypt; eastern part of Turkey and south western part of Russia.

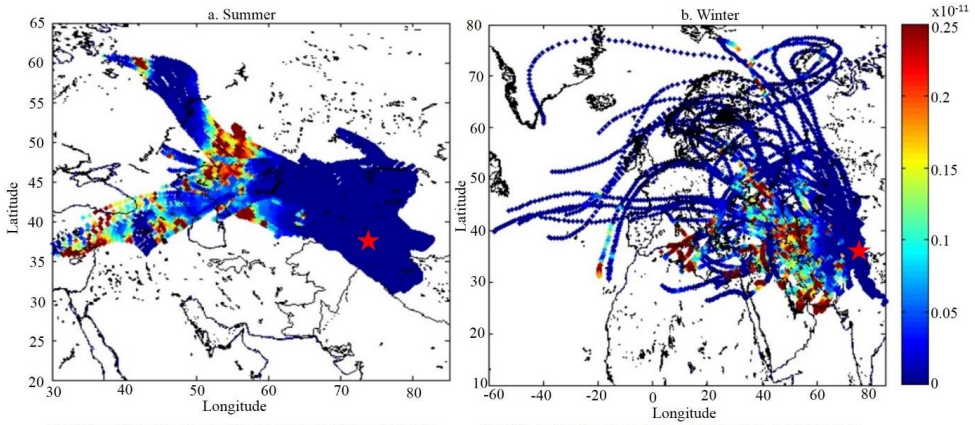

Figure 6. Source contribution regions of pollutants identified using an emissions inventory (Representative Concentration Pathways) coupled with back trajectories (a. 77 simulated days, b. 63 simulated days). Red star indicates the position of the study area.

Formatted: Font: Bold

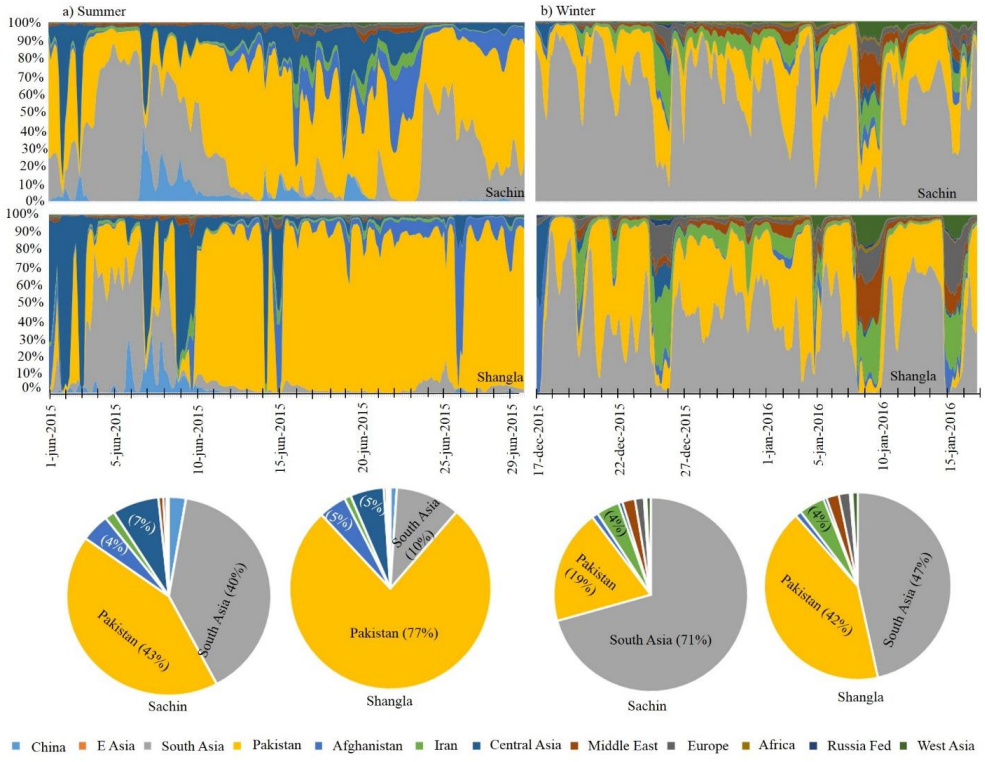

Figure 7. Source contribution regions of carbon monoxide for selected sites identified by WRF-STEM during (a) summer and (b) winter seasons.

Formatted: Font: Bold

Table 1. Concentration of black carbon~~BC~~, organic carbon~~OC~~, and dust in summer, autumn, and winter samples in 2015 and 2016.

Glacier/ Site	No.	Elevation (masl) min–max	BC min–max (avg) (ngg^{-1})	OC min–max (avg) (ngg^{-1})	Dust min–max (avg) (μgg^{-1})	Type[a] / snow age in days	OC/BC[b]	Year
Summer (May 2015/ May 2016)								
Barpu	6	2901–3405	877–5994 (2938)	244–1228 (691)	292–5250 (1998)	DCI	0.07–1.38	2015
Gulkin	31	2741–3319	82–5676 (1327)	238–8514 (1594)	31–2039 (648)	DCIS	0.169–3.76	2015/16
Henarche	4	2569–2989	778–10502 (4820)	275–4176 (1628)	225–2723 (993)	Ice	0.04–1.63	2015
Mear	8	2961–3539	222–3656 (1593)	703–6588 (2992)	33–656 (211)	DCI	0.72–4.88	2015
Passu	14	2663–3158	87–734 (346)	132–1810 (741)	28–524 (196)	DCI	1.85–4.80	2015
Sachin	35	3414–3895	257–4127 (1769)	128–7592 (3348)	5.6–2495 (314)	DCIS	0.08–0.53	2015/16
Total	98							
Autumn (October 2016)								
Gulkin	7	2741–3319	125–1028 (451)	266–3574 (1276)	60–767 (253)	DCIS	1.29–3.59	2016
Sachin	6	3414–3895	4342–6481 (5314)	543–3478 (1571)	124–1348 (546)	DCIS	0.11–0.53	2016
Total	13							
Winter (Dec 2015/ Jan 2016)								
S1-Sost	6	2873–3092	482–5957 (2506)	378–2934 (1039)	29–311 (131)	2–17 d	0.25–0.78	2015
S2-Hopar	2	2602–2794	229–1064 (646)	330–1976 (1153)	23–129 (76)	1–15 d	1.4–1.8	2016
S3-Tawas	1	2437	650	1320	16	8–17 d	2.03	2016
S4-Astore	3	2132–2396	450–2640 (1305)	914–3645 (2161)	55–171 (97)	4–7 d	1.38–2.33	2016
S5-Shangla	2	2324–2373	367–1110 (739)	1302–2856 (2079)	13–49 (31)	8–9 d	2.5–3.5	2016
S6-Kalam	4	1933–2101	79–123 (107)	214–558 (347)	4–6 (5)	1 d	2.3–5	2016
Total	18							

[a] type = snow or ice type; DCI = debris-covered ice; DCIS = debris-covered ice and aged snow

[b] range of OC/BC in individual samples

Table 2. Snow albedo reduction (%) ~~at 0.975 μm~~ by ~~BC~~black carbon, dust, and ~~BC~~ black carbon plus dust at the site with the lowest average pollutant concentration (S6) and the site with the highest average pollutant concentration (S1), under different ~~M~~mass ~~A~~absorption ~~C~~cross section values.

Pollutant	Mass ~~A~~Absorption Cross section (m^2/g)	Low concentration site (S6)			High concentration site (S1)		
		Daytime min	Daytime max	Daily mean	Daytime min	Daytime max	Daily mean
B~~C~~lack carbon	7.5	2.8	5.1	1.8	15.6	23.9	9.0
	11	3.7	6.9	2.3	19.2	28.6	10.5
	15	4.6	8.3	2.9	22.3	32.5	12.0
Dust	7.5	0.1	0.2	0.07	0.9	1.6	0.05
	11	0.1	0.2	0.07	0.9	1.6	0.05
	15	0.1	0.2	0.07	0.9	1.6	0.05
Black carbon~~C~~ and dust	7.5	2.9	5.2	1.8	15.7	24.0	8.8
	11	3.8	6.8	2.4	19.2	28.6	10.5
	15	4.6	8.3	2.9	22.3	32.5	12.0

Formatted: Centered
Formatted Table
Formatted: Centered
Formatted: Centered
Formatted: Centered
Formatted: Centered
Formatted: Centered
Formatted: Centered
Formatted: Centered
Formatted: Centered
Formatted: Centered

Concentrations and source regions of light absorbing ~~impurities~~ particles in snow/ice in northern Pakistan and their impact on snow albedo

Chaman Gul[1,2,5], Siva Praveen Puppala[2], Shichang Kang[1,3,5], Bhupesh Adhikary[2], Yulan Zhang[1], Shaukat Ali[4], Yang Li[3], Xiaofei Li[1]

[1]State Key Laboratory of Cryosphere Science, Northwest Institute of Eco-Environment and Resources, Chinese Academy of Sciences, Lanzhou 73000, China

[2]International Centre for Integrated Mountain Development (ICIMOD), G.P.O. Box 3226, Kathmandu, Nepal

[3]CAS Center for Excellence in Tibetan Plateau Earth Sciences, Beijing, 100101, China

[4]Global Change Impact Studies Centre (GCISC), Ministry of Climate Change, Islamabad, Pakistan

[5]University of Chinese Academy of Sciences, Beijing, China

Correspondence to: Chaman Gul (chaman.gul@icimod.org; chaman@lzb.ac.cn)

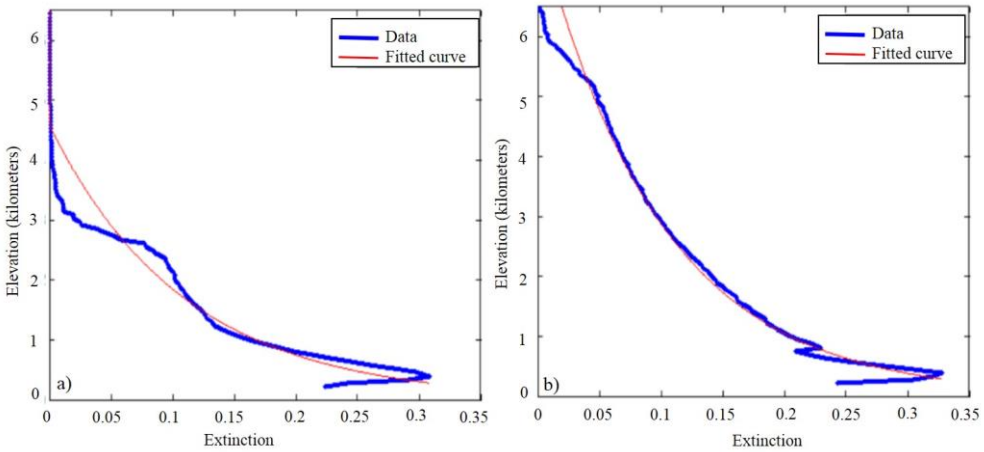

Figure S1. CALPISO extinction profile for a) winter (December, January), and b) summer (May, June)

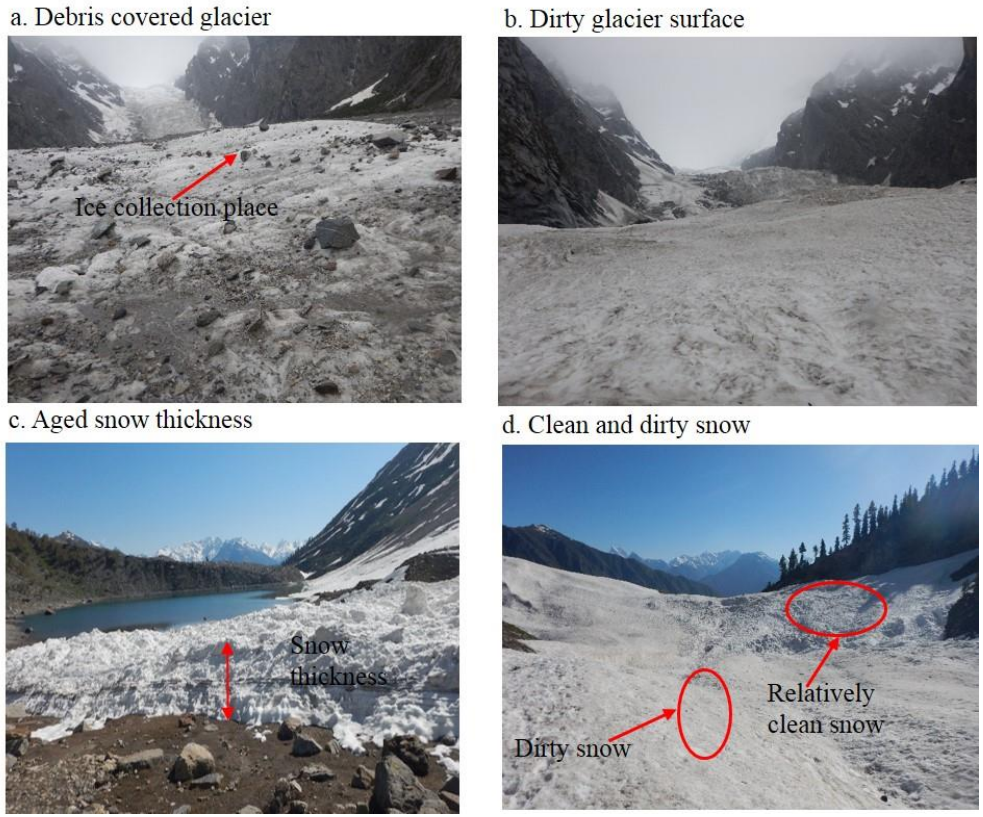

Figure S2. Appearance of different summer snow/ice sampling sites on a) b) Gulkin glacier, c) near Sachin glacier, and d) Sachin glacier

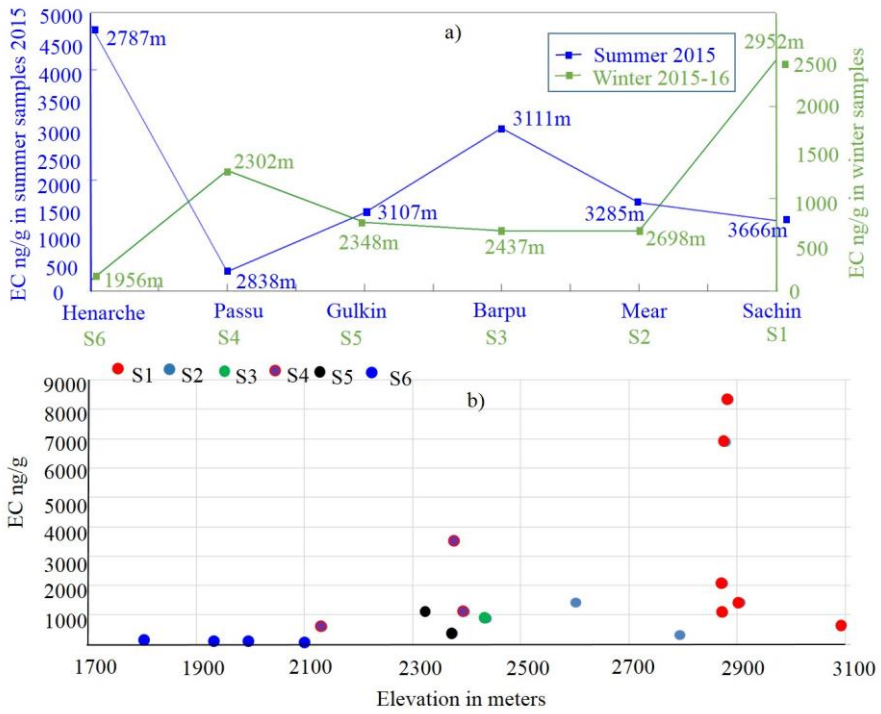

Figure S3. a) Average concentration of ~~EC~~ black carbon at sites S1 to S6 sampled in winter and glaciers sampled in summer; b) individual sample concentration in winter samples.

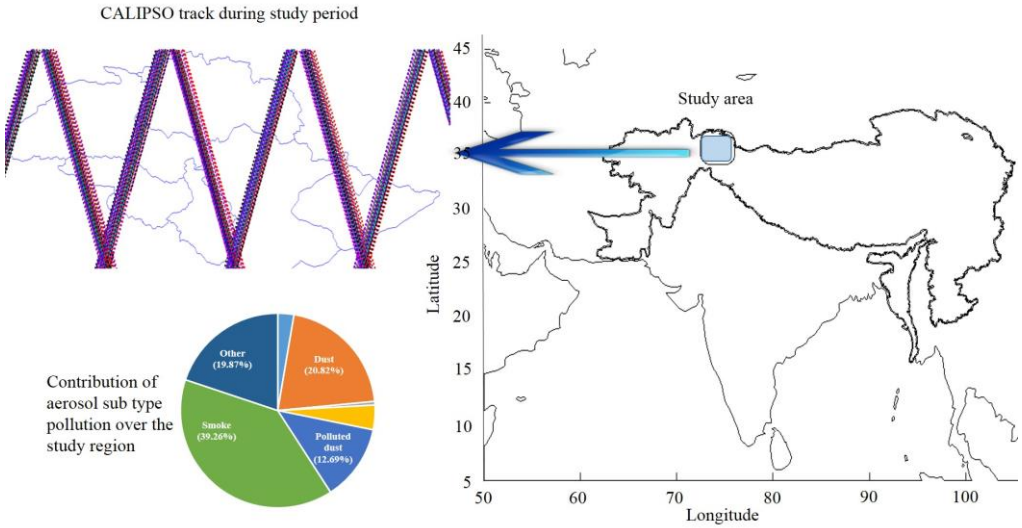

Figure S4. Contribution of subtype aerosols (%) in the atmosphere along the track of CALIPSO during the selected month June in 2006-2014

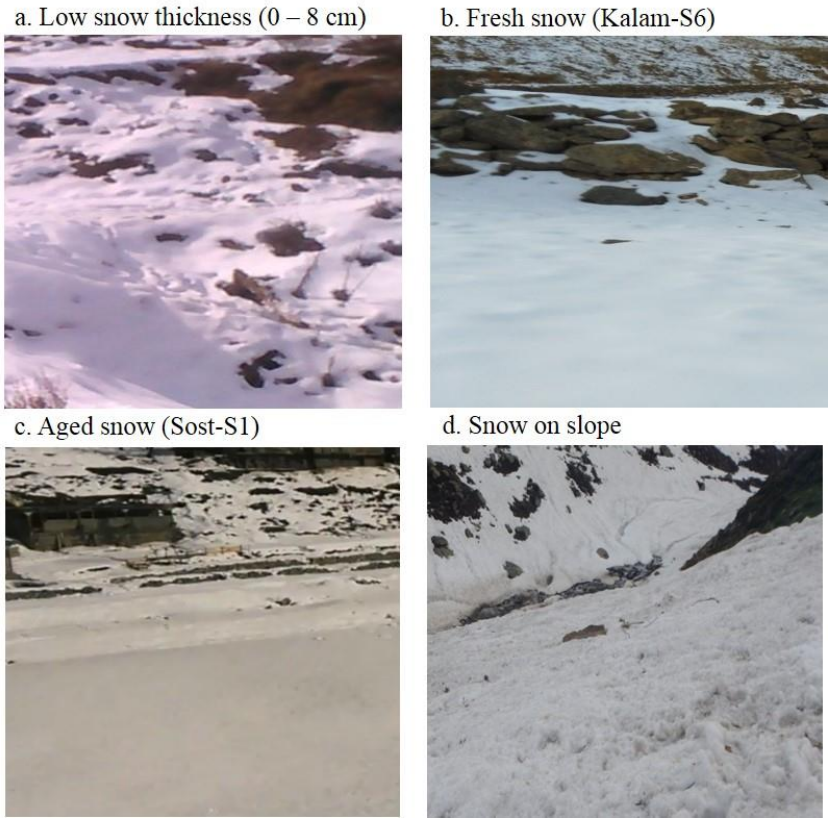

Figure S5. Appearance of different snow areas sampled in winter

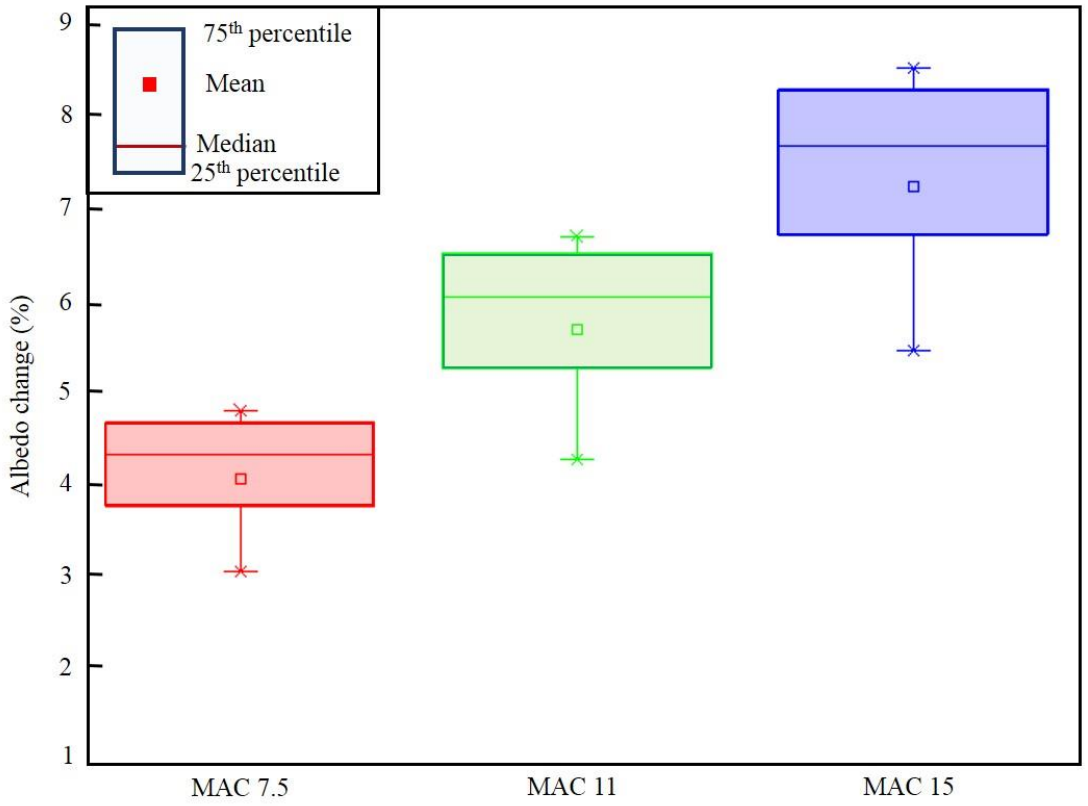
75th percentile
Mean
Median
25th percentile
Albedo change (%)
9
8
7
6
5
4
3
2
1
MAC 7.5
MAC 11
MAC 15

32

Figure S6. Albedo reduction (%) range between sulfate coated and uncoated black carbon calculated for different Mass Absorption Cross section (MAS) and the low concentration site S6.

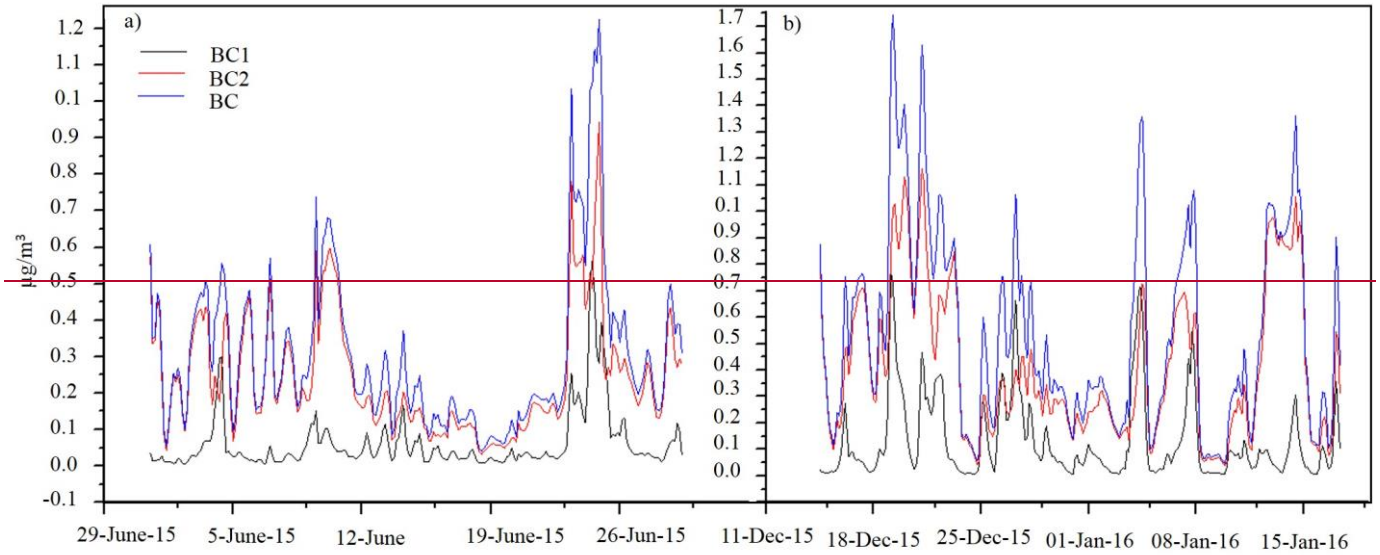

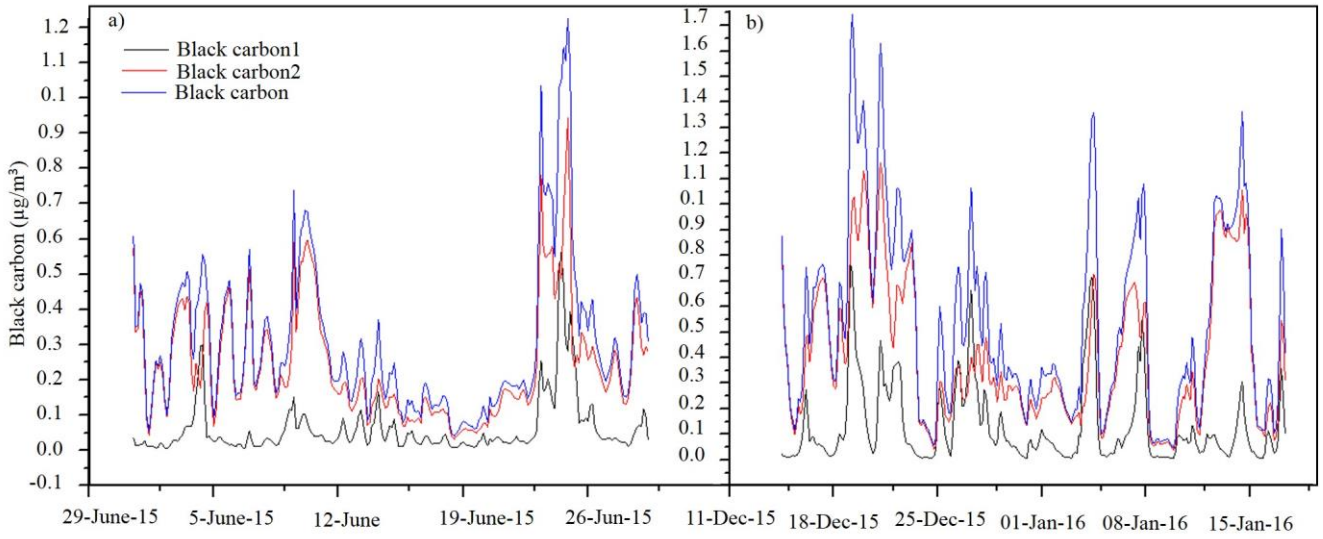

Figure S7. Concentration of ~~black carbon (BC1~~black carbon1, ~~B~~black carbon~~C~~2 and ~~BC~~black carbon~~)~~ on the Sachin glacier calculated using the WRF-STEM model: a) summer, b) winter.

Tables

Table S1 Parameters used for sensitivity analysis with SNICAR model for winter snow samples under the input parameters of direct incident radiation and mid-latitude winter, clear-sky conditions.

1 = solar zenith angle

2 = snow grain effective radius (µm)

3 = snowpack thickness (m)

4 = snowpack density (kg m^{-3})

5 = albedo of underlying ground (a. visible, 0.3-0.7µm, b. near-infrared, 0.7-5.0µm)

6 = ~~MAC~~ Mass Absorption Cross section scaling factor (experimental) for ~~BC~~black carbon

7= BC concentration (ppb, uncoated)

8 = dust concentration (ppm, 5.0–10.0 µm diameter)

9 = volcanic ash concentration (ppm)

10 = experimental particle 1 concentration (ppb)

Site	1	2	3	4	5a	5b	6	7	8	9	10
Kalam-S6	80.34	150	0.08	200	0.2	0.4	7.5/11/15	100	5.5	0	0
Kalam-S6	71.25	150	0.08	200	0.2	0.4	7.5/11/15	100	5.5	0	0
Kalam-S6	63.96	150	0.08	200	0.2	0.4	7.5/11/15	100	5.5	0	0
Kalam-S6	59.21	150	0.08	200	0.2	0.4	7.5/11/15	100	5.5	0	0
Kalam-S6	57.66	150	0.08	200	0.2	0.4	7.5/11/15	100	5.5	0	0
Kalam-S6	59.54	150	0.08	200	0.2	0.4	7.5/11/15	100	5.5	0	0
Kalam-S6	64.57	150	0.08	200	0.2	0.4	7.5/11/15	100	5.5	0	0

Formatted: Font: 10 pt, Check spelling and grammar

Kalam-S6	72.07	150	0.08	200	0.2	0.4	7.5/11/15	100	5.5	0	0
Kalam-S6	81.31	150	0.08	200	0.2	0.4	7.5/11/15	100	5.5	0	0
Kalam-S6	88.95	150	0.08	200	0.2	0.4	7.5/11/15	100	5.5	0	0
Sost-S1	82.61	350	0.04	320	0.19	0.35	7.5/11/15	1000	57	0	0
Sost-S1	73.66	350	0.04	320	0.19	0.35	7.5/11/15	1000	57	0	0
Sost-S1	66.45	350	0.04	320	0.19	0.35	7.5/11/15	1000	57	0	0
Sost-S1	61.64	350	0.04	320	0.19	0.35	7.5/11/15	1000	57	0	0
Sost-S1	59.66	350	0.04	320	0.19	0.35	7.5/11/15	1000	57	0	0
Sost-S1	61.36	350	0.04	320	0.19	0.35	7.5/11/15	1000	57	0	0
Sost-S1	65.93	350	0.04	320	0.19	0.35	7.5/11/15	1000	57	0	0
Sost-S1	72.98	350	0.04	320	0.19	0.35	7.5/11/15	1000	57	0	0
Sost-S1	81.80	350	0.04	320	0.19	0.35	7.5/11/15	1000	57	0	0
Sost-S1	88.95	350	0.04	320	0.19	0.35	7.5/11/15	1000	57	0	0

54

Table S2. EC concentrations in glacier ice and snow and plains snow in north Pakistan, and other regions

Location	Lat/long	Elevation (masl)	Min. EC (ngg^{-1})	Max. EC (ngg^{-1})	Time period (years)	Sample type/snow age	Reference
Mera Glacier, Nepal	27.72°N 86.8°E	6376	3	13	1999–2010	Ice core (rBC)	Ginot et al., 2014
Numanani, China	30.45°N 81.27°E	5900	4	14	Annual mean 2004	Ss (EC)	Xu et al., 2006
Greenland	72.6°N, 38.5°W	3209	4.2	30.1	1994 – 1996		Slater et al., 2002
NCO-P, Nepal	27.95°N, 86.82°E	5079	26	68.2	March – May 2006		Yasunari et al., 2010
Kangwure, China	28.47°N 85.82°E	6000	22	122	Annual mean 2001	Ss (EC)	Xu et al., 2007
Qiangyong, China	28.83°N 90.25°E	5400	43	143	Annual mean 2001	Ss (EC)	Xu et al., 2008
Zhadang, China	30.47°N 90.50°E	5802	334	473	2001–2010		Qu et al., 2014
Muji glacier, China	39.19°N 73.74° E	5062	25	731	2012		Yang et al., 2015
Zhadang, China	30.47°N 90.5°E	5802	114	1114	2005–2006		Ming et al., 2009
Tien Shan, China	43.1°N 86.82°E	4050		3000	2011	bottom firn-pack	Xu et al., 2012
Mera glacier, Nepal	27.72°N 86.8°E	5400		3535	2009		Kaspari et al., 2014
Northern China			60	4020	Jan-14		Wang et al., 2016
Urumqi glacier, China	43.10°N 86.80°E	4040	16	4093	2013		Ming et al., 2016
LHG glacier, China	39.17°N 96.17°E	5480		28,636	summer 2013-14	superimposed ice	Li et al., 2016
Present study							
Passu glacier	36.45°N 74.85°E	2838	87	734	May-June 2015	DCI (EC)	This study
Sachin glacier	35.32°N 74.76°E	3666	492	1789	May-June 2015	DCI & snow (EC)	This study
Sachin glacier	35.32°N 74.76°E	3666	543	3478	Oct-16	DCI & snow	This study
Gulkin glacier	36.42°N 74.77°E	3066	266	3574	Oct-16	DCI	This study
Mear glacier	36.15°N 74.82°E	3281	222	3656	May-June 2015	DCI (EC)	This study

Gulkin glacier	36.42°N 74.77°E	3066	81	5676	May-June 2015	DCI (EC)	This study
Barpu glacier	36.18°N 74.08°E	3055	877	5994	May-June 2015	DCI (EC)	This study
Henarche glacier	36.05°N 74.57°E	2941	778	10,502	May-June 2015	Surface ice (EC)	This study
S6-Kalam	35.43°N 72.6°E	1958	79	123	8-Jan-16	1–2 days	This study
S3-Tawas	36.39°N 73.36°E	2437		650	2-Jan-16	8–17 days	This study
S2- Hopar	36.22°N 74.75°E	2698	229	1064	1-Jan-16	1–15 days	This study
S5-Shangla	34.83°N 74.82°E	2348	367	1111	6–7 Jan 2016	8–9 days	This study
S4-Astore	35.37°N 74.80°E	2302	450	2640	3–4 Jan 2016	4–7 days	This study
S1- Sost	36.78°N 74.93°E	2951	482	5957	30–31 Dec 2015	2–17 days	This study

Table S3. Broadband albedo values ~~at 0.975 µm wavelength~~ for selected solar zenith angles, and daily mean albedo reduction (%)

Pollutant		Site S6 (low ~~EC~~ BC and dust)				Site S1 (high ~~EC~~ BC and dust)		
	SZA	MAC 7.5	MAC 11	MAC 15	SZA	MAC 7.5	MAC 11	MAC 15
~~EC~~ BC only	80.34	0.79	0.78	0.77	82.61	0.59	0.56	0.52
	71.25	0.77	0.75	0.74	73.66	0.54	0.50	0.46
	63.96	0.75	0.74	0.72	66.45	0.50	0.46	0.42
	59.21	0.74	0.72	0.71	61.64	0.48	0.43	0.40
	57.66	0.74	0.72	0.71	59.66	0.47	0.43	0.39
	59.54	0.74	0.72	0.71	61.36	0.48	0.43	0.39
	64.57	0.75	0.74	0.72	65.93	0.50	0.46	0.42
	72.07	0.77	0.76	0.74	72.98	0.54	0.49	0.46
	81.31	0.80	0.78	0.77	81.80	0.59	0.55	0.51
	88.95	0.82	0.81	0.80	88.95	0.64	0.60	0.57
	Daily mean reduction (%)	1.77	2.35	2.87		8.70	10.49	12.03
Dust only	80.34	0.83	0.83	0.83	82.61	0.76	0.76	0.76
	71.25	0.81	0.81	0.81	73.66	0.73	0.73	0.73
	63.96	0.80	0.80	0.80	66.45	0.71	0.71	0.71
	59.21	0.79	0.79	0.79	61.64	0.70	0.70	0.70
	57.66	0.79	0.79	0.79	59.66	0.70	0.70	0.70
	59.54	0.79	0.79	0.79	61.36	0.70	0.70	0.70
	64.57	0.80	0.80	0.80	65.93	0.71	0.71	0.71
	72.07	0.81	0.81	0.81	72.98	0.73	0.73	0.73

	81.31	0.83	0.83	0.83	81.80	0.76	0.76	0.76
	88.95	0.85	0.85	0.85	88.95	0.78	0.78	0.78
	Daily mean reduction (%)	0.07	0.07	0.07		0.05	0.05	0.05
	80.34	0.79	0.78	0.77	82.61	0.59	0.55	0.52
	71.25	0.77	0.75	0.74	73.66	0.54	0.50	0.46
	63.96	0.75	0.73	0.72	66.45	0.50	0.46	0.42
	59.21	0.74	0.72	0.71	61.64	0.48	0.43	0.40
	57.66	0.74	0.72	0.70	59.66	0.47	0.42	0.39
~~EC~~ BC and dust	59.54	0.74	0.72	0.71	61.36	0.48	0.43	0.39
	64.57	0.75	0.74	0.72	65.93	0.50	0.45	0.42
	72.07	0.77	0.76	0.74	72.98	0.54	0.49	0.46
	81.31	0.79	0.78	0.77	81.80	0.59	0.55	0.51
	88.95	0.82	0.81	0.80	88.95	0.64	0.60	0.57
	Daily mean reduction (%)	1.80	2.36	2.90		8.75	10.51	12.03
	80.34	0.83	0.83	0.83	82.61	0.77	0.77	0.77
	71.25	0.81	0.81	0.81	73.66	0.75	0.75	0.75
	63.96	0.80	0.80	0.80	66.45	0.73	0.73	0.73
	59.21	0.79	0.79	0.79	61.64	0.72	0.72	0.72
	57.66	0.79	0.79	0.79	59.66	0.71	0.71	0.71
No ~~EC~~BC/ no dust	59.54	0.79	0.79	0.79	61.36	0.72	0.72	0.72
	64.57	0.79	0.80	0.80	65.93	0.73	0.73	0.73
	72.07	0.81	0.81	0.81	72.98	0.75	0.75	0.75
	81.31	0.83	0.83	0.83	81.80	0.77	0.77	0.77

	88.95	0.85	0.85	0.85	88.95	0.79	0.79	0.79

MAC = Mass Absorption Cross section, SZA = Solar Zenith Angle

Formatted: Font: 9 pt

Table S4. Radiative forcing for selected solar zenith angles (Wm^{-2}) and daily mean (%)

Pollutant	Site S6 (low EC and dust)				Site S1 (high EC and dust)			
	SZA	MAC 7.5	MAC 11	MAC 15	SZA	MAC 7.5	MAC 11	MAC 15
	80.34	4.90	6.47	8.00	82.61	23.87	29.10	33.71
	71.25	5.86	7.72	9.53	73.66	27.50	33.25	38.21
	63.96	6.57	8.65	10.65	66.45	29.96	36.01	41.16
	59.21	7.00	9.70	11.33	61.64	31.39	37.58	42.82
~~**EC**~~ **BC**	57.66	7.14	9.38	11.54	59.66	31.93	38.18	43.44
only	59.54	6.97	9.16	11.29	61.36	31.47	37.67	42.91
	64.57	6.51	8.58	10.56	65.93	30.13	36.19	41.35
	72.07	5.78	7.61	9.40	72.98	27.75	33.53	38.52
	81.31	4.79	6.33	7.83	81.80	24.23	29.51	34.16
	88.95	3.93	5.20	6.44	88.95	20.88	25.62	29.86
	Daily mean	2.40	3.18	3.90	-	10.74	12.95	14.85
	80.34	0.20	0.20	0.20	82.61	1.43	1.43	1.43
	71.25	0.24	0.24	0.24	73.66	1.71	1.71	1.71
	63.96	0.27	0.27	0.27	66.45	1.91	1.91	1.91
Dust	59.21	0.29	0.29	0.29	61.64	2.03	2.03	2.03
only	57.66	0.30	0.30	0.30	59.66	2.08	2.08	2.08
	59.54	0.29	0.29	0.29	61.36	2.04	2.04	2.04
	64.57	0.27	0.27	0.27	65.93	1.93	1.93	1.93
	72.07	0.24	0.24	0.24	72.98	1.73	1.73	1.73

	81.31	0.20	0.20	0.20	81.80	1.38	1.38	1.38
	88.95	0.16	0.16	0.16	88.95	1.21	1.21	1.21
	Daily mean	0.10	0.10	0.10	-	0.67	0.67	0.67
~~EC~~ BC and dust	80.34	5.00	6.55	8.07	82.61	24.03	29.16	33.71
	71.25	5.98	7.82	9.61	73.66	27.70	33.33	38.22
	63.96	6.70	8.75	10.75	66.45	30.17	36.09	41.17
	59.21	7.14	9.32	11.43	61.64	31.61	37.68	42.83
	57.66	7.28	9.49	11.64	59.66	32.15	38.27	43.45
	59.54	7.11	9.28	11.38	61.36	31.69	37.76	42.92
	64.57	6.65	8.68	10.66	65.93	30.34	36.27	41.36
	72.07	5.89	7.71	9.48	72.98	27.95	33.61	38.52
	81.31	4.89	6.41	7.90	81.80	24.39	29.58	34.16
	88.95	4.01	5.26	6.49	88.95	21.01	25.67	29.85
	Daily mean	2.45	3.20	3.93	-	10.81	12.98	14.86

MAC = Mass Absorption Cross section, SZA = Solar Zenith Angle

Table S5. Potential source countries for pollutants: a) identified using wind vector analysis; b) identified using trajectory analysis; and c) identified using the WRF-STEM model

Method	Region	Countries
a) Wind vector	East Asia	~~Thailand, Myanmar~~South west China.
	Central Asia	Tajikistan, Kyrgyzstan, Uzbekistan, Azerbaijan, Turkmenistan
	South Asia	~~Bay of Bengal,~~ India, Pakistan, Afghanistan
	Middle East	Syria, Iraq, Lebanon, Armenia.
	West Asia	Iran, Turkey
	Europe	Western parts of Russia.
b) Trajectory analysis	Central Asia	Uzbekistan, Western part Turkmenistan, Kazakhstan, Azerbaijan
	South Asia	Pakistan
	Middle East	Iraq, Armenia, Syria, United Arab Emirates, Jordan
	West Asia	Iran, Georgia, Turkey, Cyprus
	Russian Federation	Western Russia.
	Europe	Ukraine
	Africa	Egypt, Libya, Tunisia
c) WRF-STEM	East Asia	Indonesia, Singapore, Malaysia, Thailand, Myanmar, Sri Lanka
	Central Asia	Mongolia, Tajikistan, Kyrgyzstan, Kazakhstan, Uzbekistan, Turkmenistan
	South Asia	Bangladesh, India, Bhutan, Nepal
	Middle East	Oman, United Arab Emirates, Qatar, Bahrain, Kuwait, Iraq, Syria, Lebanon, Palestinian Territory, Israel, Jordan, Saudi Arabia, Yemen

Russian Federation	Russia
West Asia	Azerbaijan, Armenia, Georgia, Turkey and Cyprus
Europe	Europe
Africa	Kenia, Somalia, Egypt, Congo
Other	China, Pakistan, Afghanistan, Iran

66